Linking star formation to black hole spectra: simulations and inference for the Einstein Telescope era

Giovanni Antinozzi, Astrophysics & Cosmology Ph.D. student @ Scuola Internazionale Superiore di Studi Avanzati, Trieste, Italy

INAF - IASF Milano Seminars – 27/05/2026

1 : Introduction

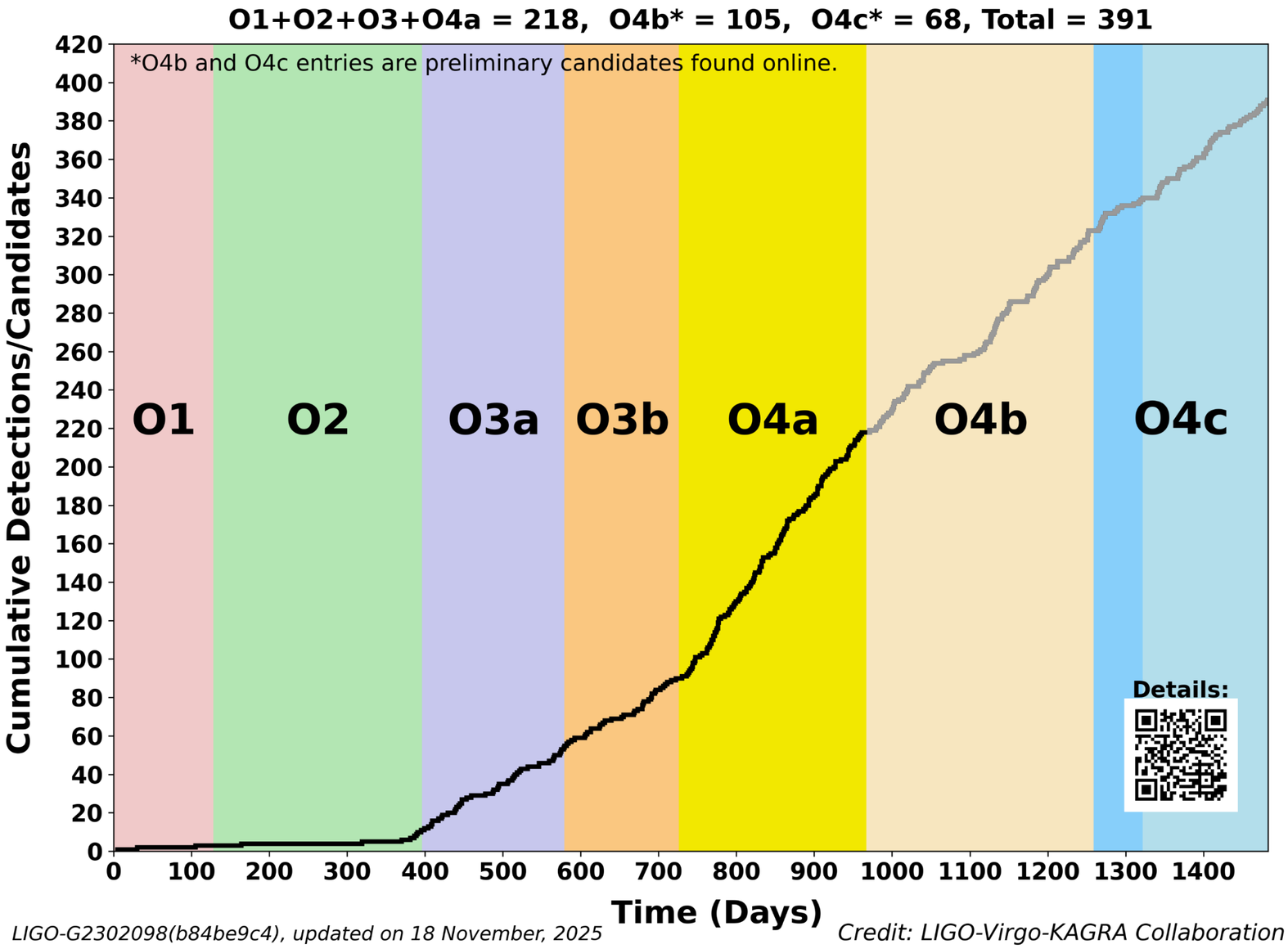

LIGO-G2302098(b84be9c4), updated on 18 November, 2025 *Credit: LIGO-Virgo-KAGRA Collaboration*


Masses in the Stellar Graveyard
Solar Masses
200
100
50
20
10
5
2
1
LIGO-Virgo-KAGRA | Aaron Geller | Northwestern

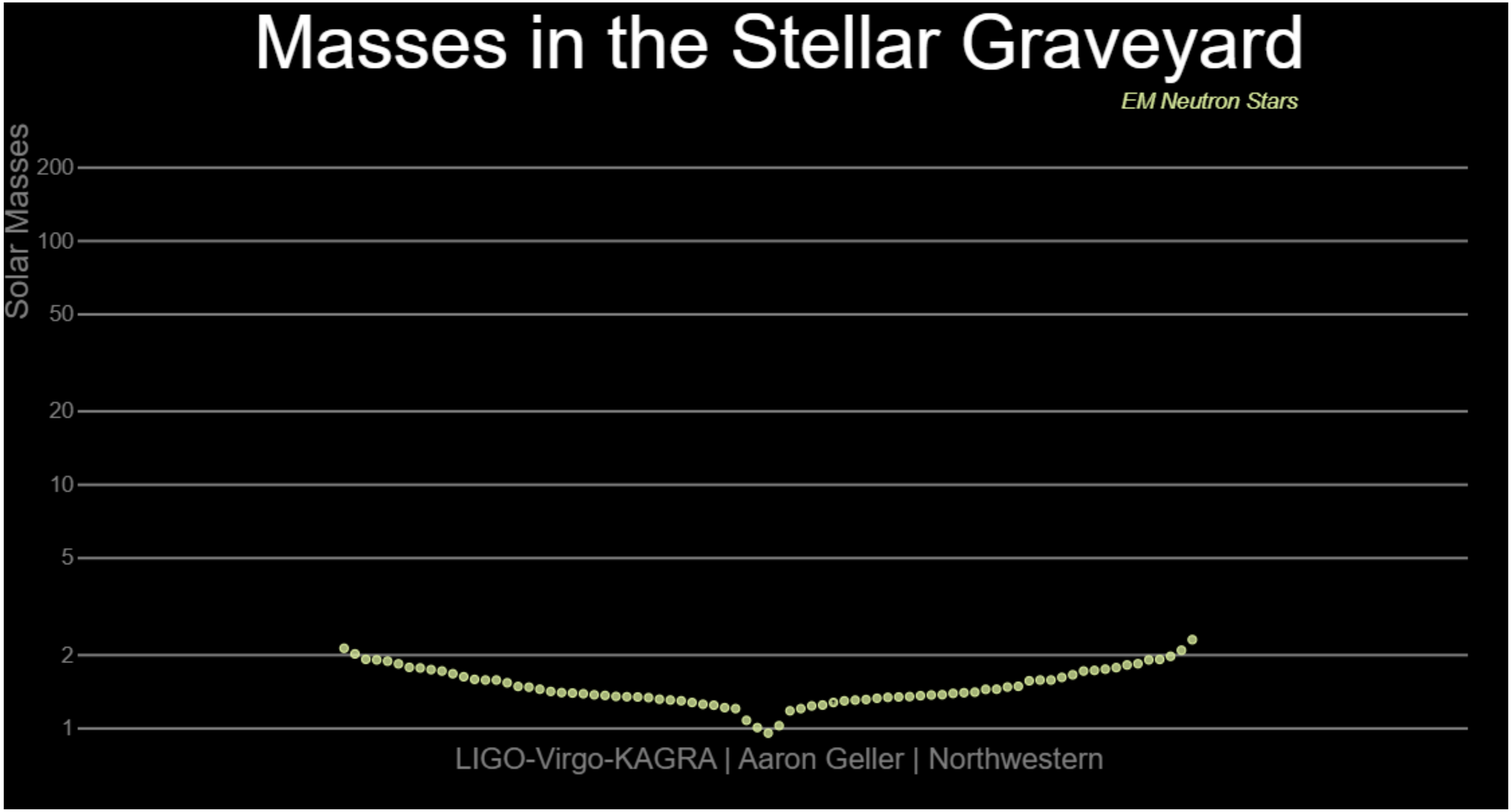
Masses in the Stellar Graveyard
EM Neutron Stars
Solar Masses
200
100
50
20
10
5
2
1
LIGO-Virgo-KAGRA | Aaron Geller | Northwestern

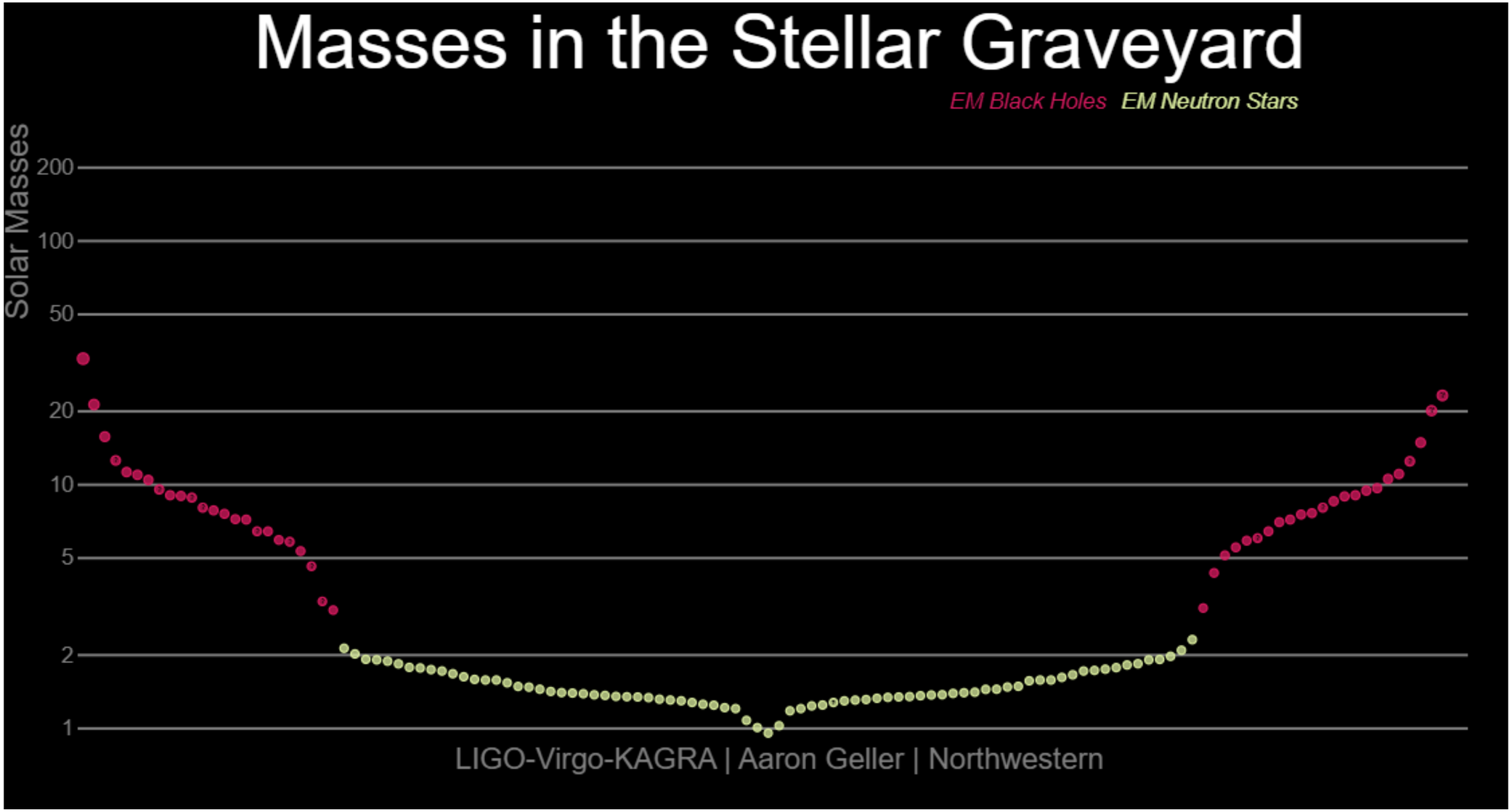
Masses in the Stellar Graveyard
EM Black Holes
EM Neutron Stars
Solar Masses
200
100
50
20
10
5
2
1
LIGO-Virgo-KAGRA | Aaron Geller | Northwestern

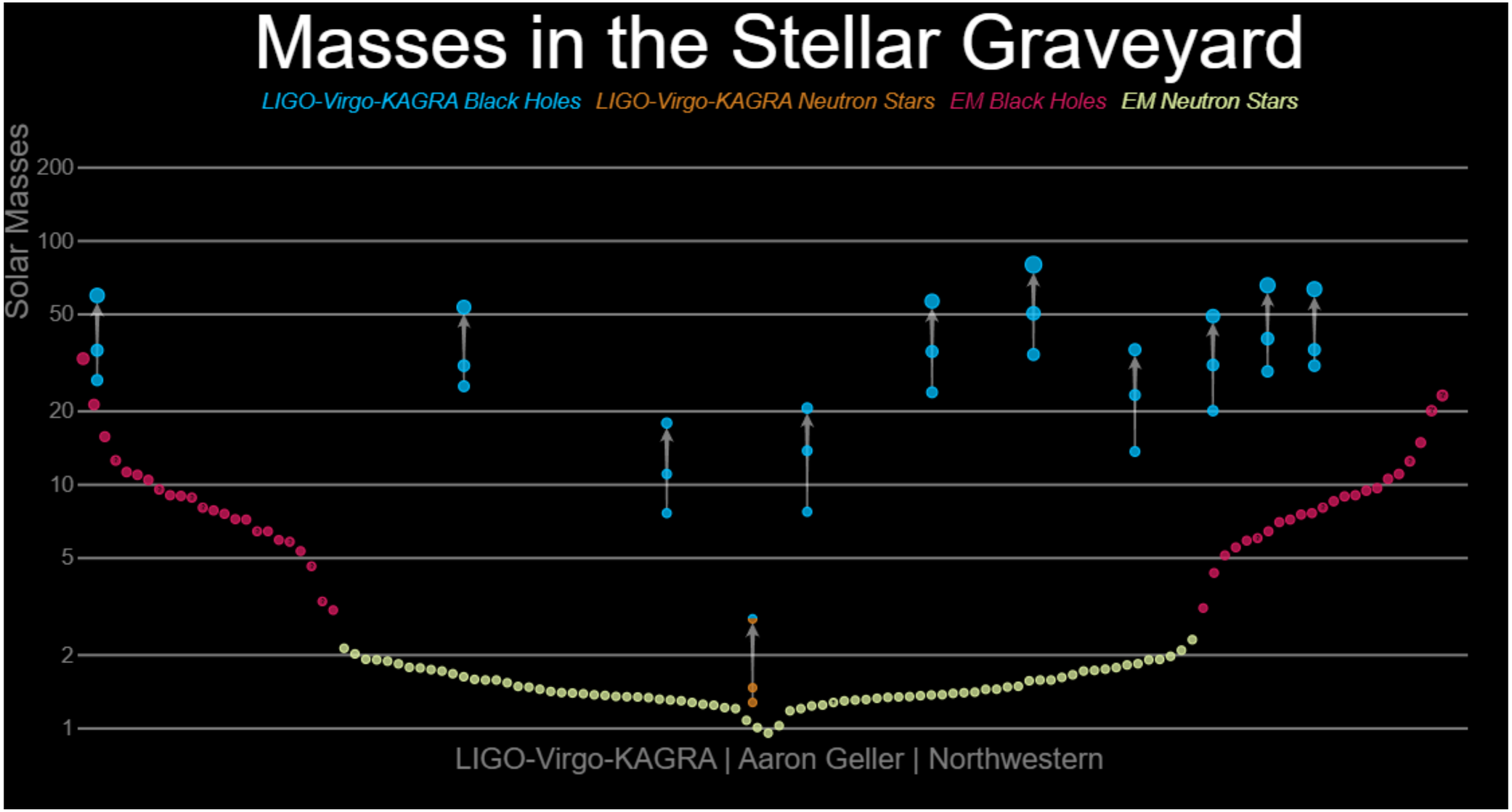
Masses in the Stellar Graveyard
LIGO-Virgo-KAGRA Black Holes
LIGO-Virgo-KAGRA Neutron Stars
EM Black Holes
EM Neutron Stars
Solar Masses
200
100
50
20
10
5
2
1
LIGO-Virgo-KAGRA | Aaron Geller | Northwestern

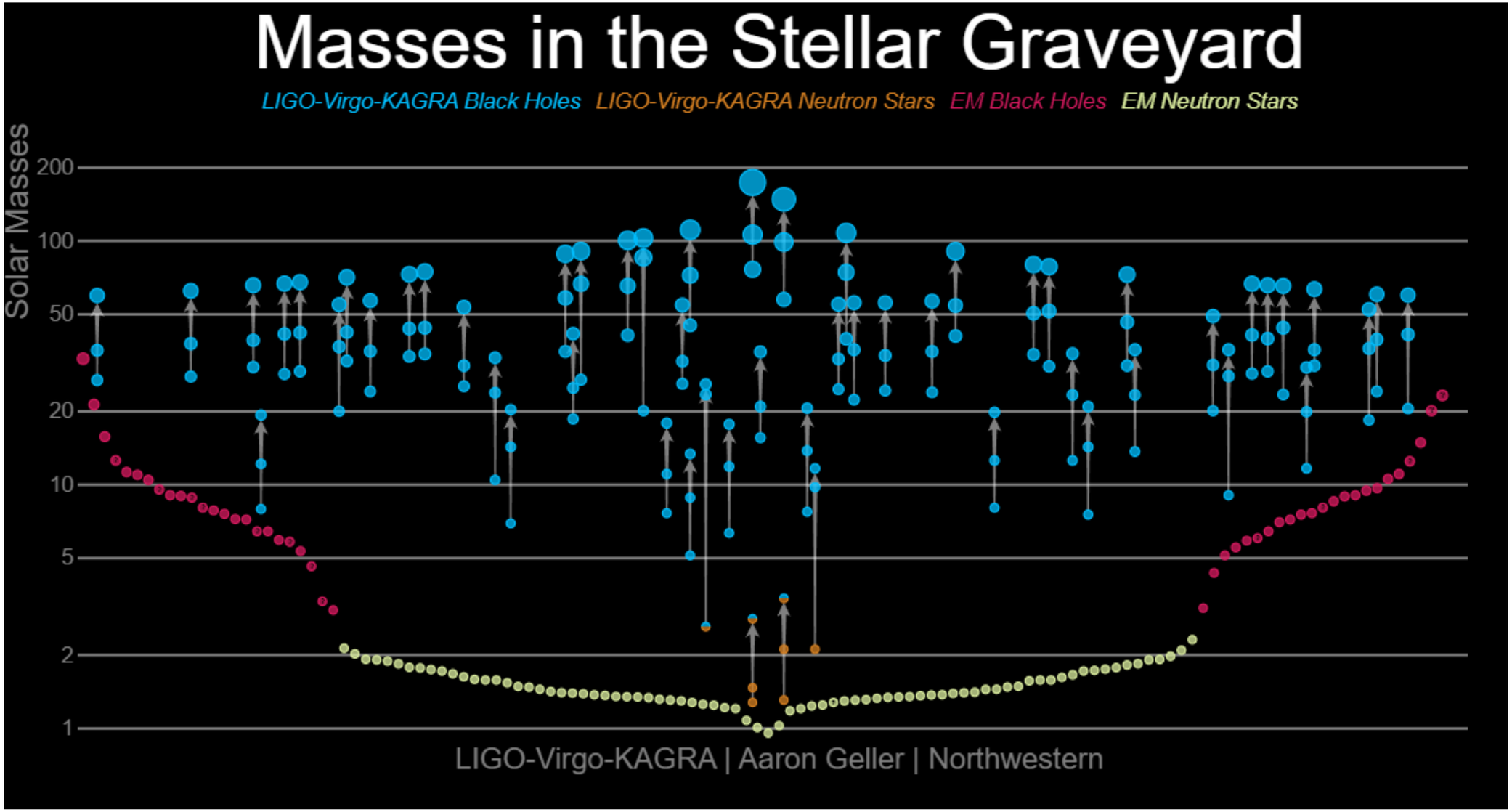
Masses in the Stellar Graveyard
LIGO-Virgo-KAGRA Black Holes
LIGO-Virgo-KAGRA Neutron Stars
EM Black Holes
EM Neutron Stars
Solar Masses
200
100
50
20
10
5
2
1
LIGO-Virgo-KAGRA | Aaron Geller | Northwestern

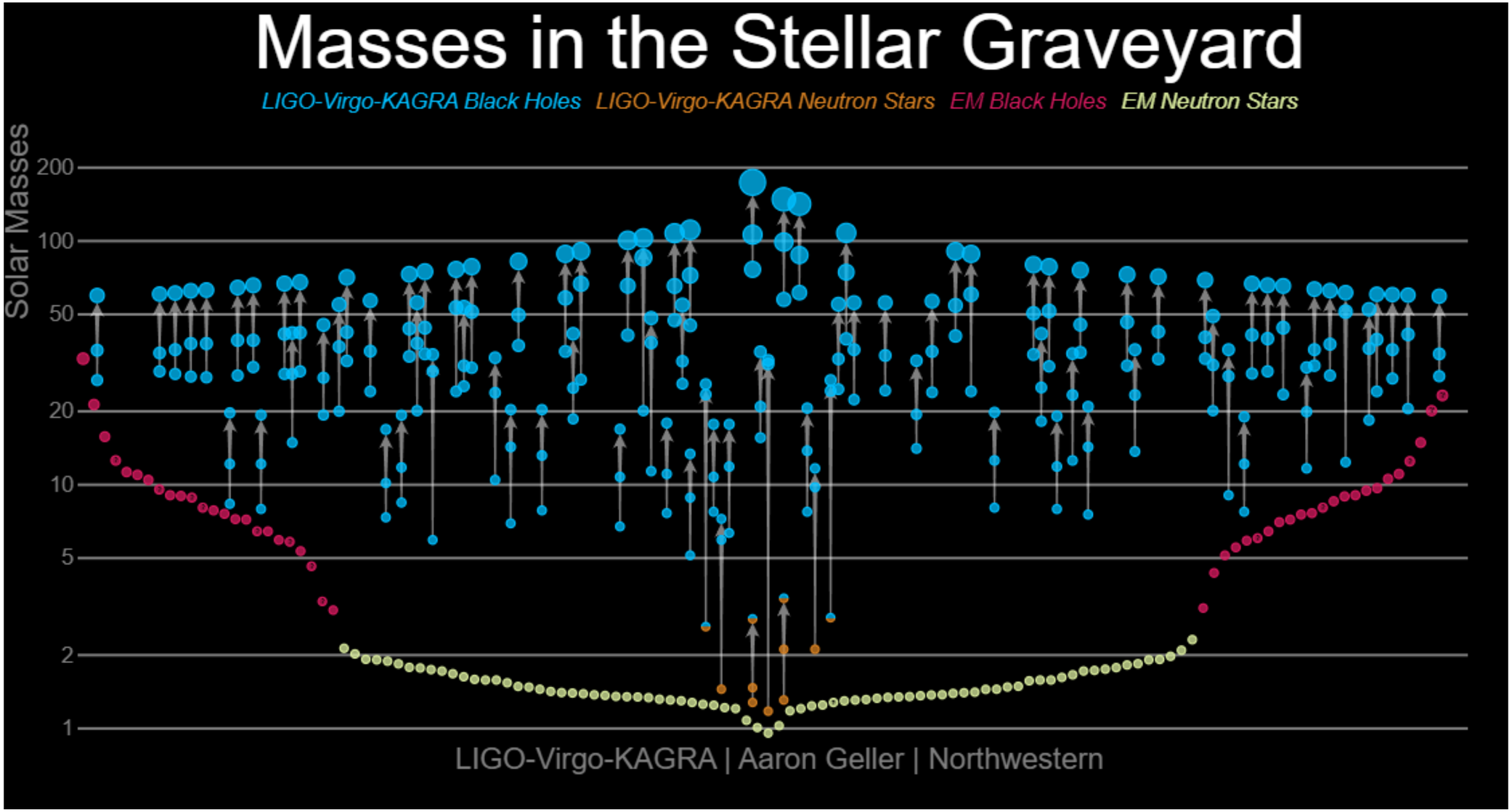
Masses in the Stellar Graveyard
LIGO-Virgo-KAGRA Black Holes
LIGO-Virgo-KAGRA Neutron Stars
EM Black Holes
EM Neutron Stars
Solar Masses
200
100
50
20
10
5
2
1
LIGO-Virgo-KAGRA | Aaron Geller | Northwestern

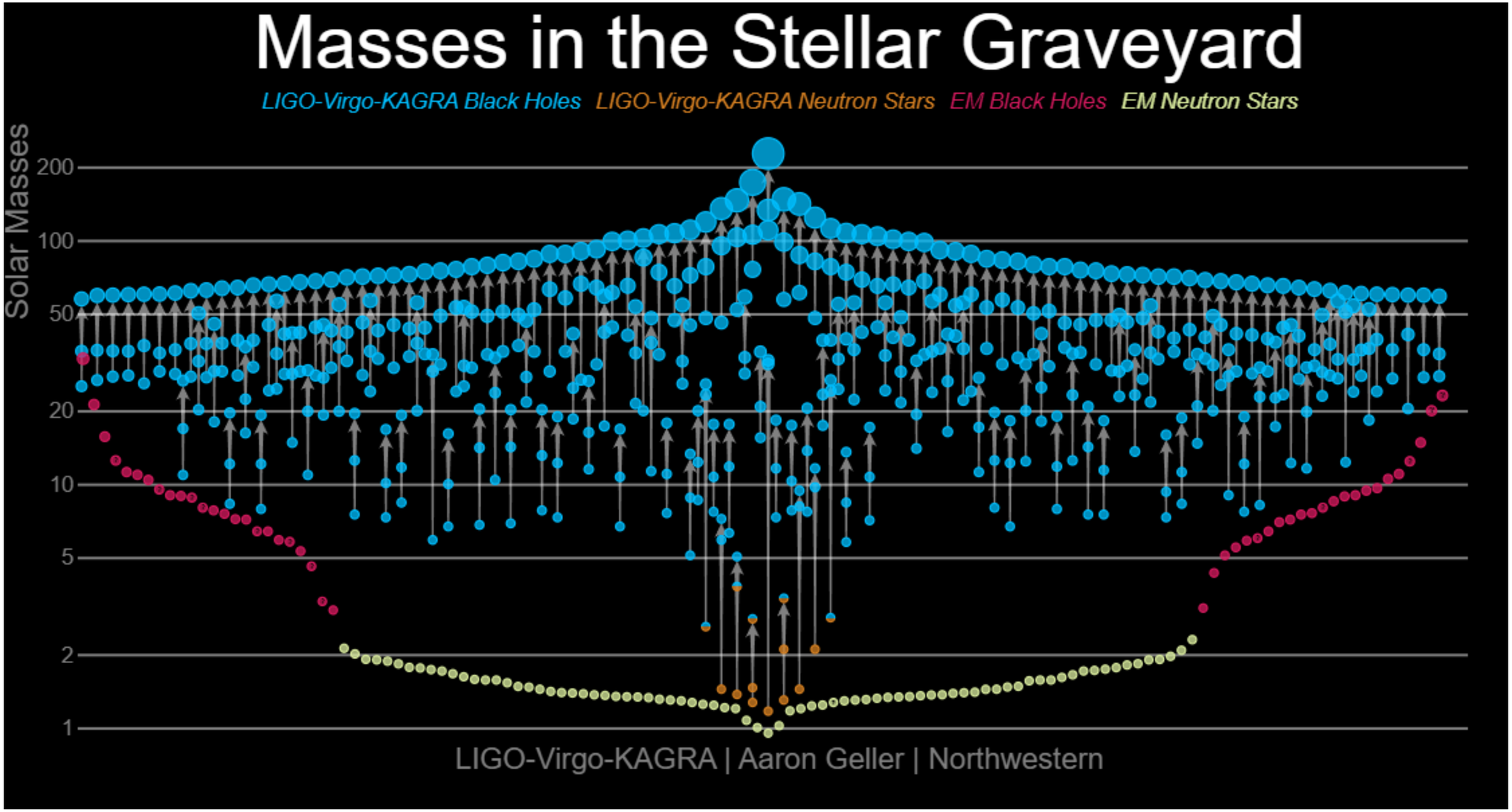
Masses in the Stellar Graveyard
LIGO-Virgo-KAGRA Black Holes
LIGO-Virgo-KAGRA Neutron Stars
EM Black Holes
EM Neutron Stars
Solar Masses
200
100
50
20
10
5
2
1
LIGO-Virgo-KAGRA | Aaron Geller | Northwestern

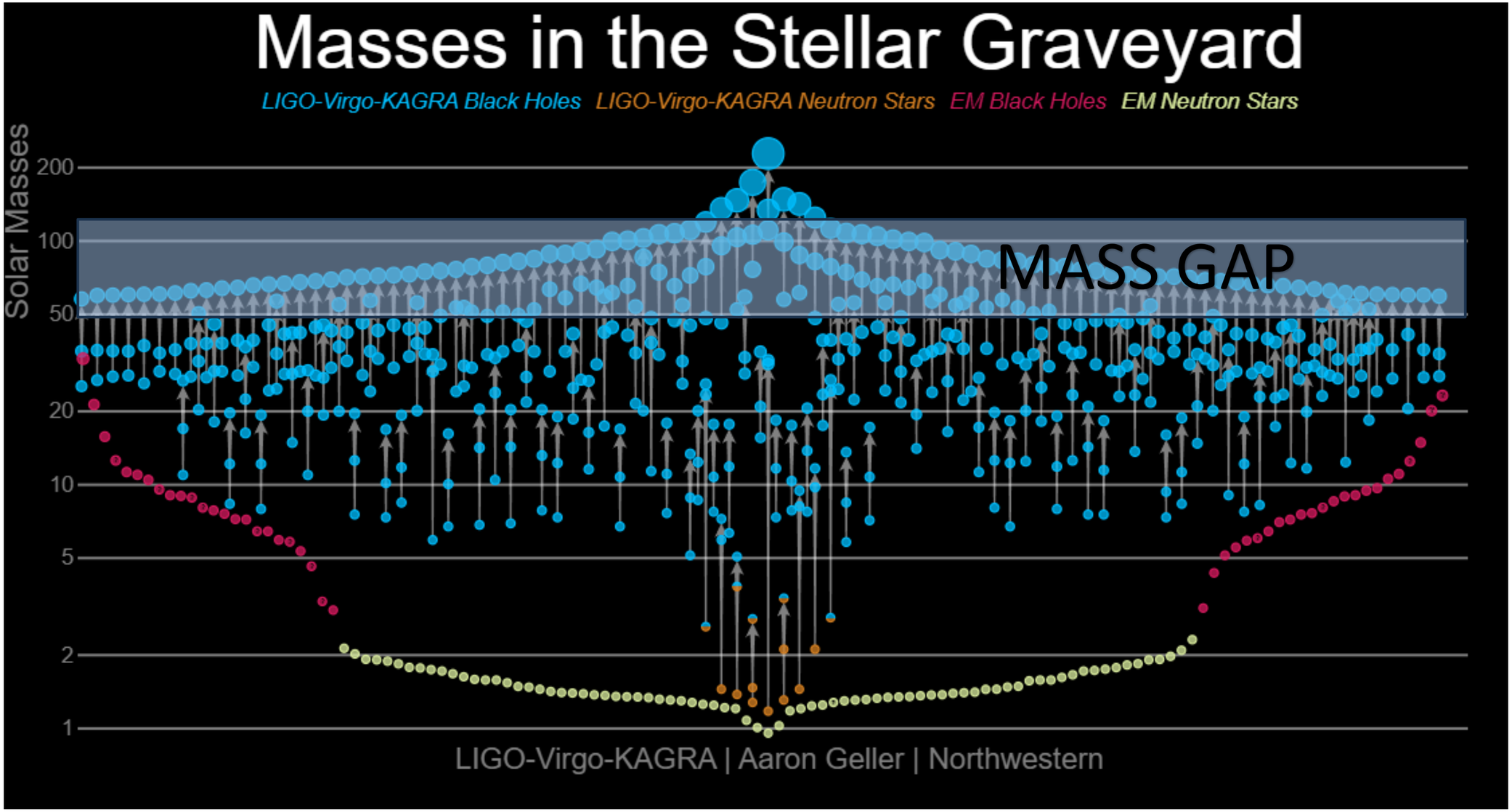
Masses in the Stellar Graveyard
LIGO-Virgo-KAGRA Black Holes
LIGO-Virgo-KAGRA Neutron Stars
EM Black Holes
EM Neutron Stars
Solar Masses
200
100
50
20
10
5
2
1
MASS GAP
LIGO-Virgo-KAGRA | Aaron Geller | Northwestern

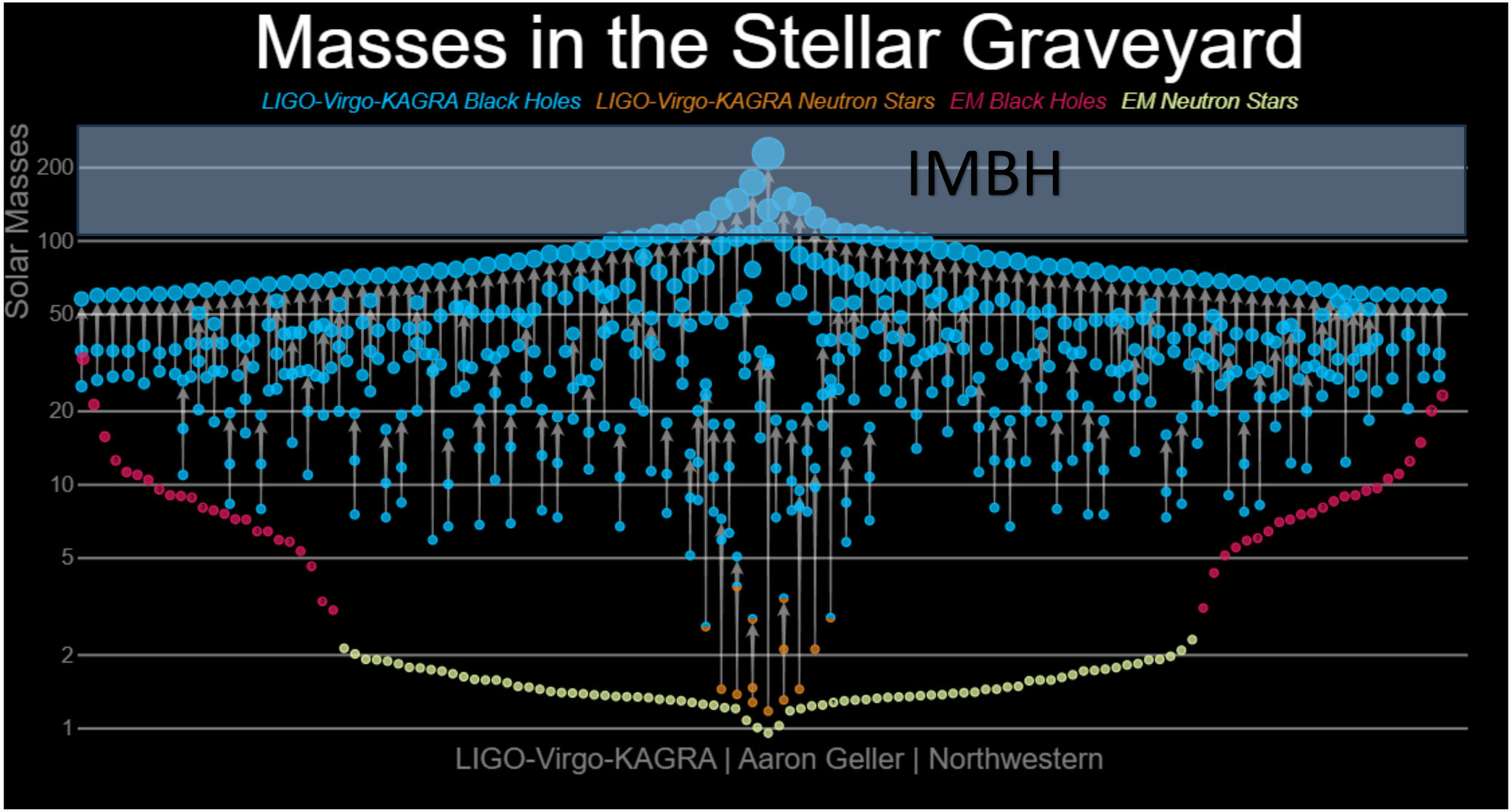
Masses in the Stellar Graveyard
LIGO-Virgo-KAGRA Black Holes
LIGO-Virgo-KAGRA Neutron Stars
EM Black Holes
EM Neutron Stars
IMBH
Solar Masses
200
100
50
20
10
5
2
1
LIGO-Virgo-KAGRA | Aaron Geller | Northwestern

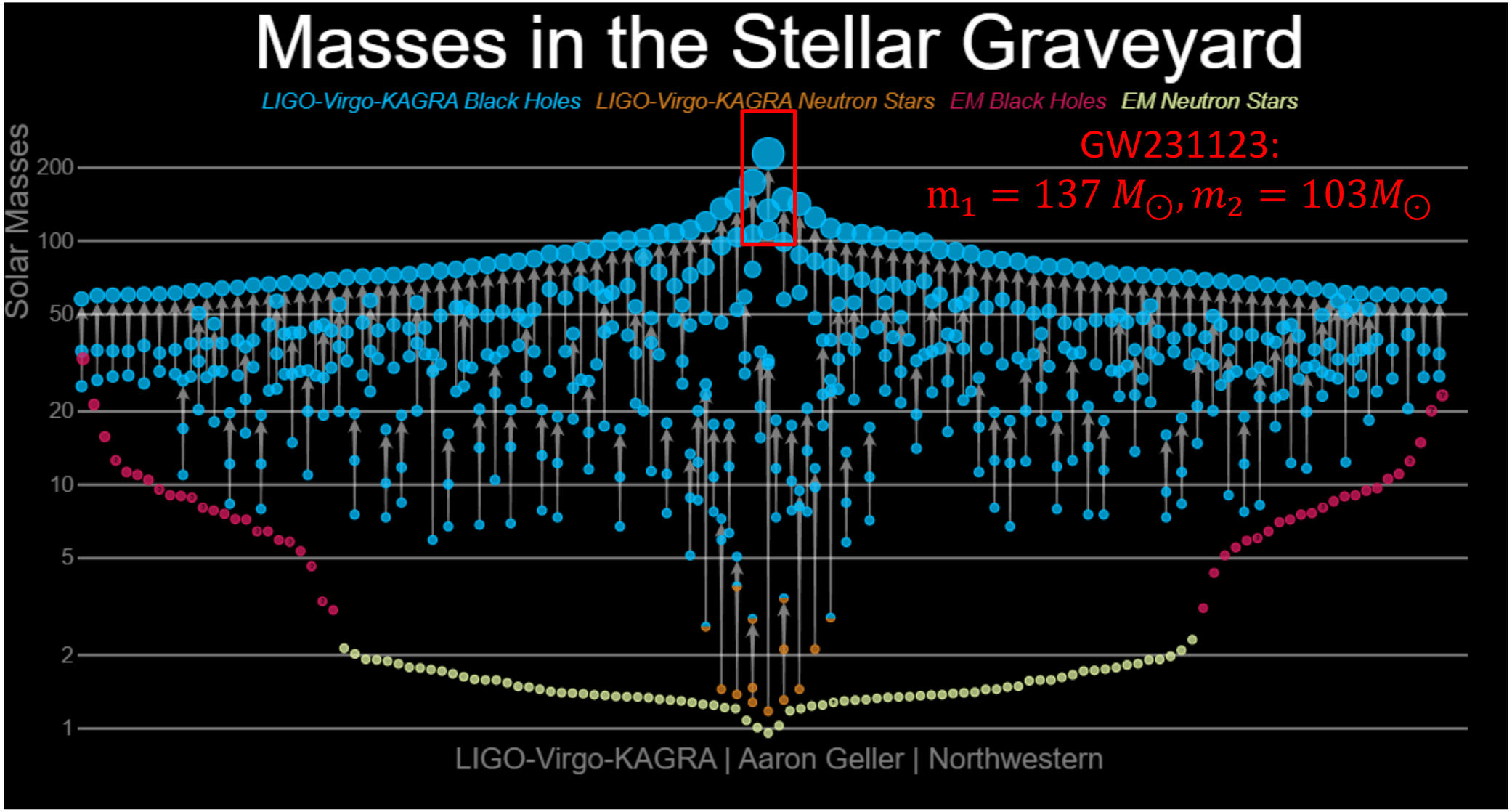
Masses in the Stellar Graveyard
LIGO-Virgo-KAGRA Black Holes
LIGO-Virgo-KAGRA Neutron Stars
EM Black Holes
EM Neutron Stars
GW231123:
$m_1 = 137\ M_\odot, m_2 = 103 M_\odot$
Solar Masses
200
100
50
20
10
5
2
1
LIGO-Virgo-KAGRA | Aaron Geller | Northwestern

Population properties inferred from observations

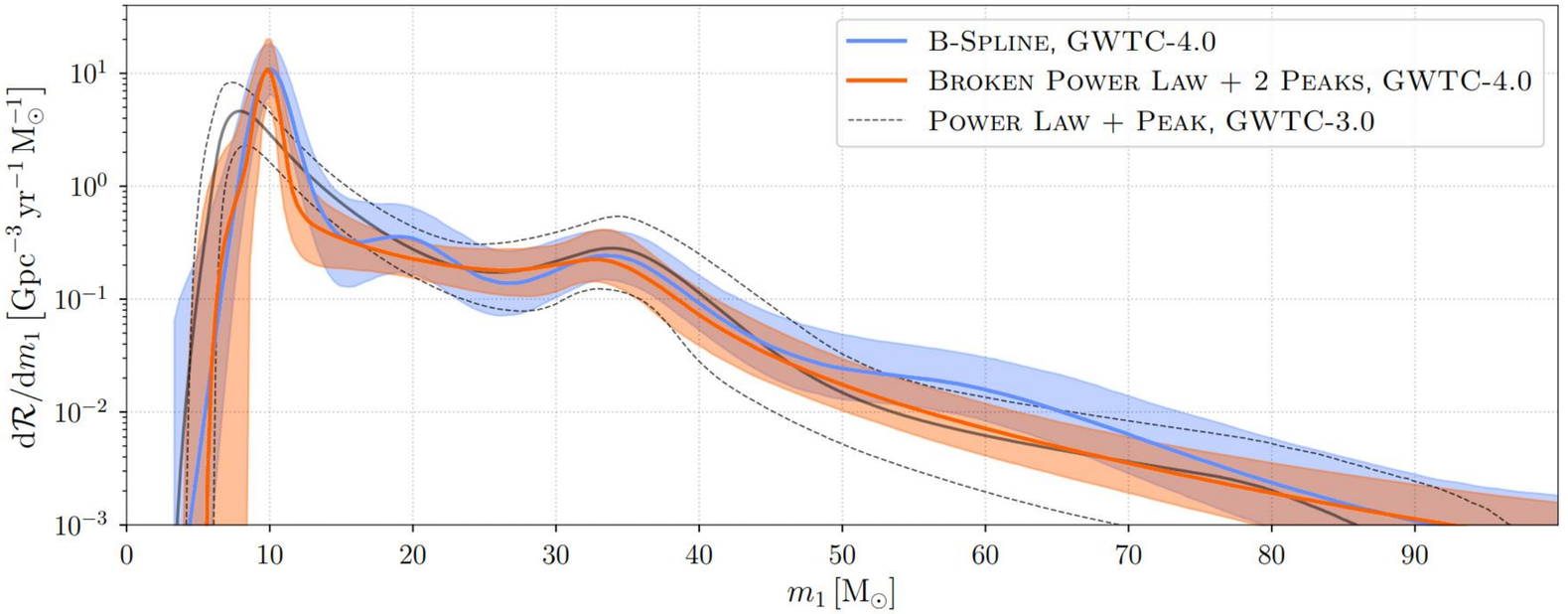

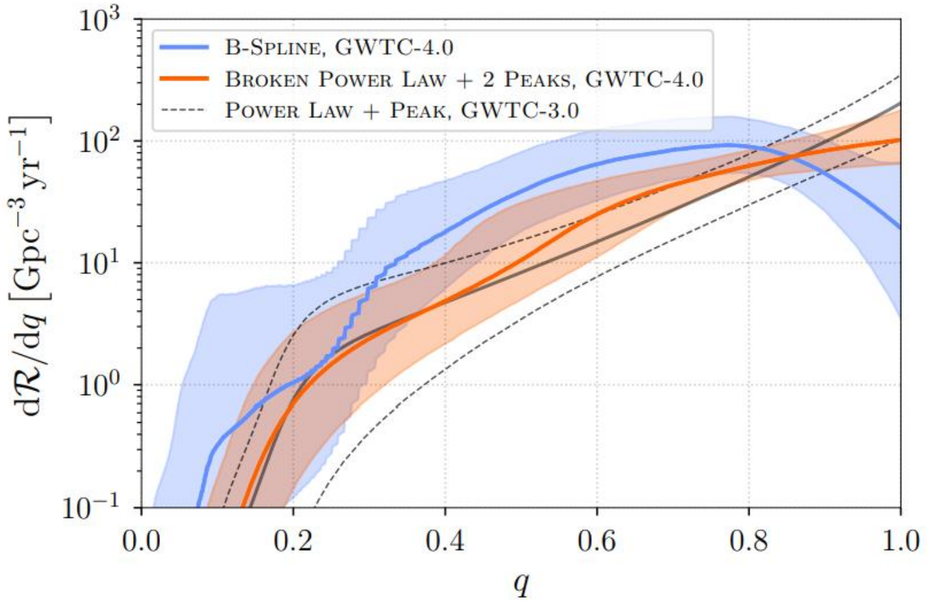

$$q = \frac{m_2}{m_1}, m_1 > m_2$$

$$\chi_{\mathrm{eff}} = \left(\frac{m_1\vec{\chi}_1 + m_2\vec{\chi}_2}{m_1 + m_2}\right)\cdot\vec{L}$$

The LIGO Scientific Collaboration, the Virgo Collaboration, the KAGRA Collaboration, A.G. Abac, I. Abouelfettouh, F. Acernese et al. , arXiv e-prints (2025)

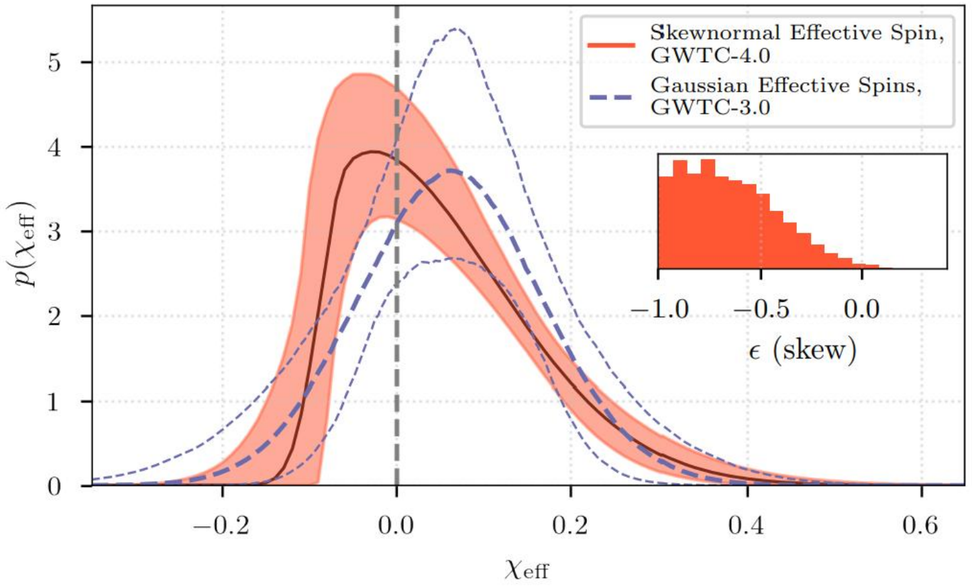

Population properties inferred from observations

Draft version May 27, 2026
Typeset using LaTeX **twocolumn** style in AASTeX631

GWTC-5.0: Population Properties of Merging Compact Binaries

The LIGO Scientific Collaboration, the Virgo Collaboration, and the KAGRA Collaboration

ABSTRACT

We present the population properties of merging compact binaries inferred using 267 mergers from the cumulative Gravitational-Wave Transient Catalog 5.0. As this data set contains no new sources with a neutron star, we primarily focus on the properties of the binary black hole mergers. We infer the merger rate of binary black holes with component masses between $2.5\,M_\odot$ and $200\,M_\odot$ to be 27.5–$49.4\,\mathrm{Gpc^{-3}\,yr^{-1}}$ (all intervals at 90% credible levels) at redshift $z = 0.2$. We find evidence for a subpopulation of binary black hole mergers that host a rapidly spinning black hole (dimensionless spins $\chi \sim 0.7$), consistent with signatures of hierarchical mergers. We find that these occur at two mass scales, the first at primary masses $\sim$ 10–$20\,M_\odot$ and the second above $\sim 45\,M_\odot$, and we estimate their total rate at $z = 0.2$ to be 0.2–$3.11\,\mathrm{Gpc^{-3}yr^{-1}}$. We infer that, above $40\,M_\odot$, the mass distribution of the less massive (secondary) black hole declines more steeply than that of the more massive (primary) one. This is consistent with a flatter mass-ratio distribution and indicates the prevalence of unequal-mass binaries with large primary masses. We find evidence for two features in the black hole mass spectrum: a peak around $10\,M_\odot$ and a change of slope at around $35\,M_\odot$. Black holes of $\sim 35\,M_\odot$ pair preferentially with companions of similar mass. Additionally, we find that the effective inspiral spin distribution of binary black holes is asymmetric about zero, based on which we infer that at least 9% of mergers occur in channels with some preference for spin-orbit alignment. We find evidence that the effective inspiral spin distribution is broader for unequal-mass binaries and that it also likely broadens with increasing redshift. Overall, our results support the presence of multiple subpopulations of merging black holes that can potentially arise from different formation pathways.

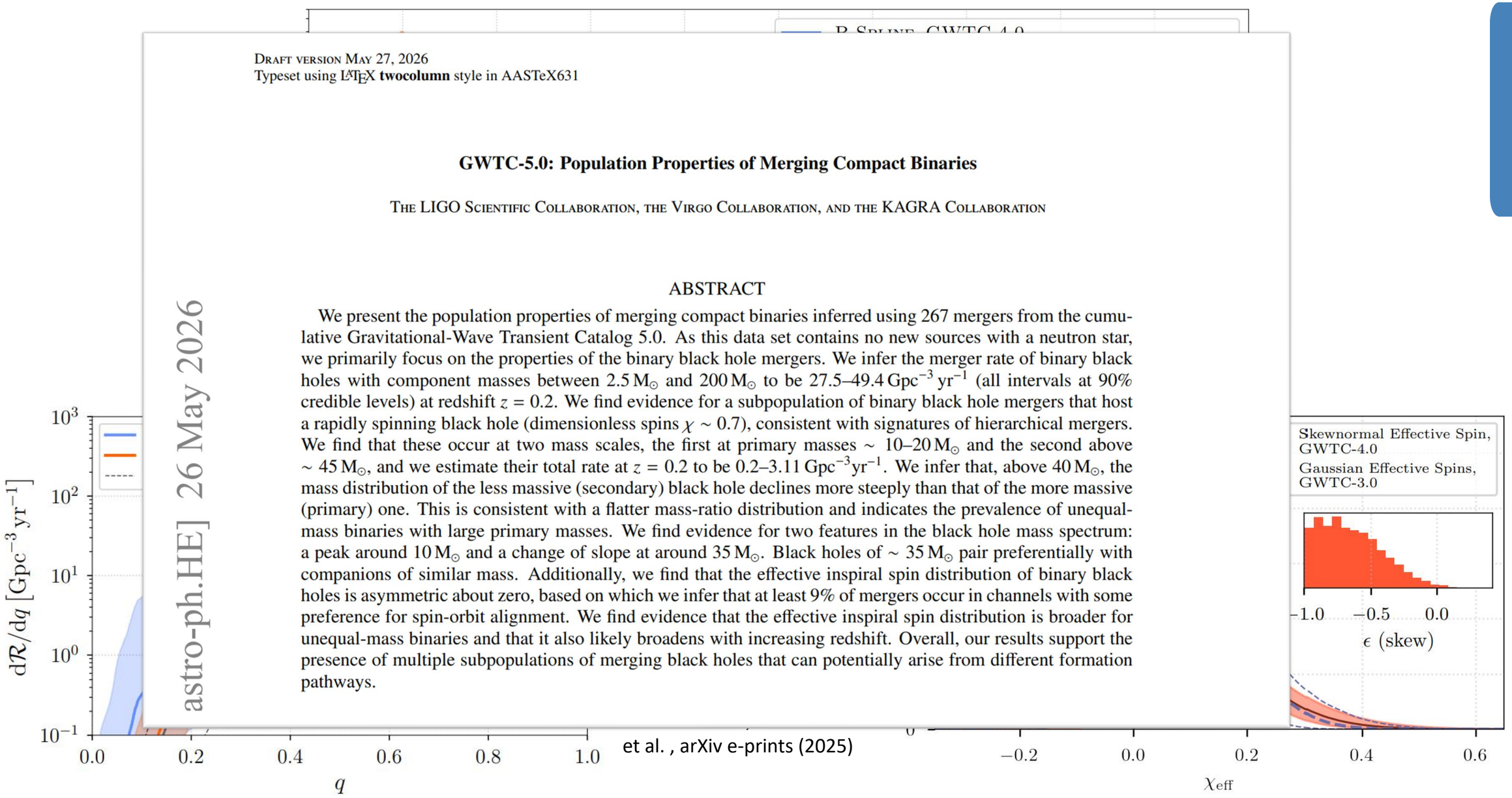

et al. , arXiv e-prints (2025)

Population properties inferred from observations

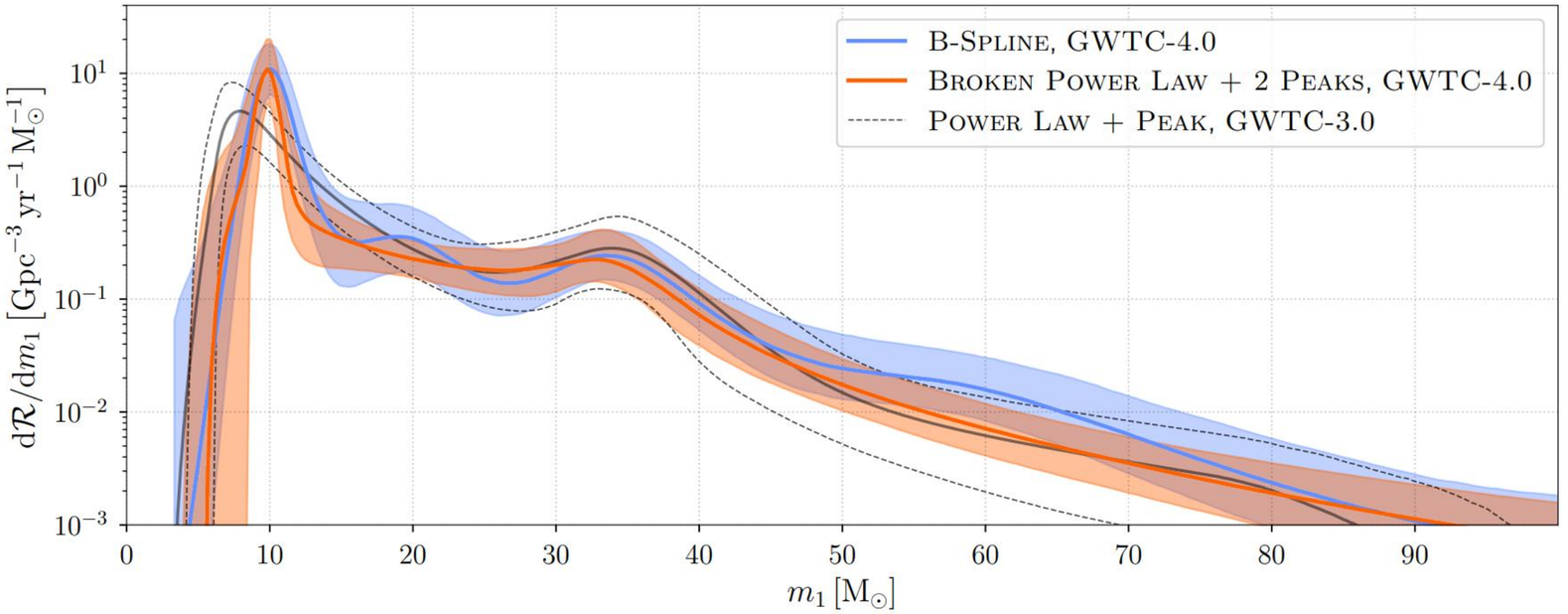

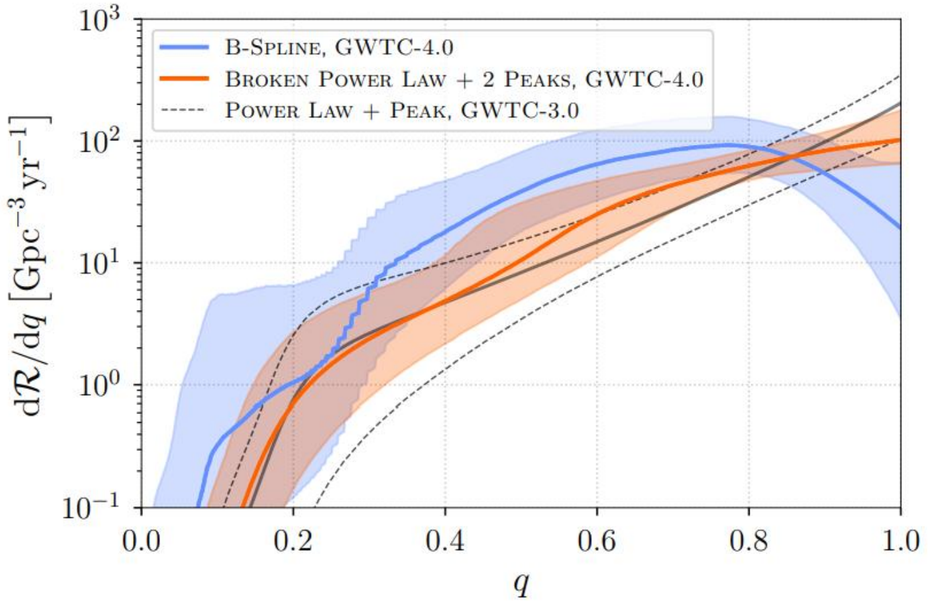

$$q = \frac{m_2}{m_1}, m_1 > m_2$$

$$\chi_{\mathrm{eff}} = \left(\frac{m_1\vec{\chi}_1 + m_2\vec{\chi}_2}{m_1 + m_2}\right)\cdot\vec{L}$$

The LIGO Scientific Collaboration, the Virgo Collaboration, the KAGRA Collaboration, A.G. Abac, I. Abouelfettouh, F. Acernese et al. , arXiv e-prints (2025)

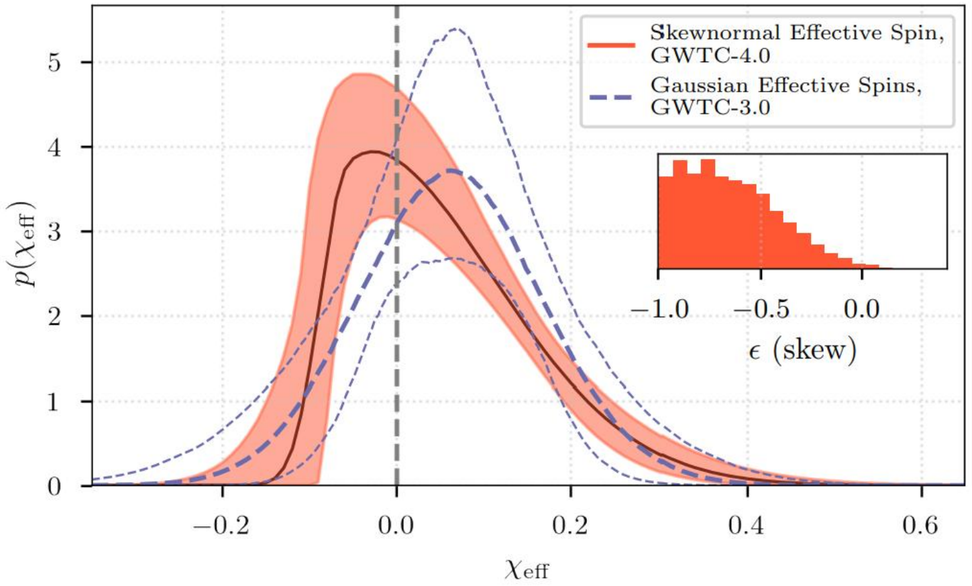

Formation channels

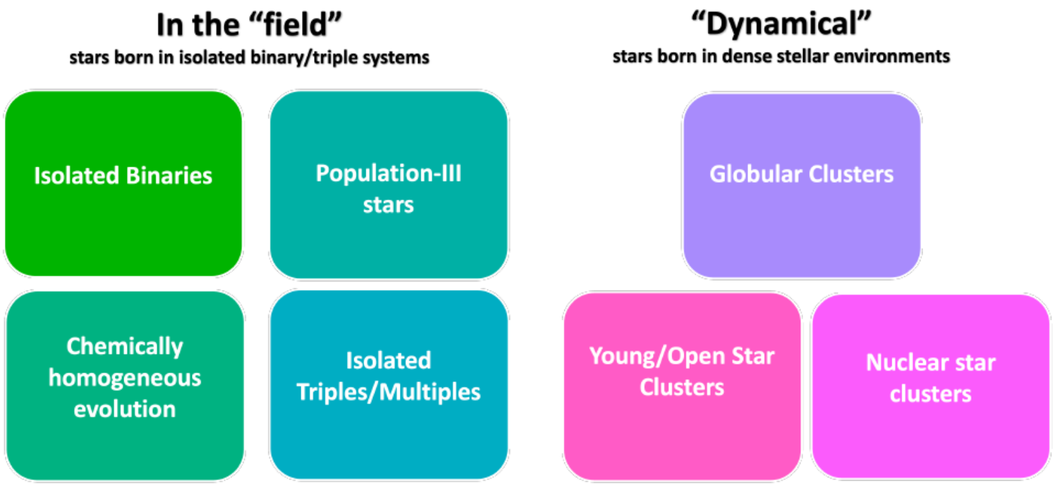

Costa G., et al., arXiv:2311,15778

Formation channels

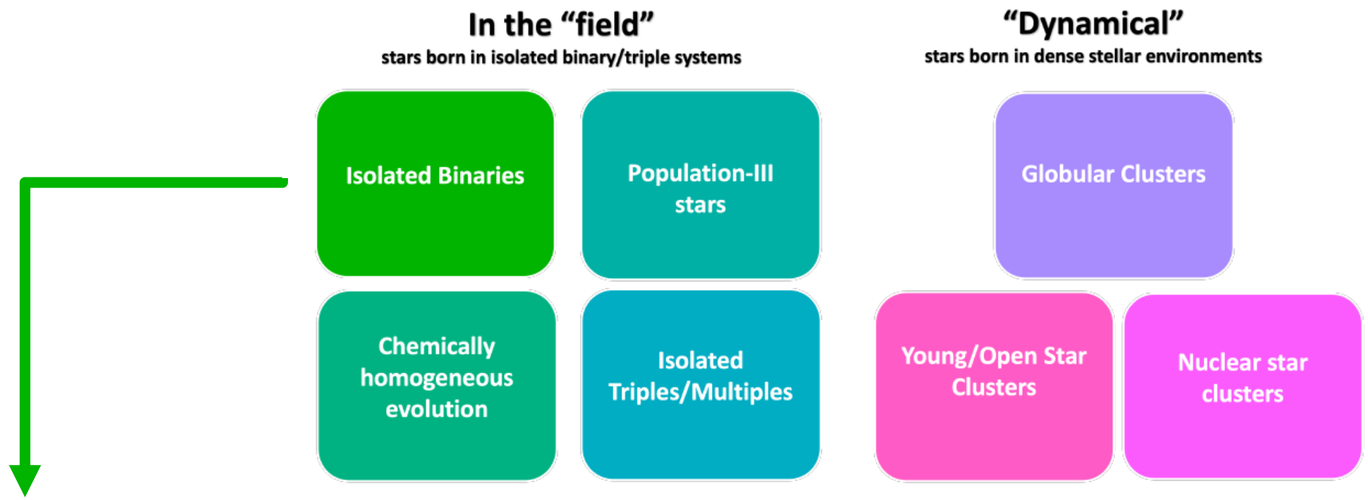

Costa G., et al., arXiv:2311,15778

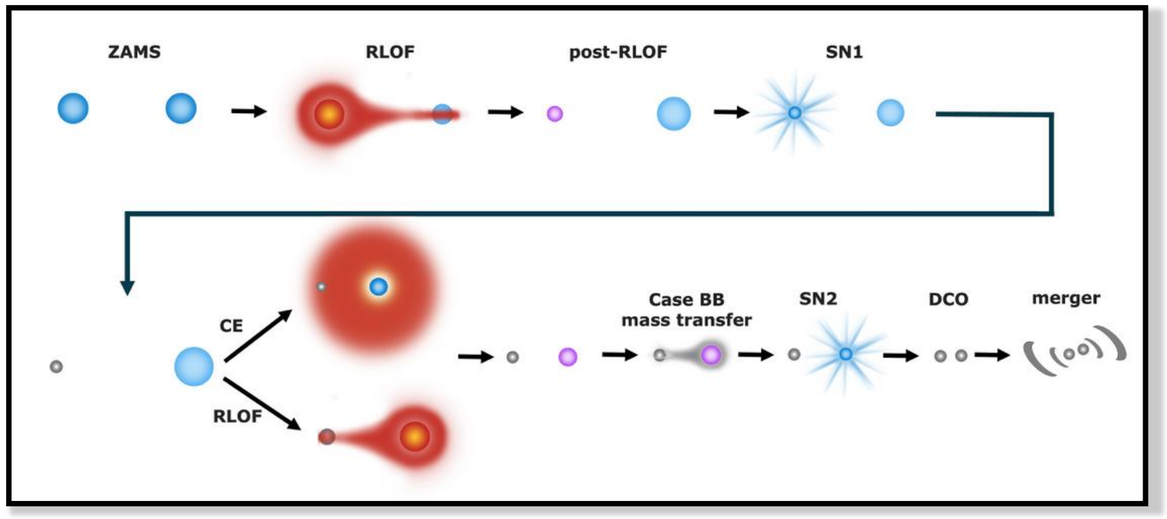

Formation channels

In the "field"
stars born in isolated binary/triple systems

- Isolated Binaries
- Population-III stars
- Chemically homogeneous evolution
- Isolated Triples/Multiples

"Dynamical"
stars born in dense stellar environments

- Globular Clusters
- Young/Open Star Clusters
- Nuclear star clusters

Costa G., et al., arXiv:2311,15778

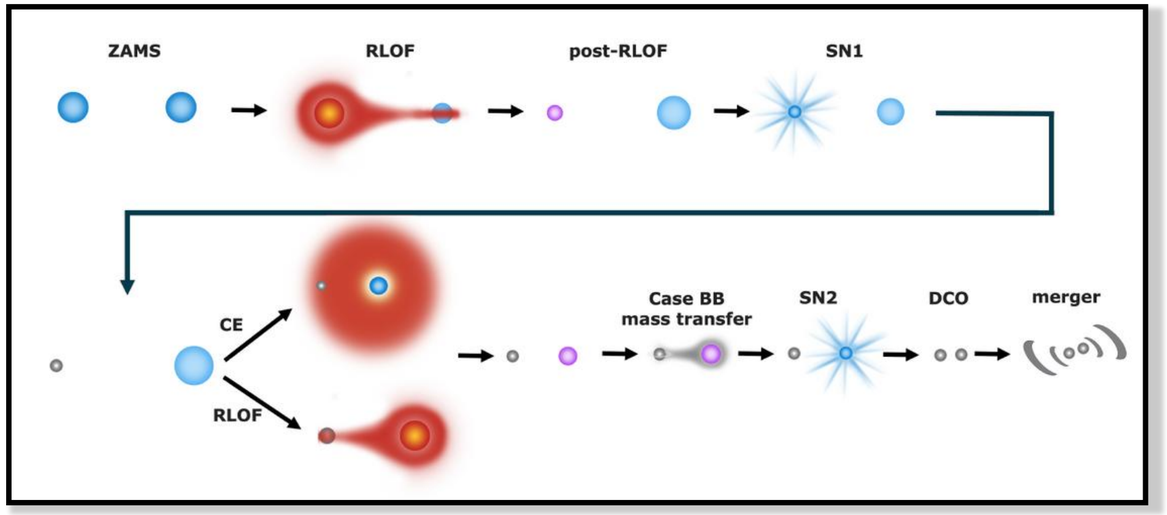

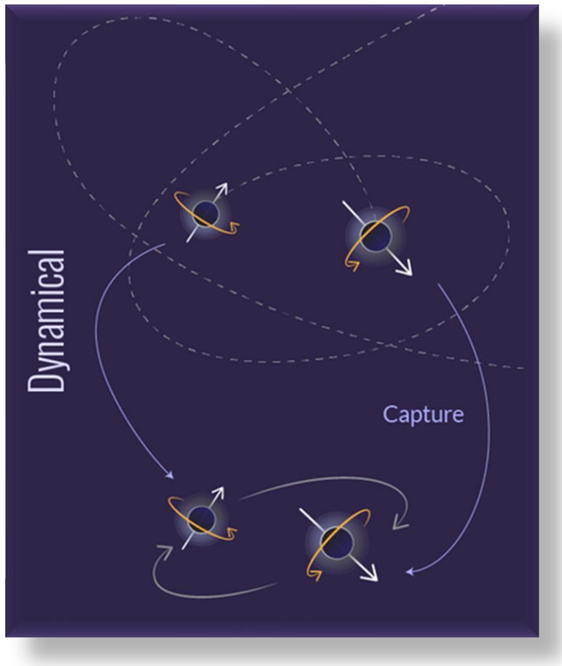

Formation channels

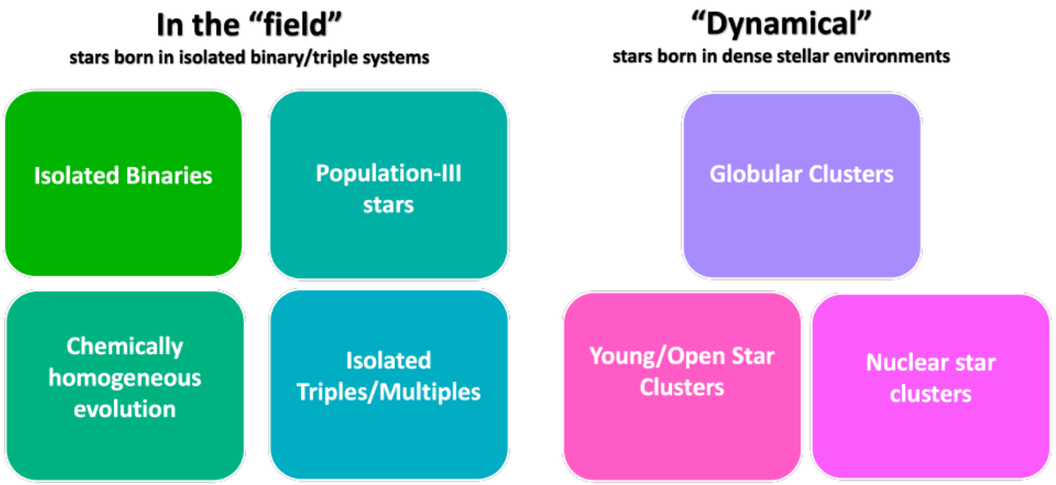

CHE

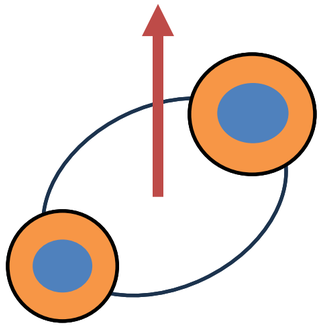

Costa G., et al., arXiv:2311,15778

Formation channels

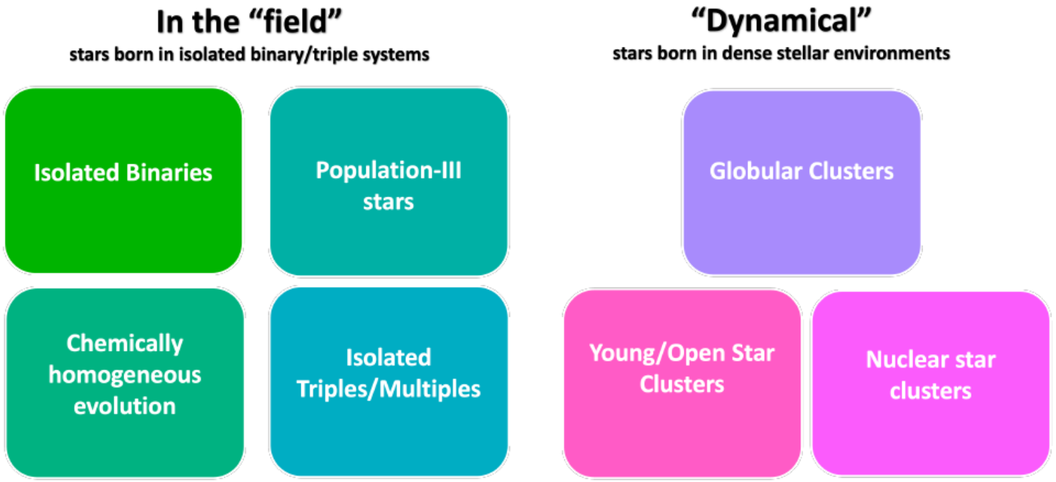

CHE

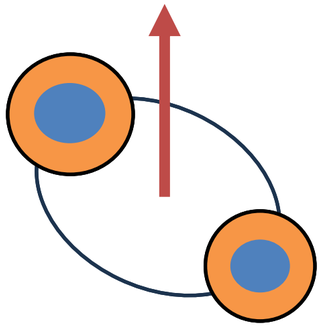

Costa G., et al., arXiv:2311,15778

Formation channels

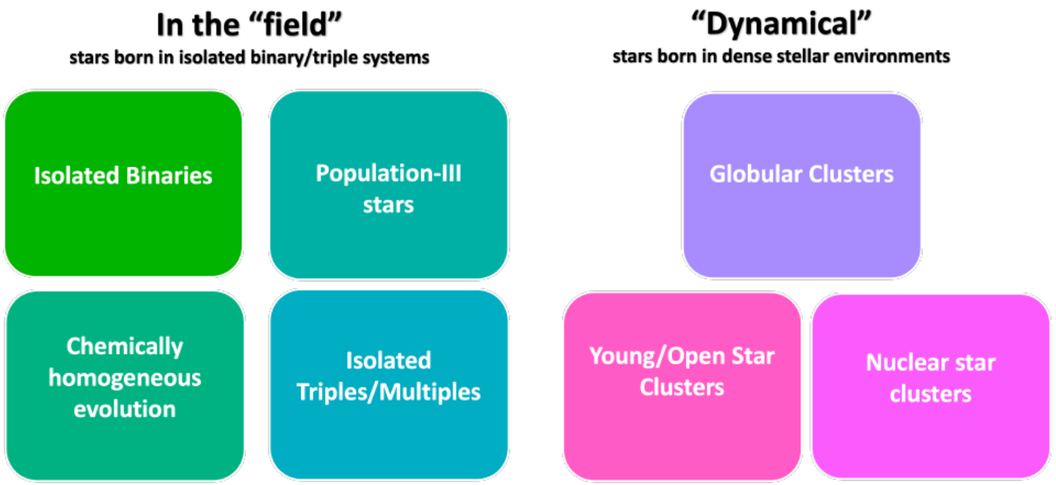

CHE

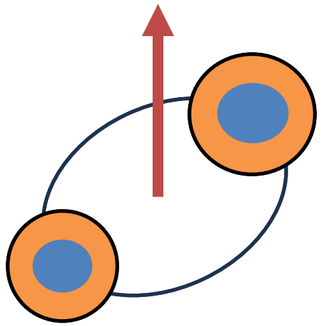

Costa G., et al., arXiv:2311,15778

Formation channels

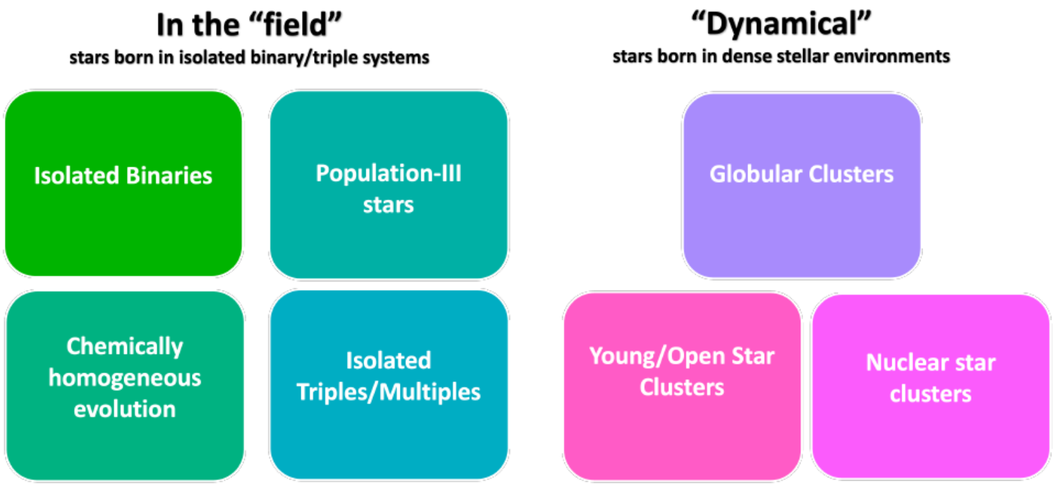

CHE

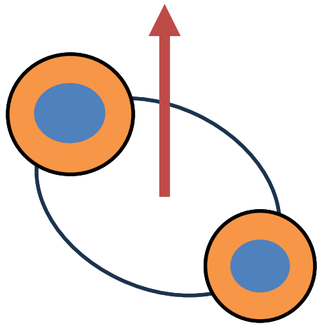

Costa G., et al., arXiv:2311,15778

Formation channels

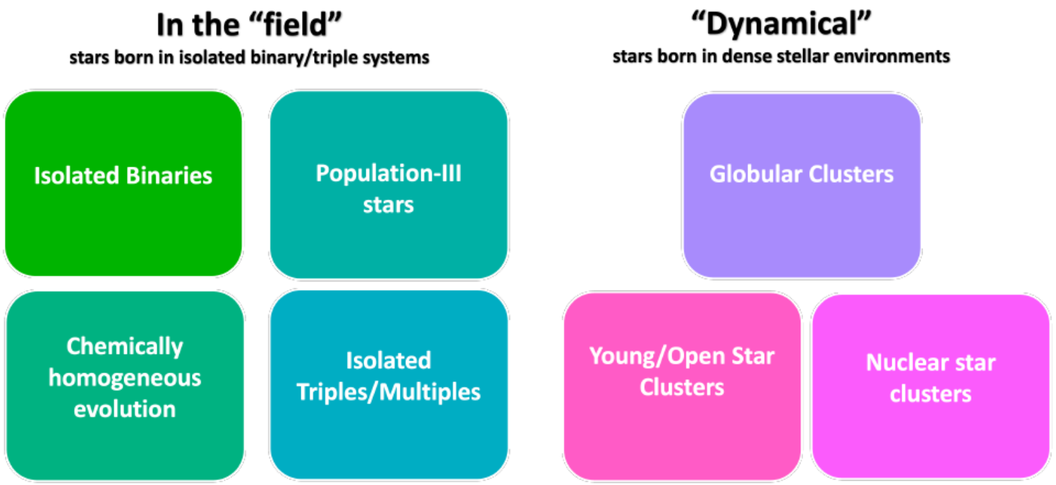

CHE

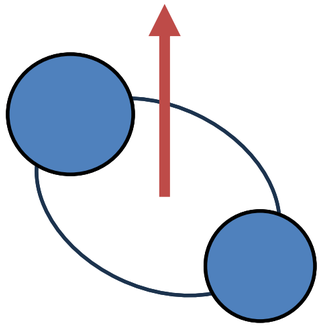

Costa G., et al., arXiv:2311,15778

Formation channels

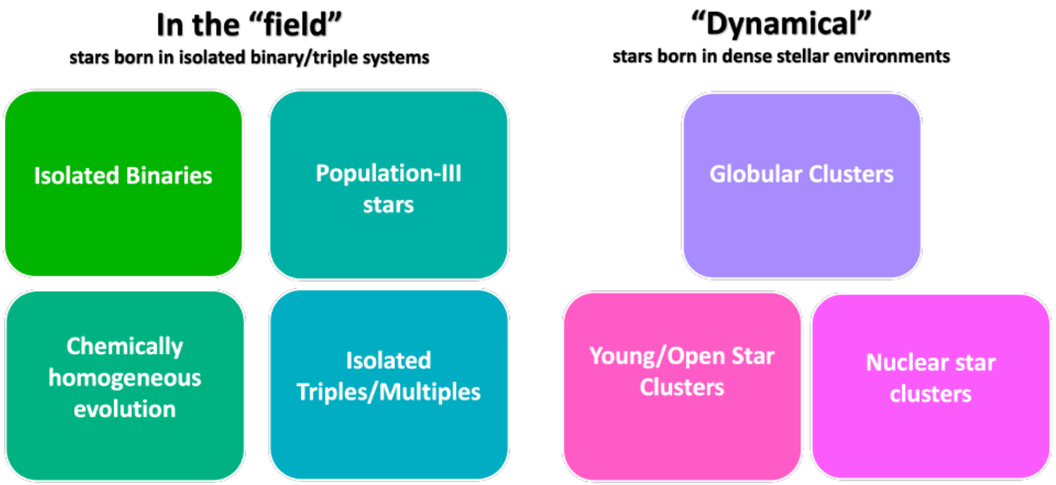

CHE

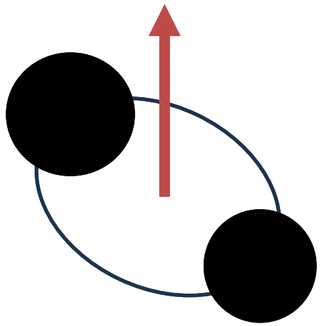

Costa G., et al., arXiv:2311,15778

Formation channels

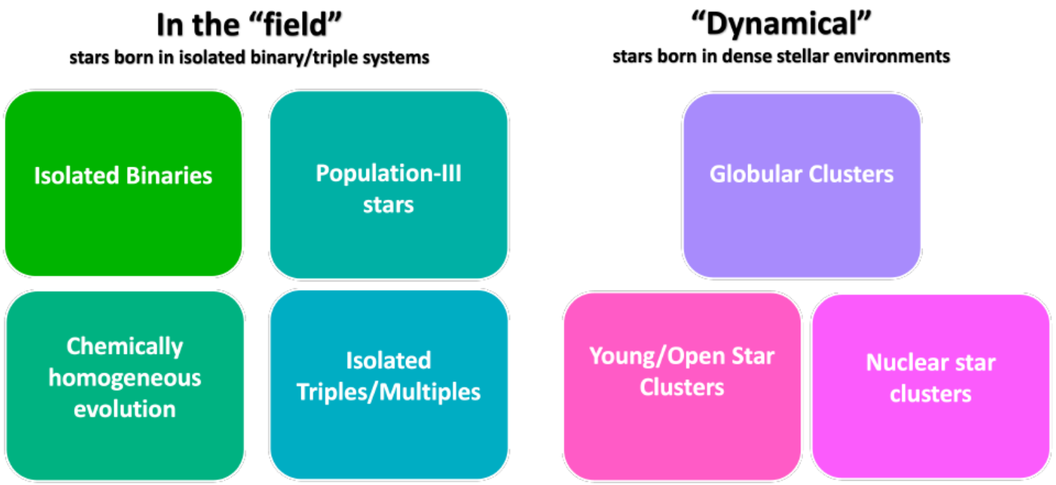

CHE

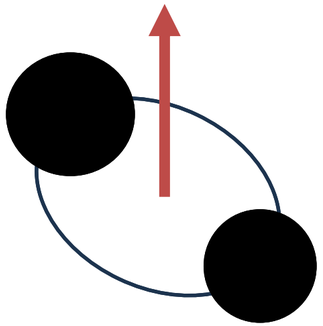

Pop III

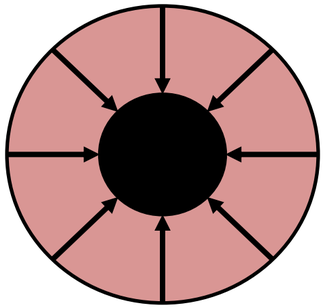

Costa G., et al., arXiv:2311,15778

Formation channels

In the "field"
stars born in isolated binary/triple systems

- Isolated Binaries
- Population-III stars
- Chemically homogeneous evolution
- Isolated Triples/Multiples

"Dynamical"
stars born in dense stellar environments

- Globular Clusters
- Young/Open Star Clusters
- Nuclear star clusters

CHE

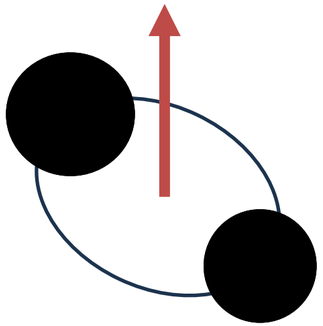

Pop III

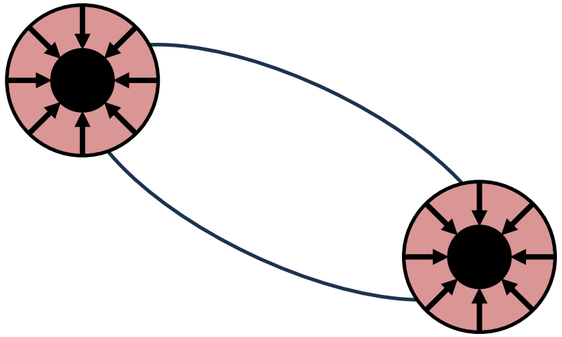

Costa G., et al., arXiv:2311,15778

Formation channels

In the "field"
stars born in isolated binary/triple systems

- Isolated Binaries
- Population-III stars
- Chemically homogeneous evolution
- Isolated Triples/Multiples

"Dynamical"
stars born in dense stellar environments

- Globular Clusters
- Young/Open Star Clusters
- Nuclear star clusters

CHE

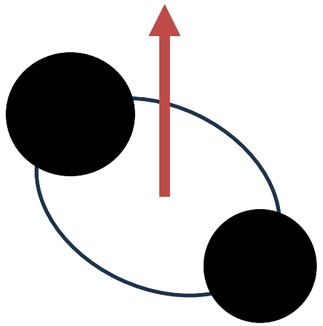

Pop III

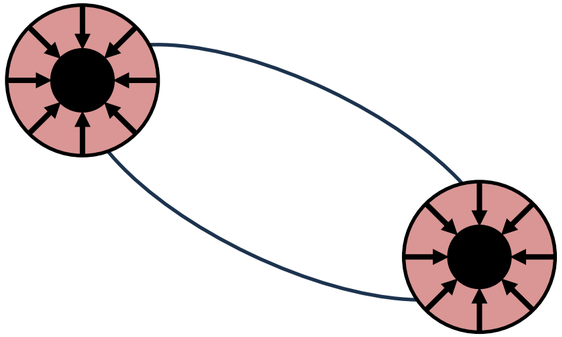

AGN disc

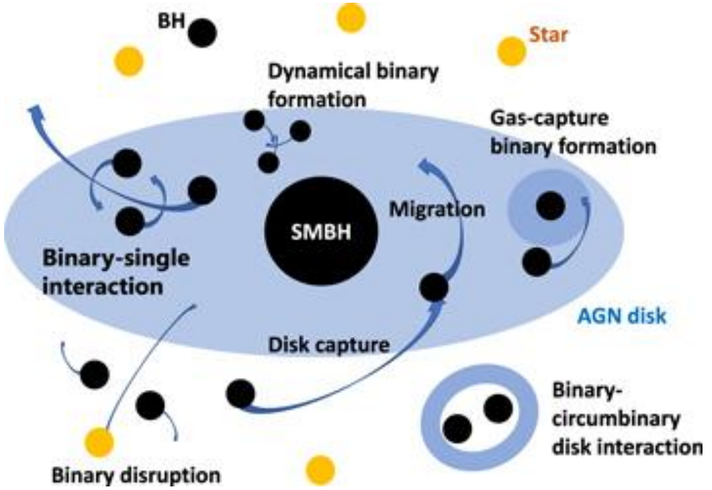

Costa G., et al., arXiv:2311,15778

BH Mass regimes

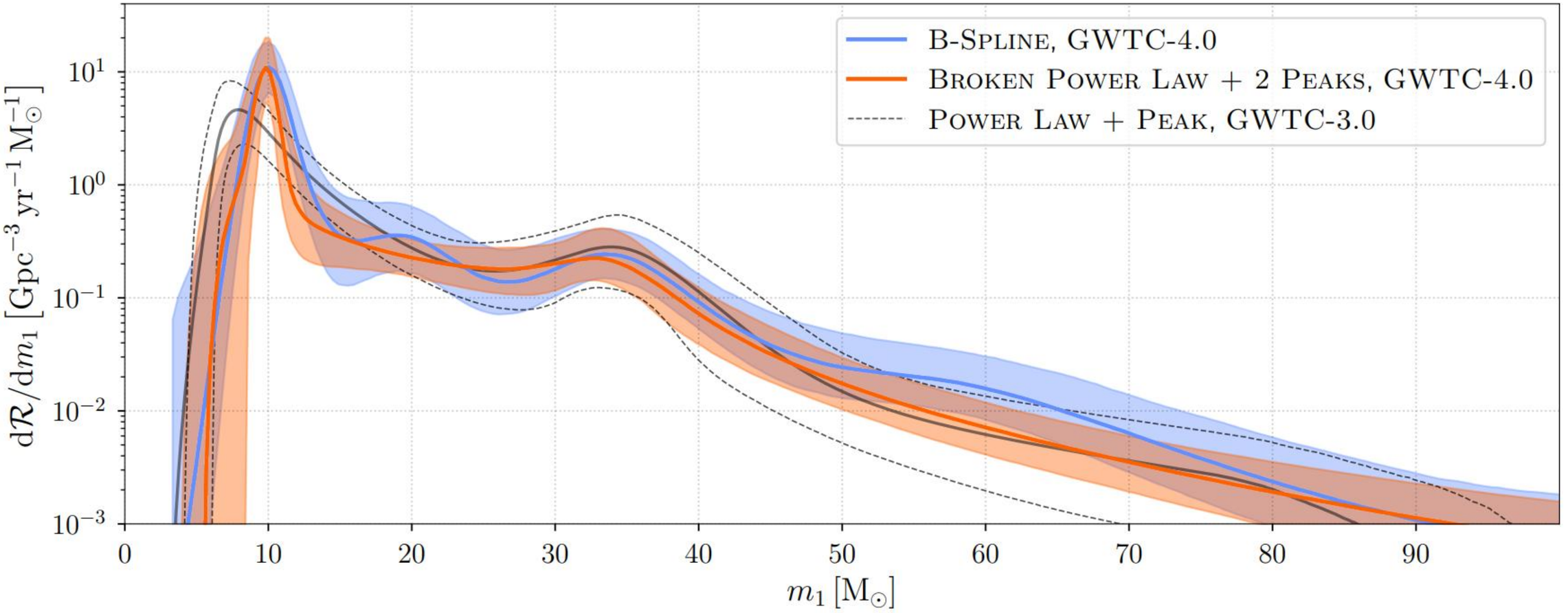

BH Mass regimes

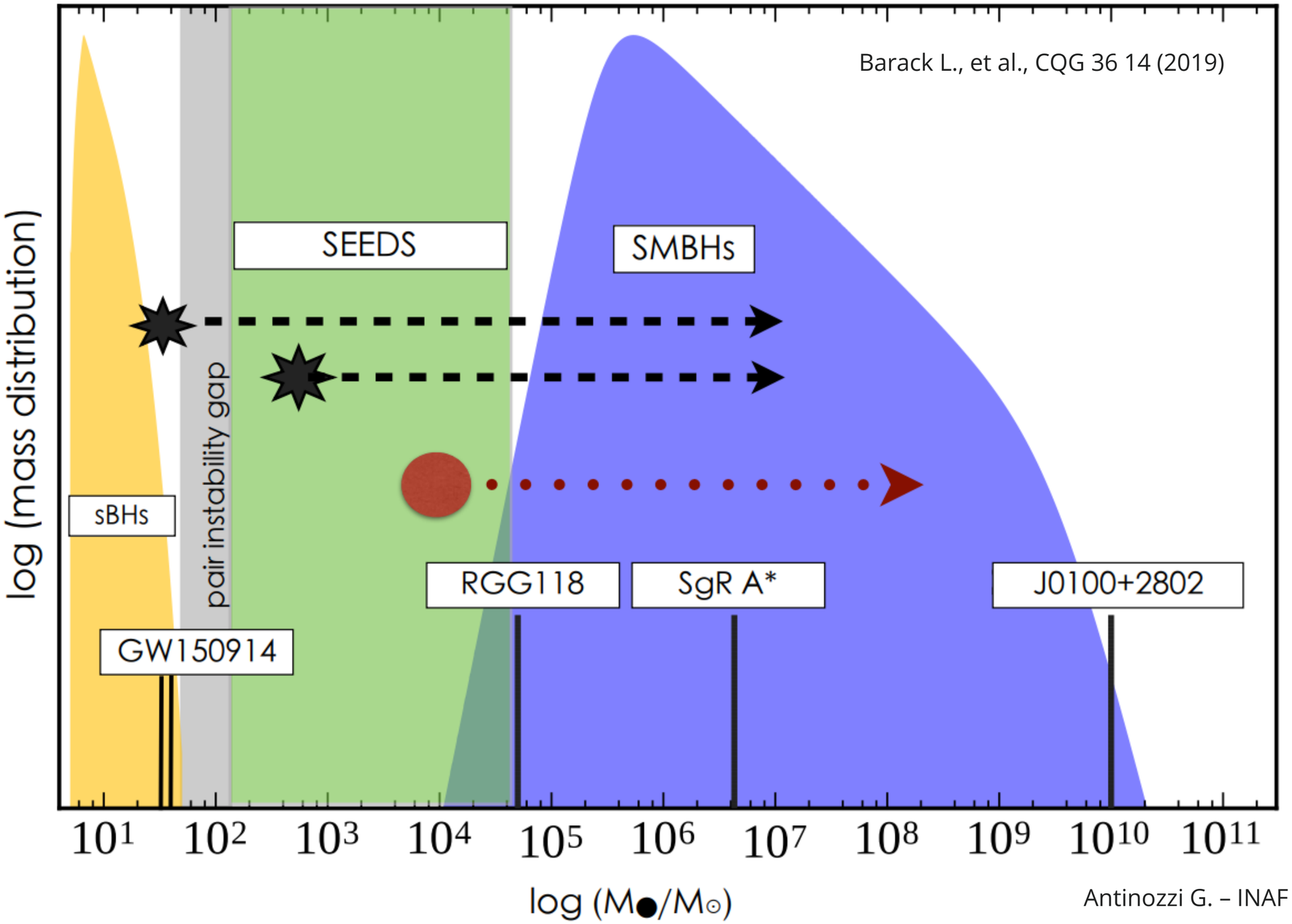

BH Mass regimes

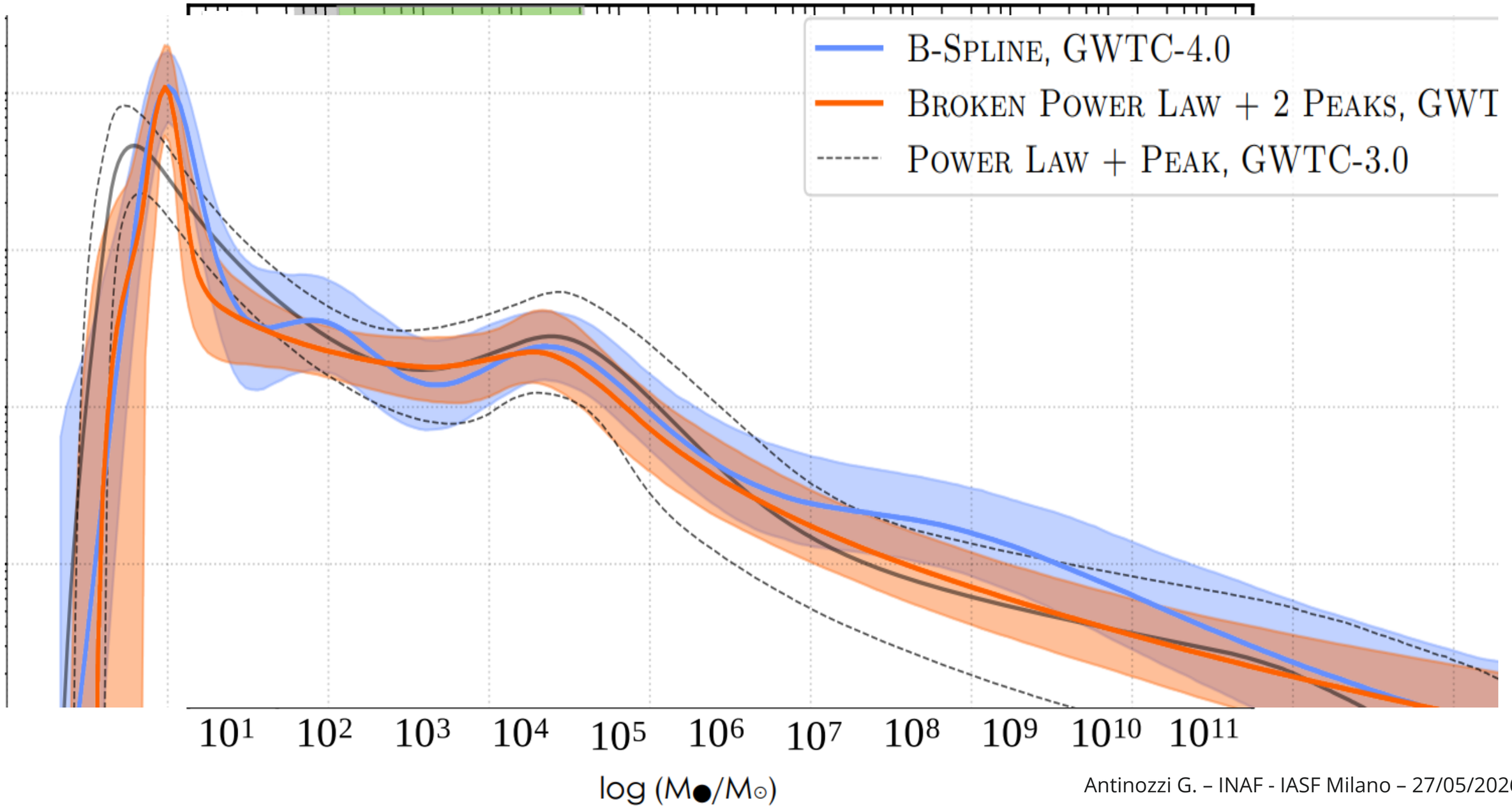

BH Mass regimes

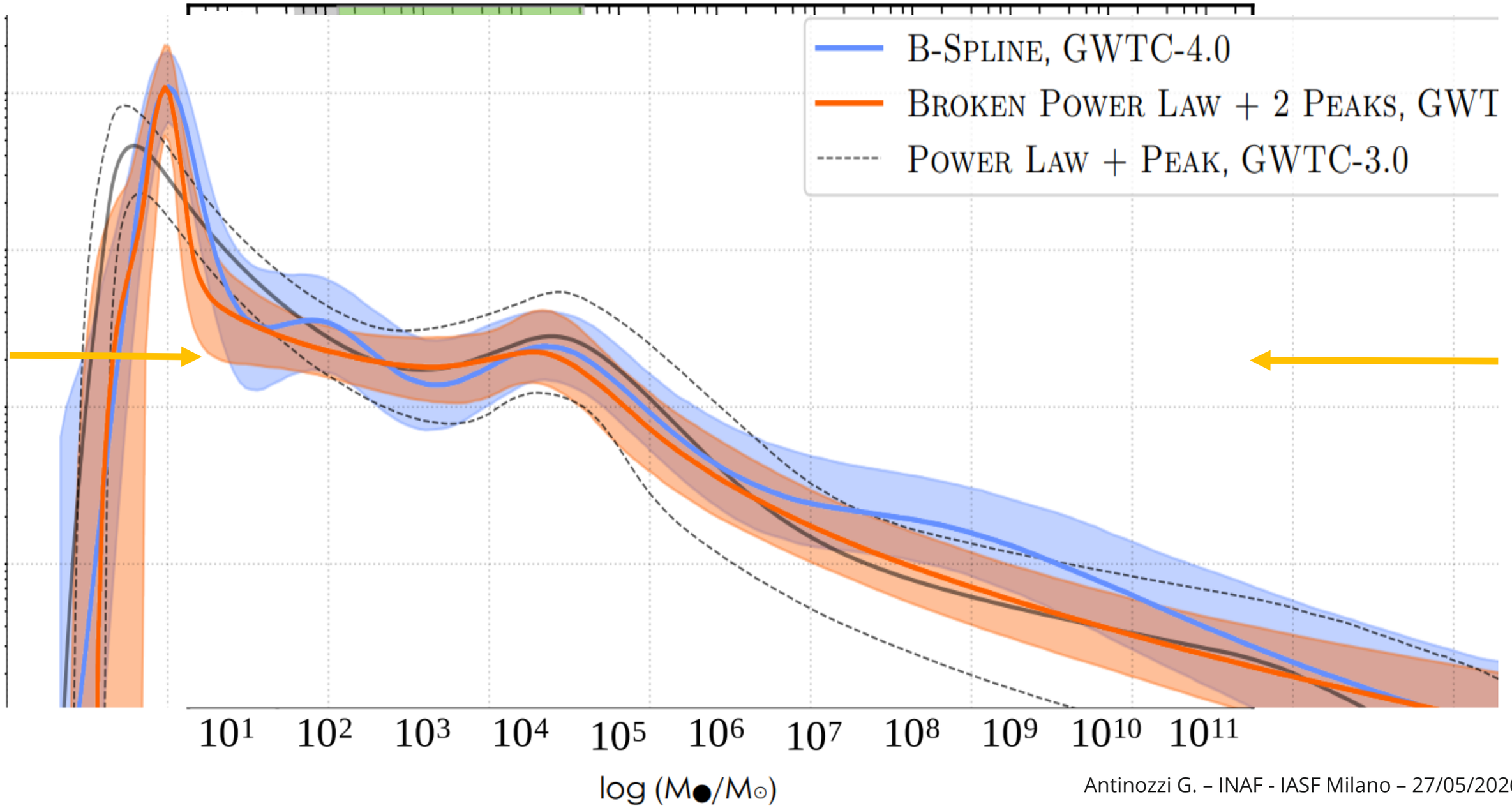

BH Mass regimes

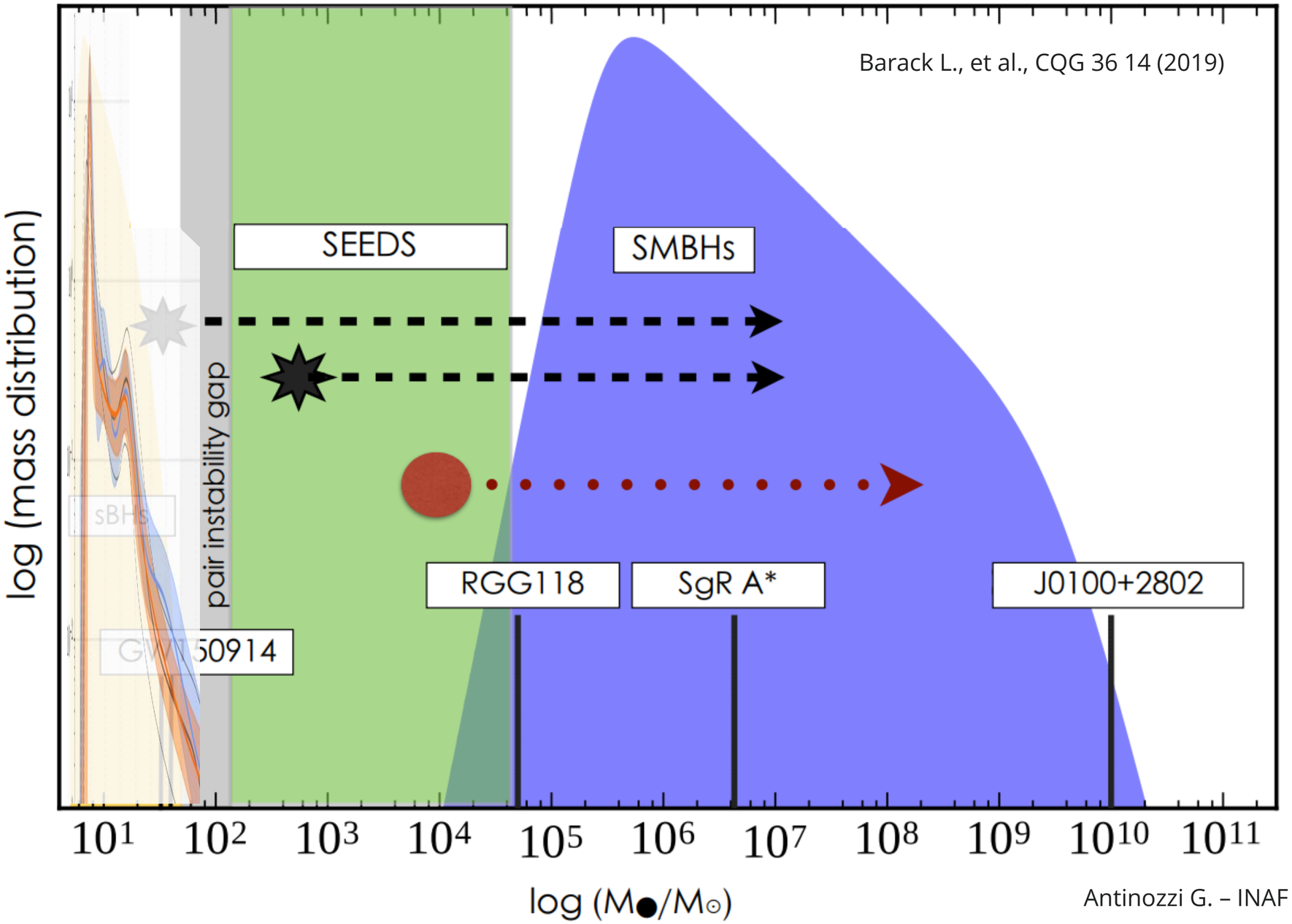

Cosmological tensions and anomalies

Tensions $(> 5\sigma)$:

a) Hubble tension H_0

b) Growth tension $S_8 = \sigma_8 \left(\frac{\Omega_m}{0.3}\right)^{0.5}$

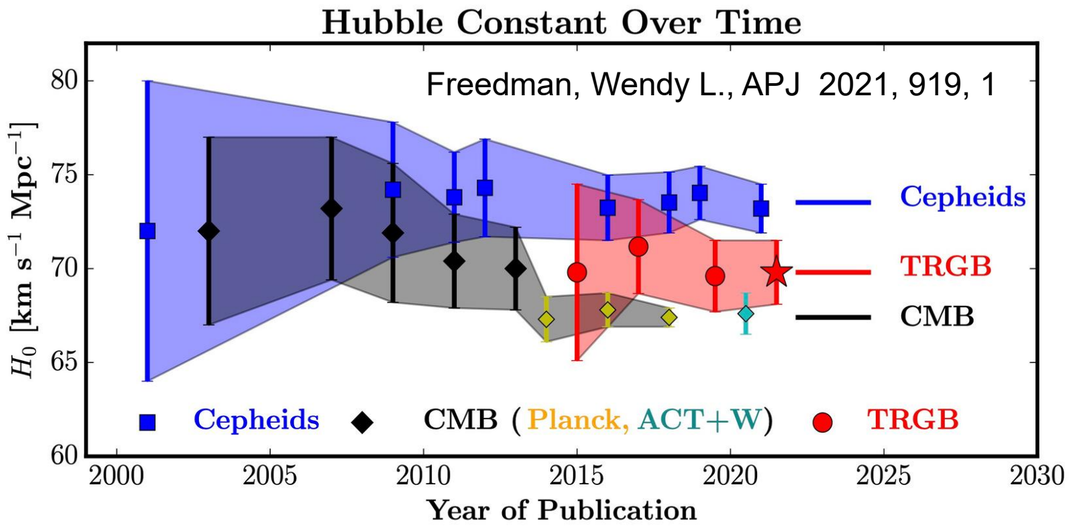

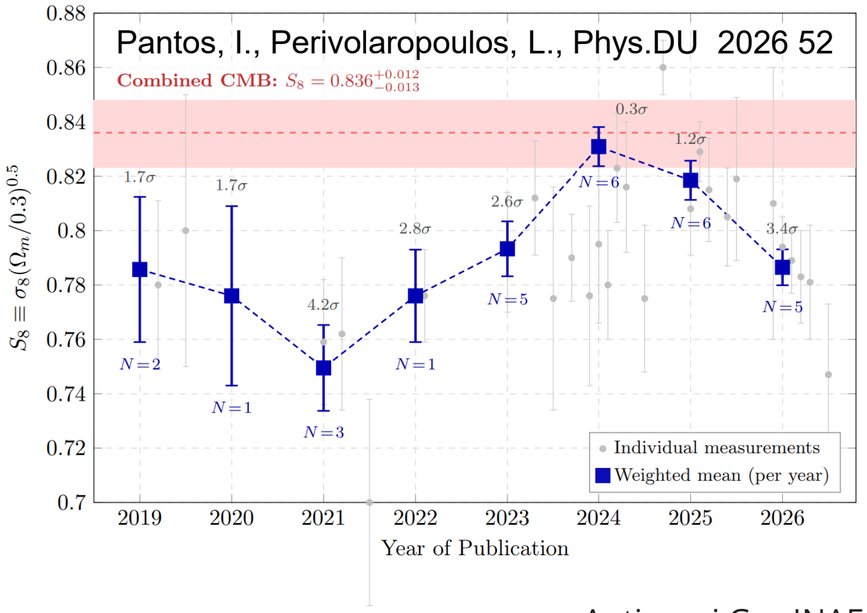

Cosmological tensions and anomalies

Tensions $(> 5\sigma)$:

a) Hubble tension H_0

b) Growth tension $S_8 = \sigma_8 \left(\frac{\Omega_m}{0.3}\right)^{0.5}$

Anomalies/Curiosities $(3 - 5\ \sigma)$:

- BBN Lithium anomaly
- Core-Cusp problem
- …

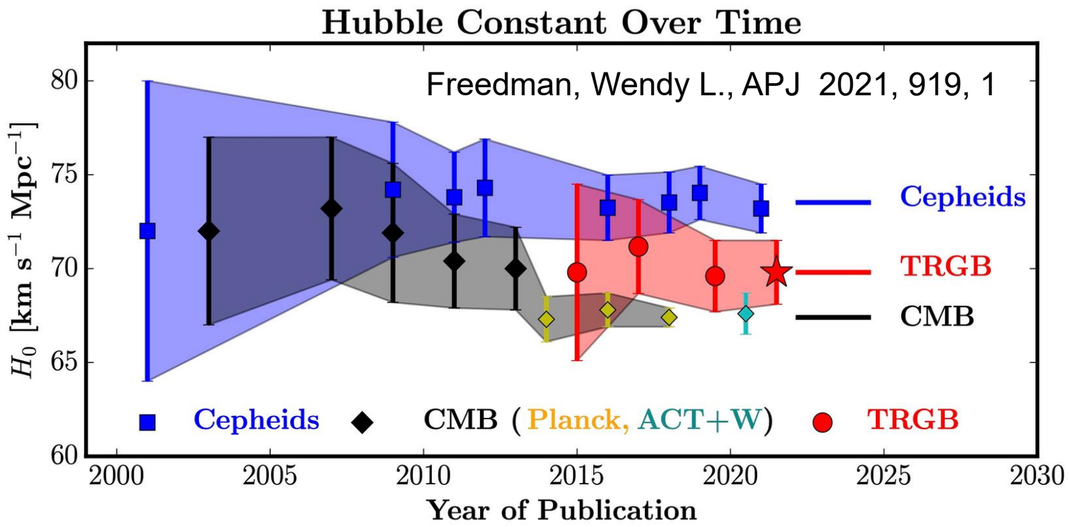

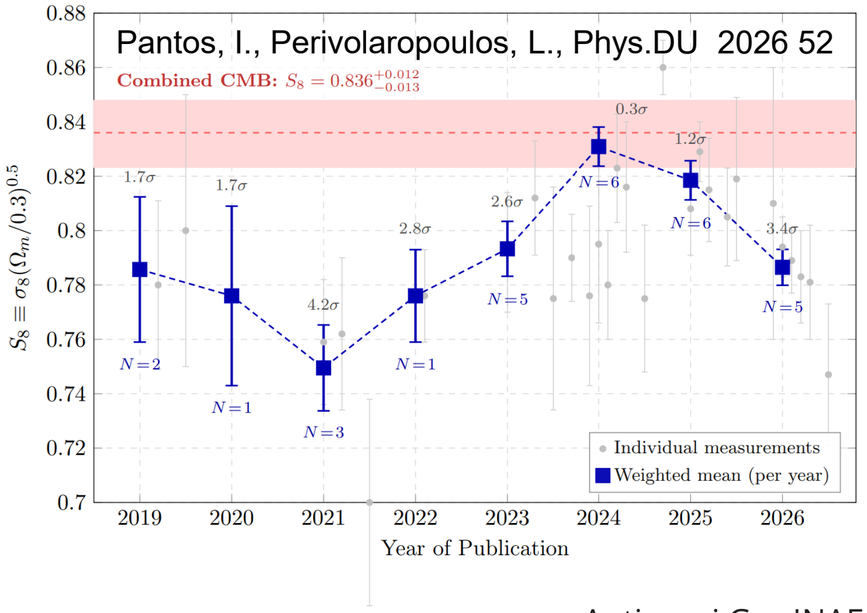

Hubble tension and standard sirens

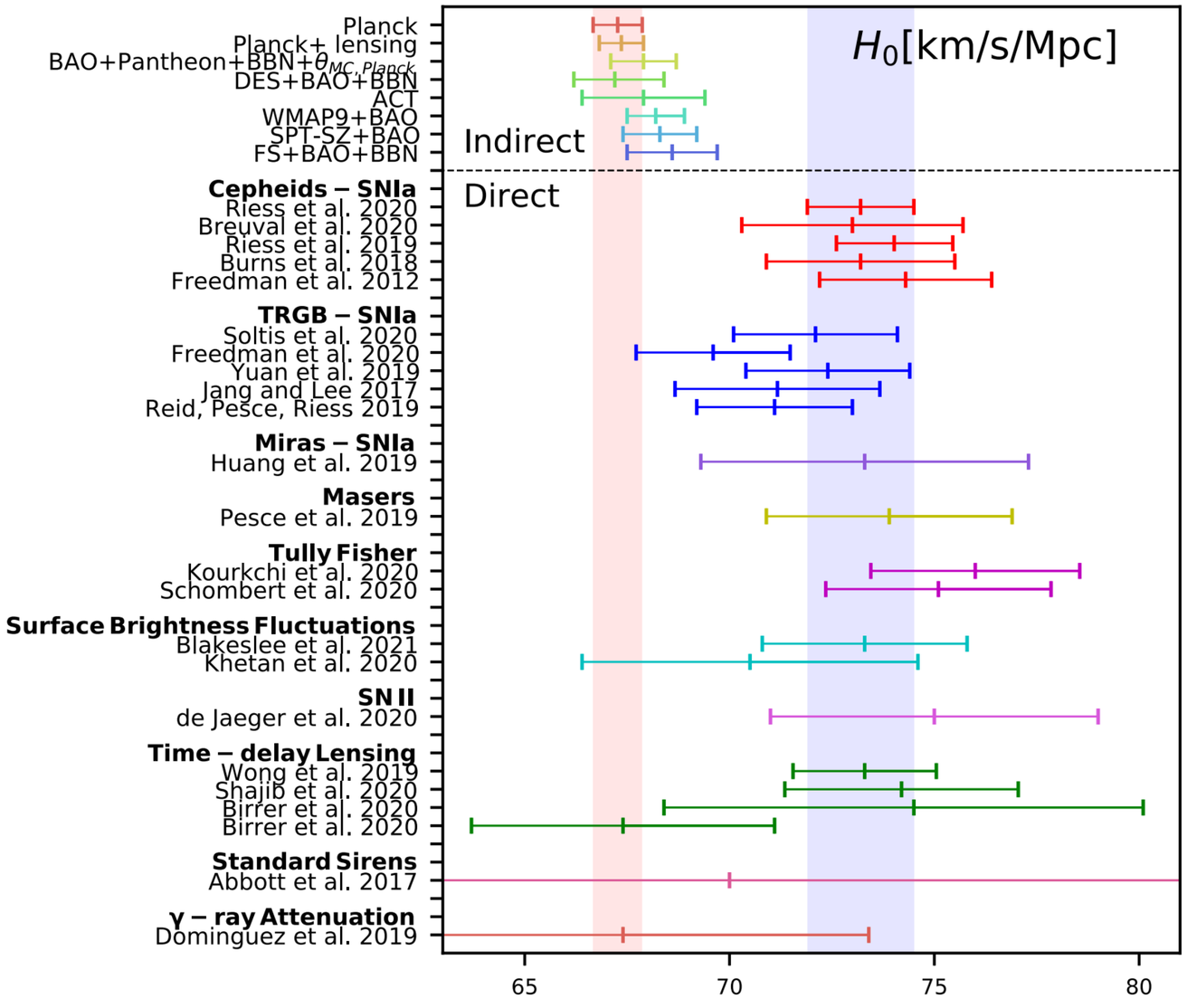

Di Valentino, E., MNRAS 2021, 502, 2

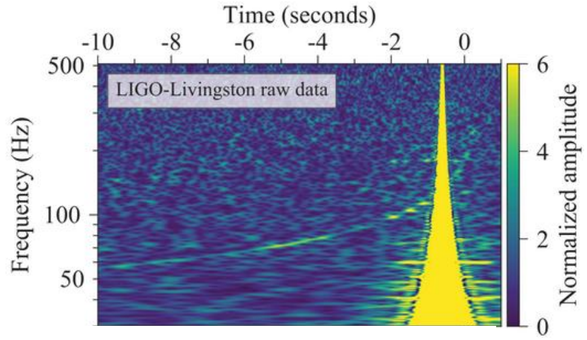

Abbott B. P., et al., LV collaboration, PhRvL 2017, 119, 16

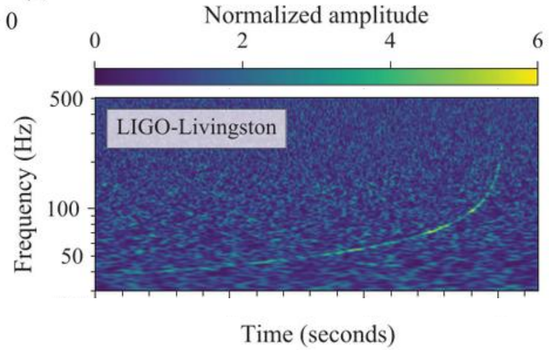

GW170817 + GRB170817A (+ Kilonova) = H_0

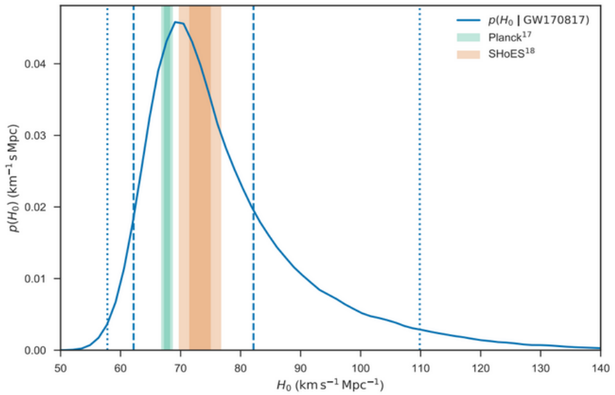

Abbott B. P. et al., LV collaboration, Nature 2017, 551, 7678

Cosmology with Standard Sirens

Binary Neutron Star (BNS)

Black Hole Neutron Star (BHNS)

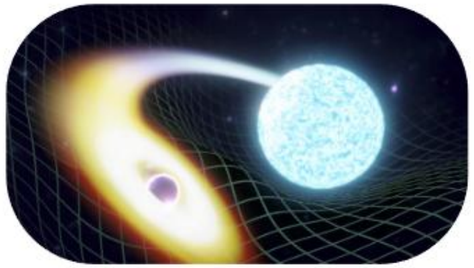

Binary Black Hole (BBH)

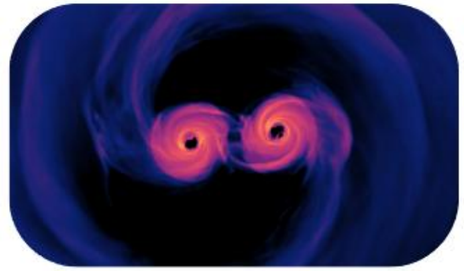

Cosmology with Standard Sirens

Binary Neutron Star (BNS)

Black Hole Neutron Star (BHNS)

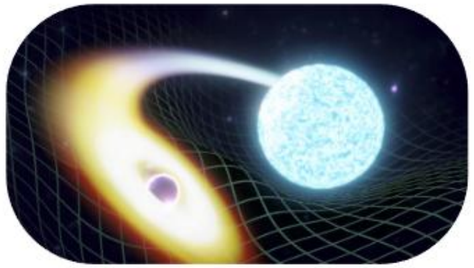

Binary Black Hole (BBH)

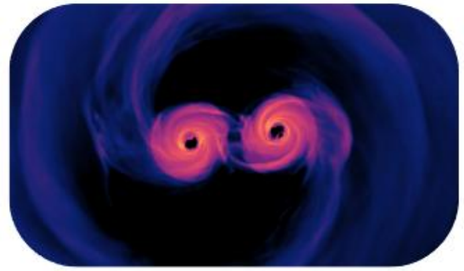

GW + Kilonova: Bright Siren

Abbott B. P. et al., LV collaboration, Nature 2017, 551, 7678

Cosmology with Standard Sirens

Binary Neutron Star (BNS)

Black Hole Neutron Star (BHNS)

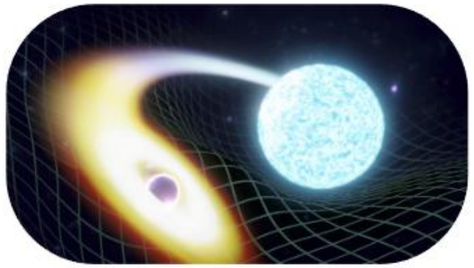

Binary Black Hole (BBH)

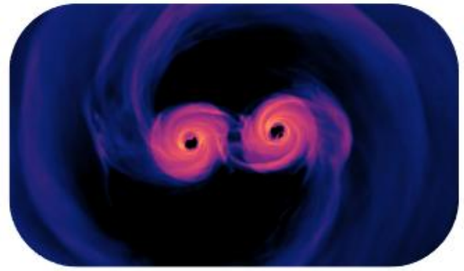

GW + Kilonova: Bright Siren

Abbott B. P. et al., LV collaboration, Nature 2017, 551, 7678

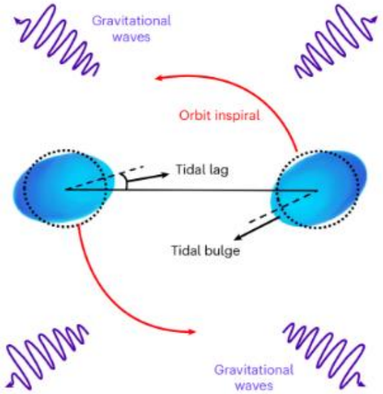

NS Tidal deformation + EoS: Love Siren

C. Messenger and J. Read, Phys. Rev. Lett. 108, 091101

Cosmology with Standard Sirens

Binary Neutron Star (BNS)

GW + Kilonova: Bright Siren

Abbott B. P. et al., LV collaboration, Nature 2017, 551, 7678

Black Hole Neutron Star (BHNS)

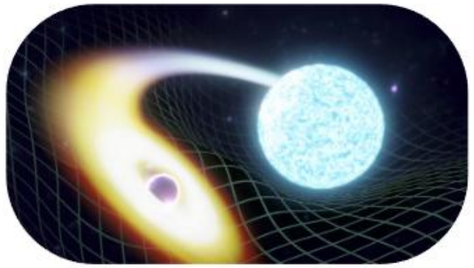

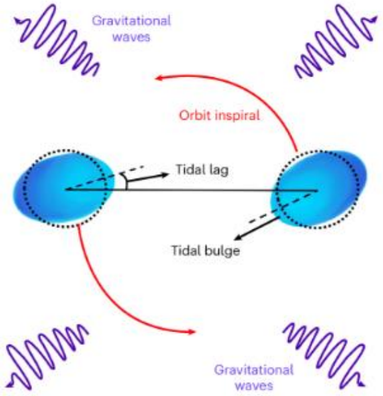

NS Tidal deformation + EoS: Love Siren

C. Messenger and J. Read, Phys. Rev. Lett. 108, 091101

Binary Black Hole (BBH)

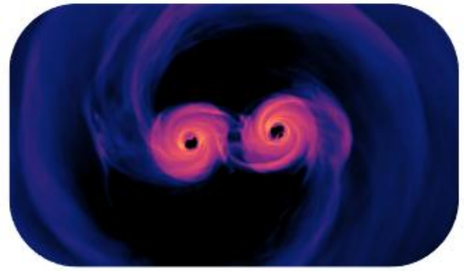

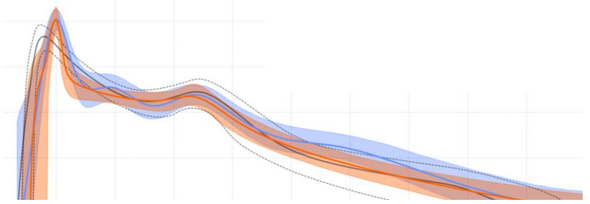

S.R. Taylor and J.R. Gair, Phys. Rev. D 86 (2012) 023502

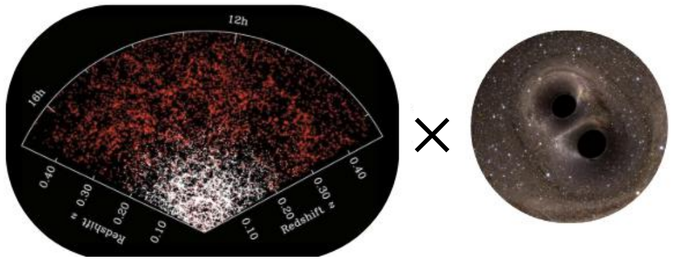

W. Del Pozzo, Phys. Rev. D 86 (2012) 043011

BH or BH+NS mass spectrum: Spectral Siren

Cross-correlation Sirens:

× Galaxies

× LSS M. Oguri, 2016, Phys Rev. D, 93, 083511

× HI U. Dupletsa, 2026, arXiv

...

Cosmology with Standard Sirens

Binary Neutron Star (BNS)

GW + Kilonova: Bright Siren

Abbott B. P. et al., LV collaboration, Nature 2017, 551, 7678

Black Hole Neutron Star (BHNS)

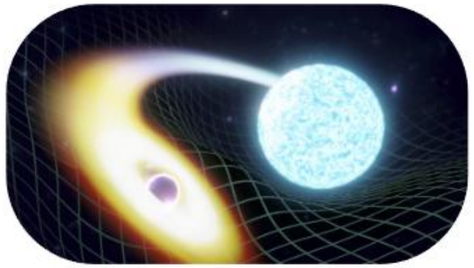

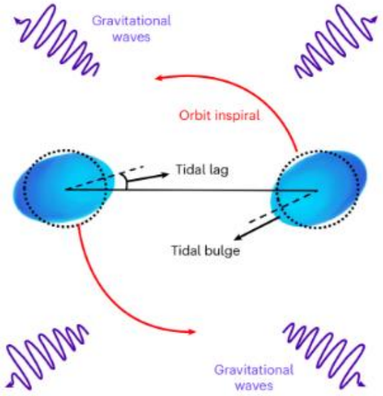

NS Tidal deformation + EoS: Love Siren

C. Messenger and J. Read, Phys. Rev. Lett. 108, 091101

Binary Black Hole (BBH)

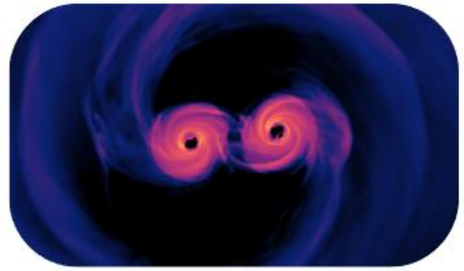

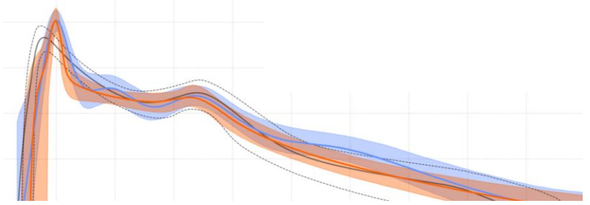

S.R. Taylor and J.R. Gair, Phys. Rev. D 86 (2012) 023502

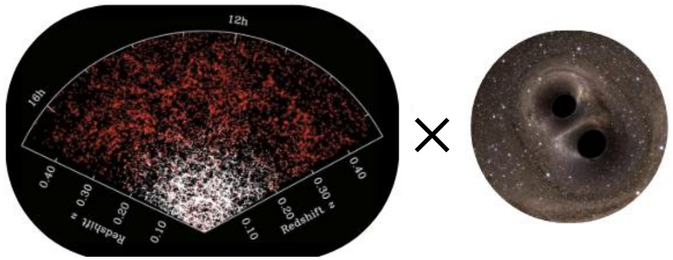

W. Del Pozzo, Phys. Rev. D 86 (2012) 043011

BH or BH+NS mass spectrum: Spectral Siren

Cross-correlation Sirens:

× Galaxies

× LSS M. Oguri, 2016, Phys Rev. D, 93, 083511

× HI U. Dupletsa, 2026, arXiv

...

Spectral Sirens

$$h_{+,\times}(t) \propto \frac{\mathcal{M}_{\mathrm{d}}}{d_{\mathrm{L}}(\mathrm{z}|H_0, \Omega_0)}$$

$$\mathcal{M}_{\mathrm{d}} = \mathcal{M}_{\mathrm{S}}(1 + \mathrm{z})$$

Spectral Sirens

$$h_{+,\times}(t) \propto \frac{\mathcal{M}_{\mathrm{d}}}{d_{\mathrm{L}}(\mathrm{z}|H_0, \Omega_0)}$$

$$\mathcal{M}_{\mathrm{d}} = \mathcal{M}_{\mathrm{S}}(1 + \mathrm{z})$$

Assumption: Source-frame mass spectrum does not evolve with redshift

$\Rightarrow$

A standard “ruler” to extract redshift information indirectly

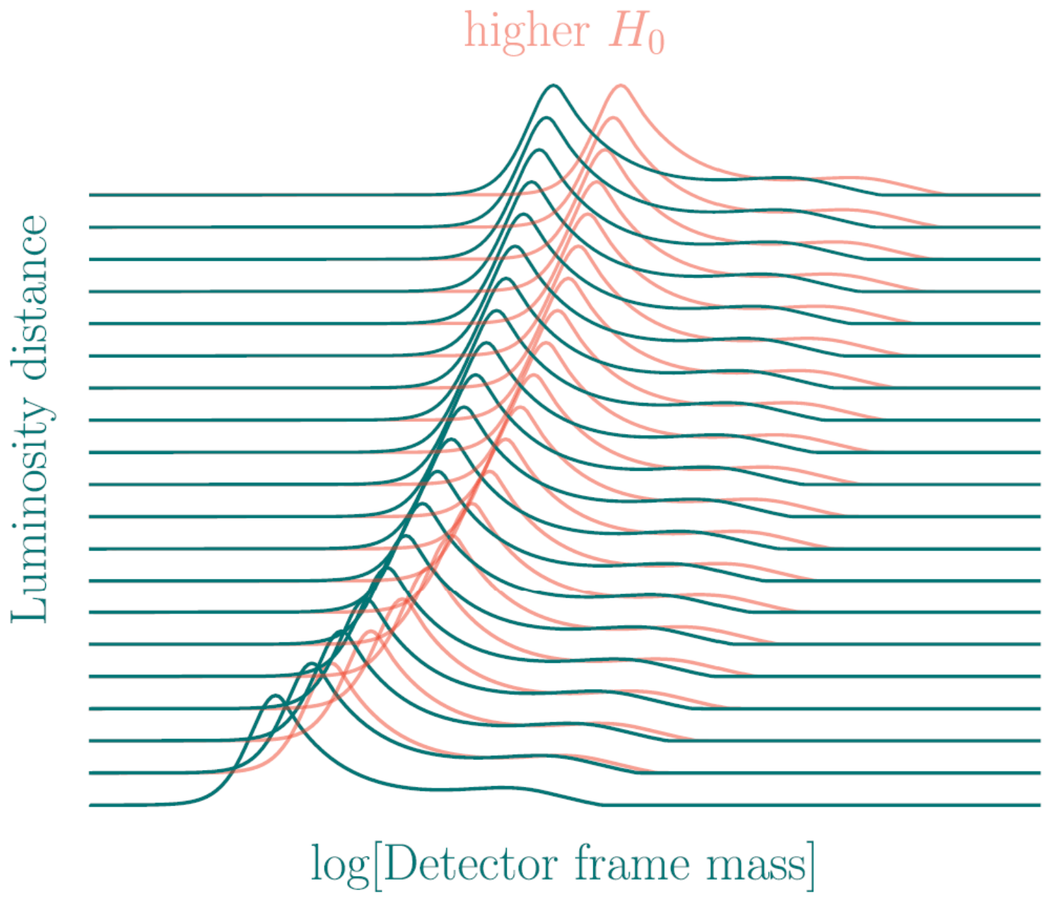

Chen, H-Y., Ezquiaga, J.M., Gupta I., CQG 2024 41 12

Spectral Sirens

$$h_{+,\times}(t) \propto \frac{\mathcal{M}_{\mathrm{d}}}{d_{\mathrm{L}}(\mathrm{z}|H_0, \Omega_0)}$$

$$\mathcal{M}_{\mathrm{d}} = \mathcal{M}_{\mathrm{S}}(1+\mathrm{z})$$

Assumption: Source-frame mass spectrum does not evolve with redshift

$\Rightarrow$

A standard “ruler” to extract redshift information indirectly

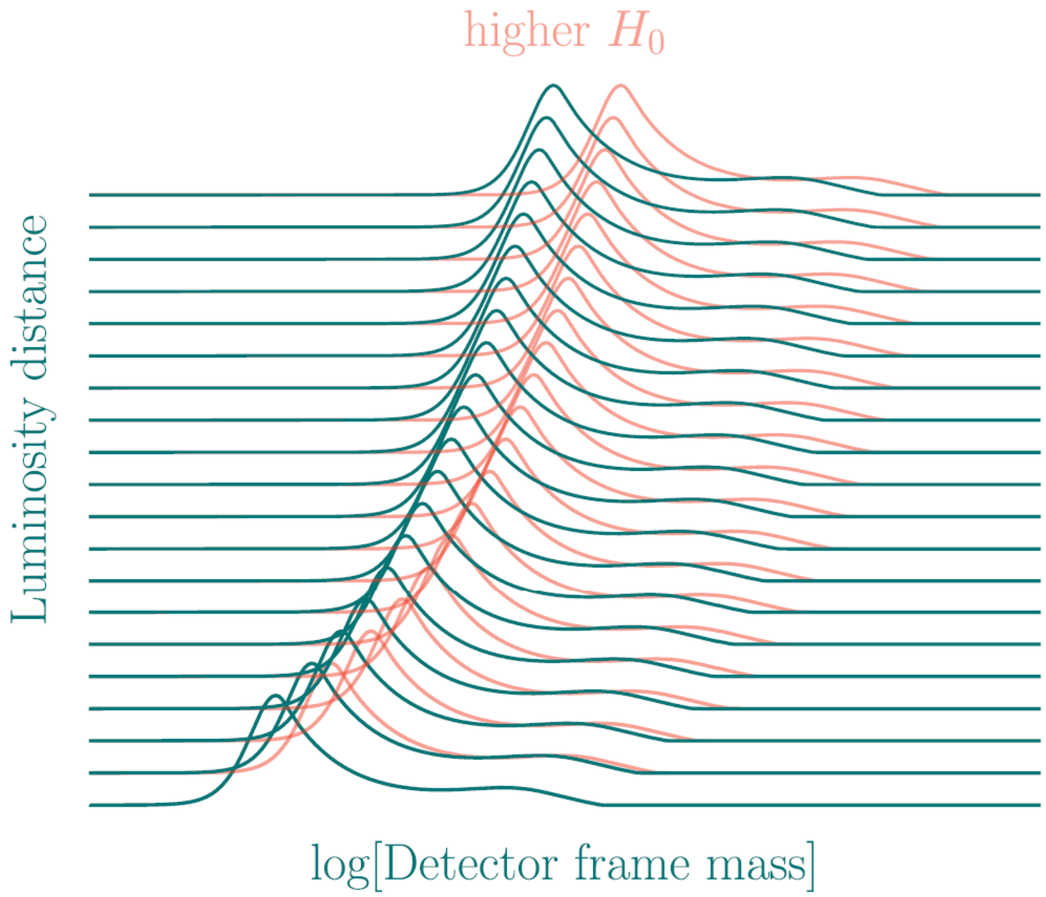

Chen, H-Y., Ezquiaga, J.M., Gupta I., CQG 2024 41 12

Recent work from Agapito A., De Renzis V., Mancarella M. arXiv 2026 suggest a weak redshift evolution (**systematic effect**) within the current redshift reach.

XG Forecasts

1

Motivations:

a) Test hints of redshift dependence
b) Progenitor-Remnant relation across the history of the Universe
c) New Physics?

XG Forecasts

Motivations:

a) Test hints of redshift dependence
b) Progenitor-Remnant relation across the history of the Universe
c) New Physics?

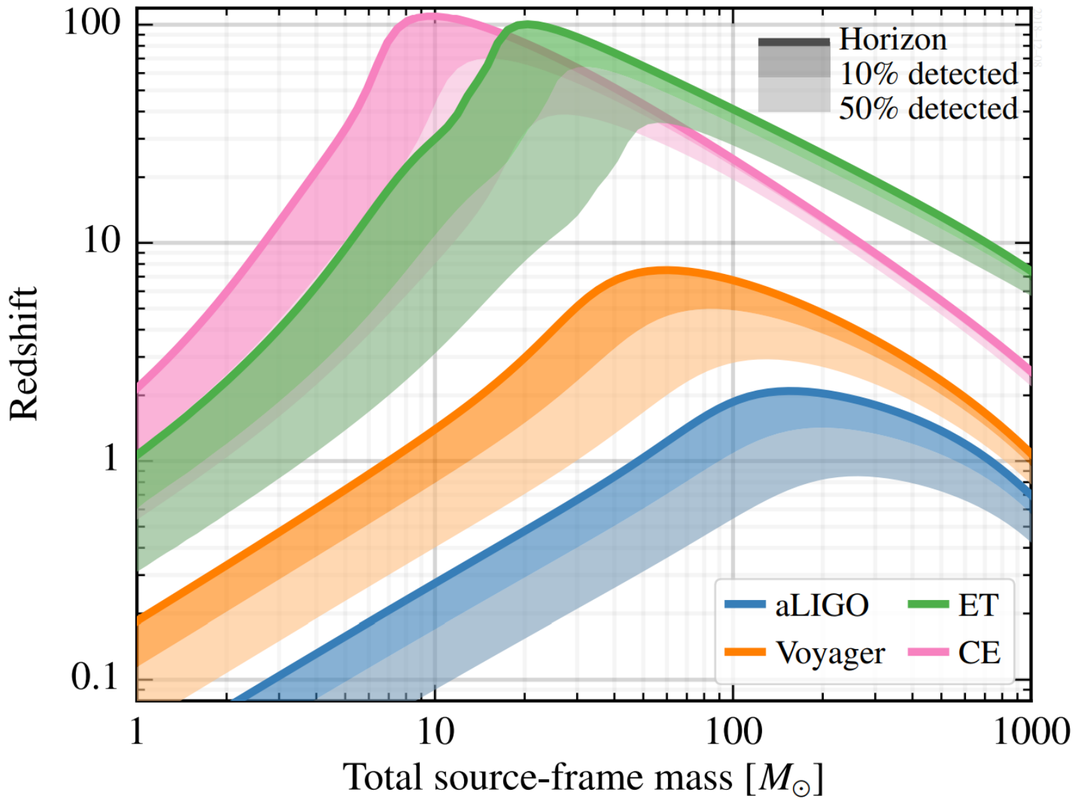

Hall Evan D., Evans M., Classical and Quantum Gravity 2019, 36, 22

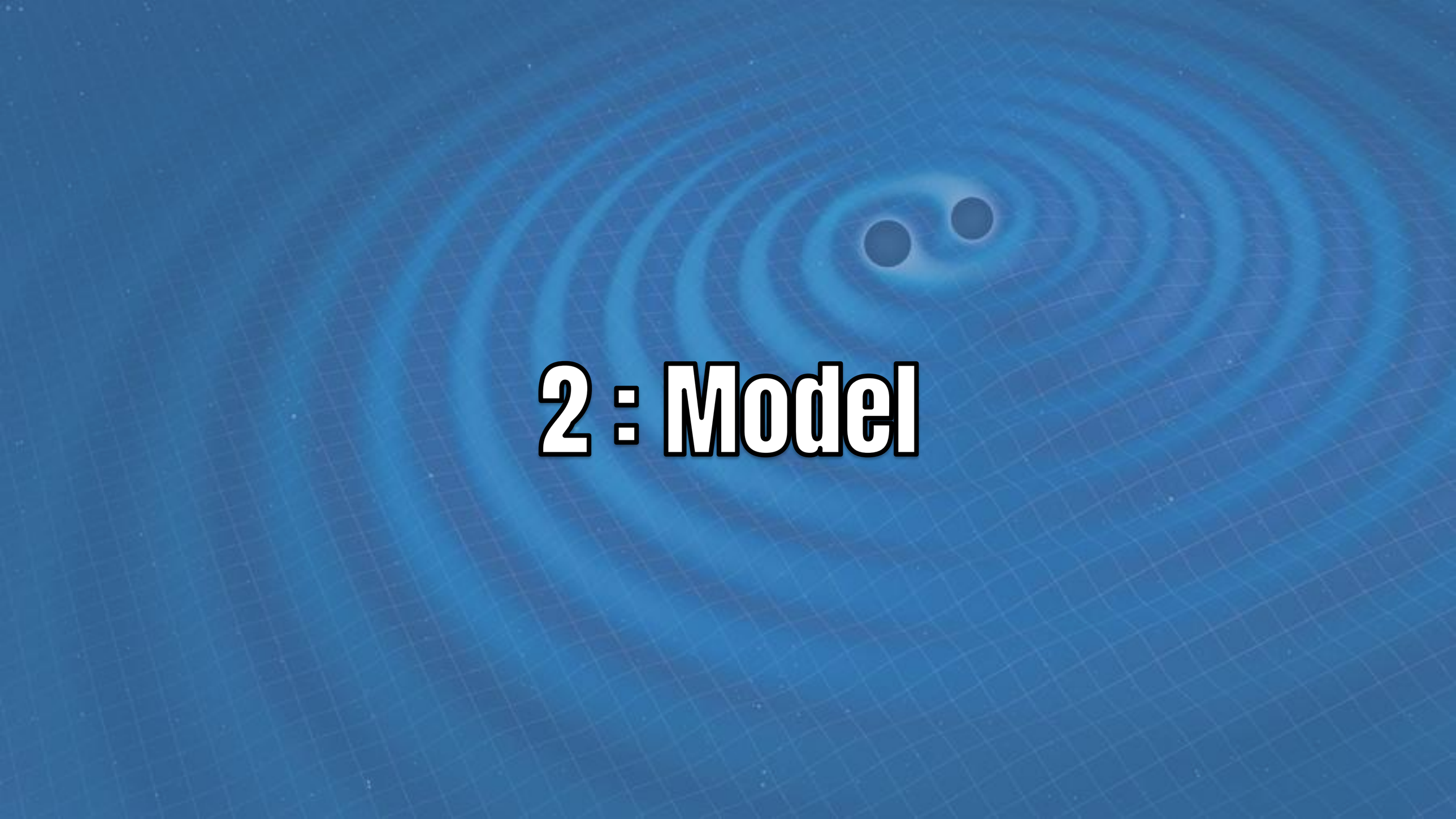
2 : Model

Theoretical model

Binary Black Hole Merger Rate Density : $\frac{d\dot{N}}{dV}(z)$

2

Theoretical model

Binary Black Hole Merger Rate Density : $\frac{d\dot{N}}{dV}(z) :=$ Convolution of Cosmic Star Formation Rate Density and Merger Distribution

2

Theoretical model

Binary Black Hole Merger Rate Density : $\frac{d\dot{N}}{dV}(z) :=$ Convolution of Cosmic Star Formation Rate Density and Merger Distribution

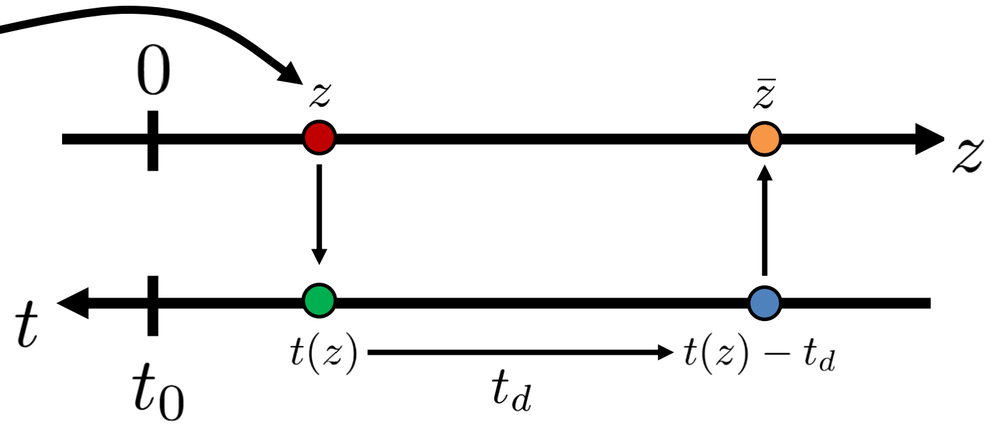

2

Theoretical model

Binary Black Hole Merger Rate Density : $\frac{d\dot{N}}{dV}(z) :=$ Convolution of Cosmic Star Formation Rate Density and Merger Distribution

Data driven Star Formation Rate Density per unit metallicity

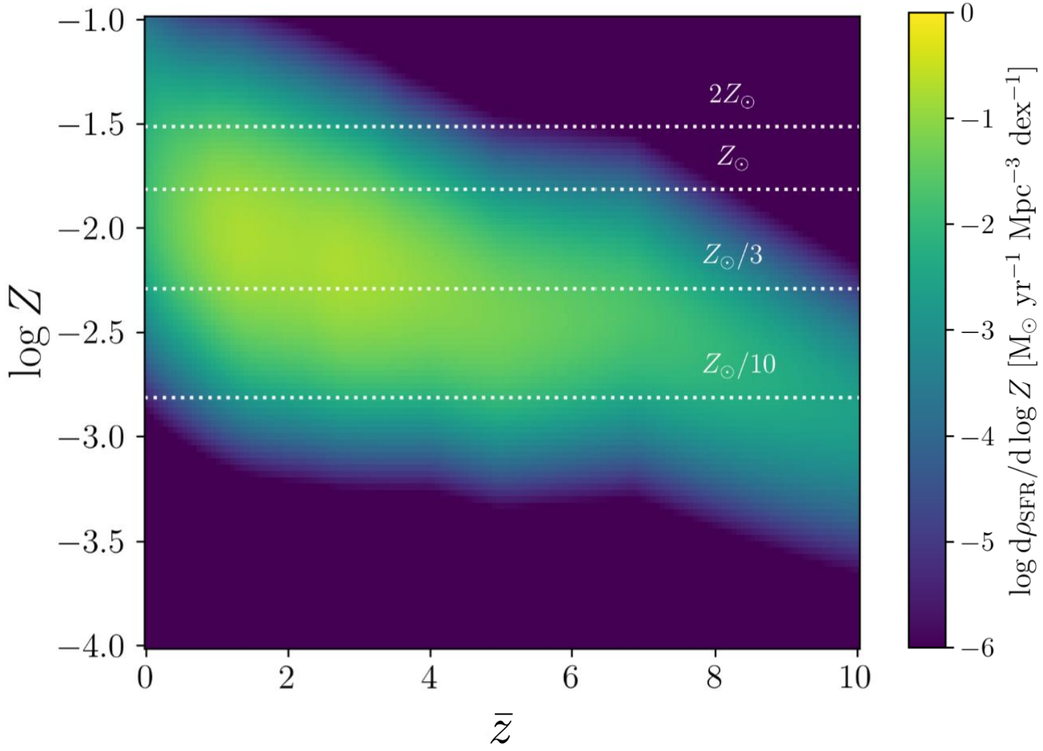

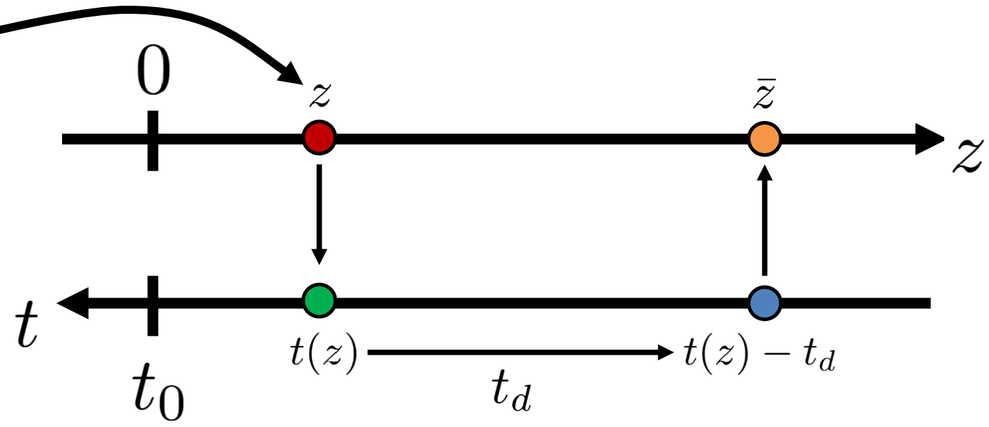

2

Theoretical model

Binary Black Hole Merger Rate Density : $\frac{d\dot{N}}{dV}(z) :=$ Convolution of Cosmic Star Formation Rate Density and Merger Distribution

Data driven Star Formation Rate Density per unit metallicity

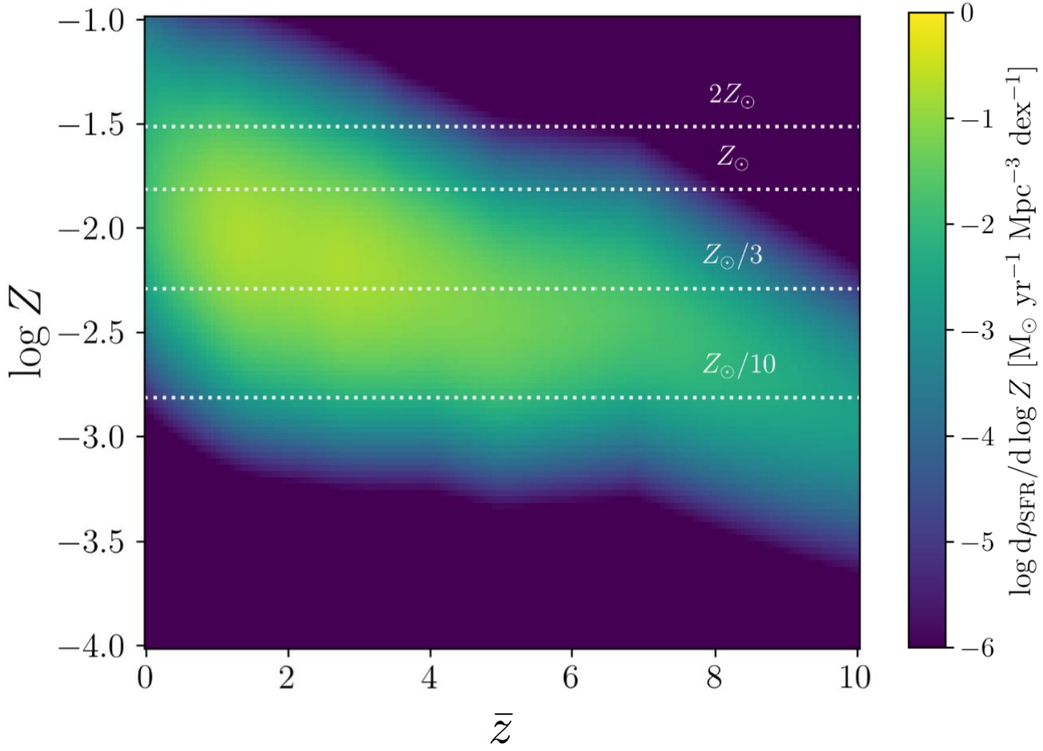

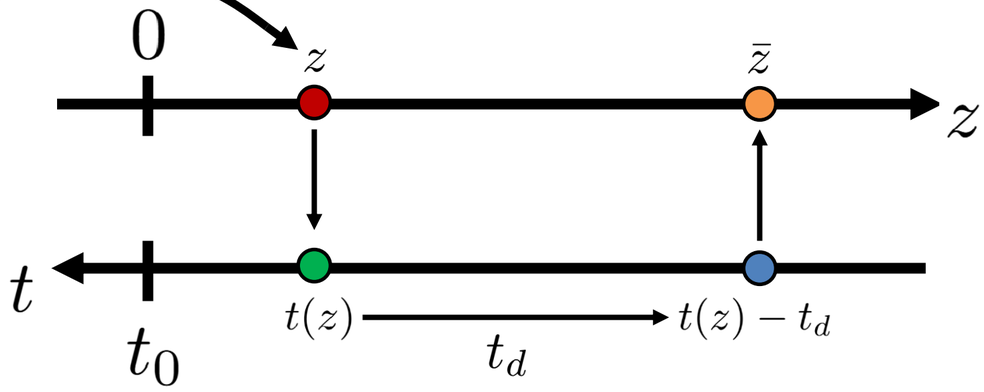

Population synthesis of isolated binaries

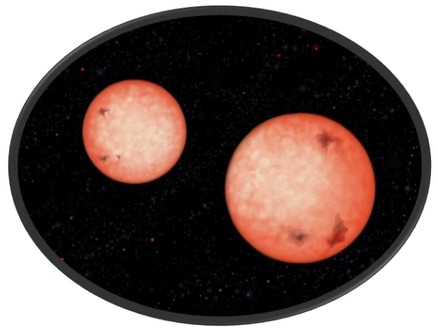

2

Theoretical model

Binary Black Hole Merger Rate Density : $\frac{d\dot{N}}{dV}(z) :=$ Convolution of Cosmic Star Formation Rate Density and Merger Distribution

Data driven Star Formation Rate Density per unit metallicity

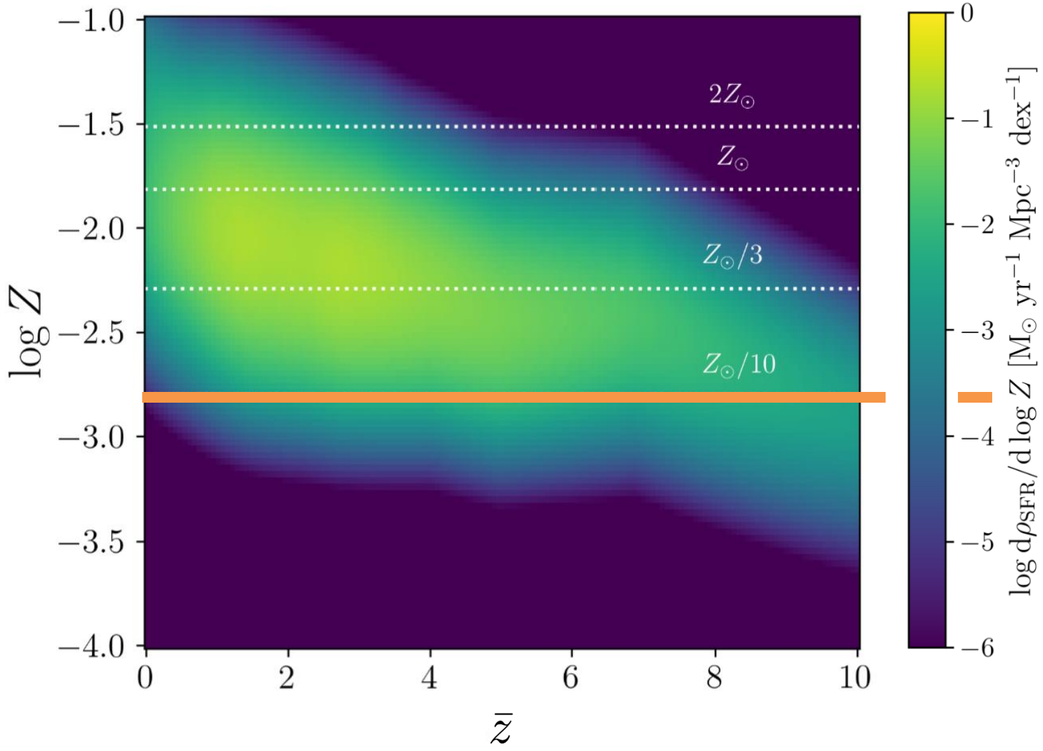

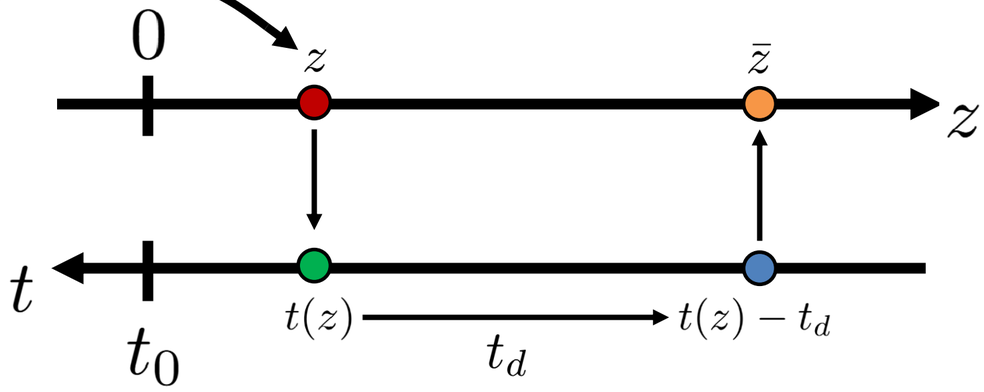

$$\int dt_d \left[\ \right] \times \frac{dp}{d\log t_d}$$

Population synthesis of isolated binaries

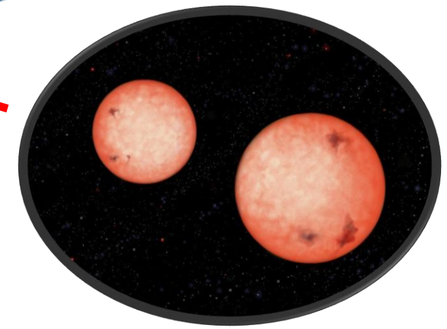

Model details

1. **SFRD computed with empirical relations from latest galaxy survey data** (more flexible than cosmological simulations and consistent with recent JWST data)

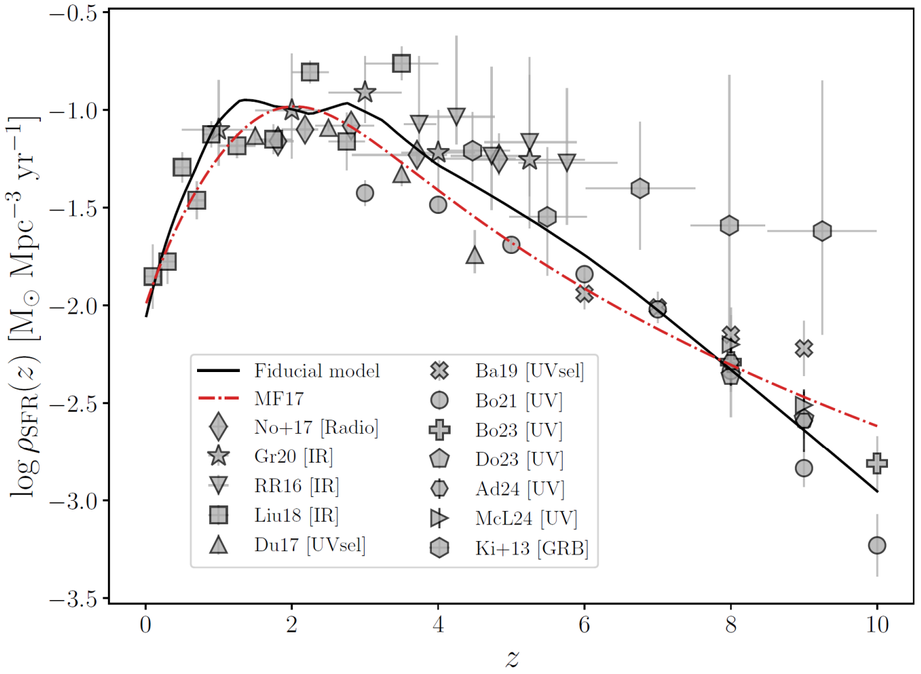

2

Model details

1. **SFRD computed with empirical relations from latest galaxy survey data** (more flexible than cosmological simulations and consistent with recent JWST data)
2. **Refined time delay distributions using simulations** (used SEVN but other pop synth codes can be used)

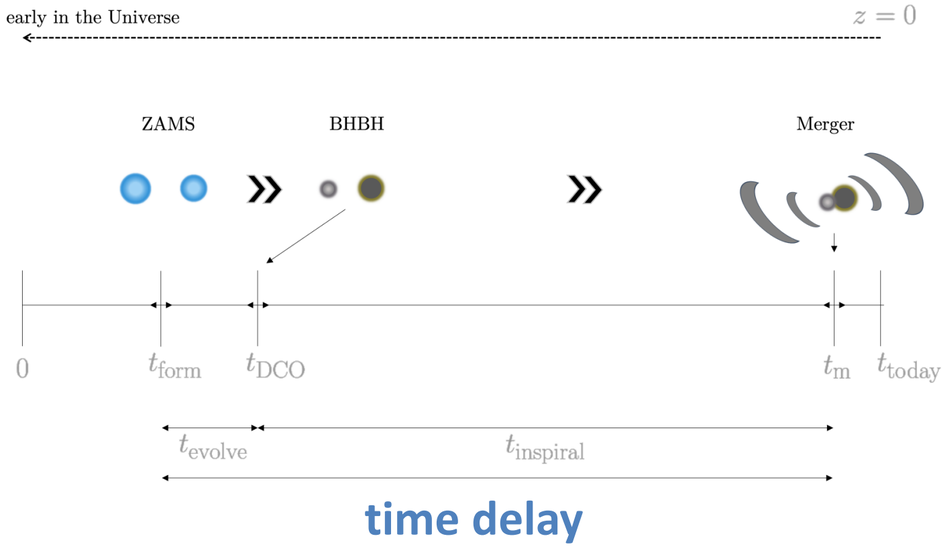

2

Model details

1. **SFRD computed with empirical relations from latest galaxy survey data** (more flexible than cosmological simulations and consistent with recent JWST data)
2. **Refined time delay distributions using simulations** (used SEVN but other pop synth codes can be used)
   An Example of construction:

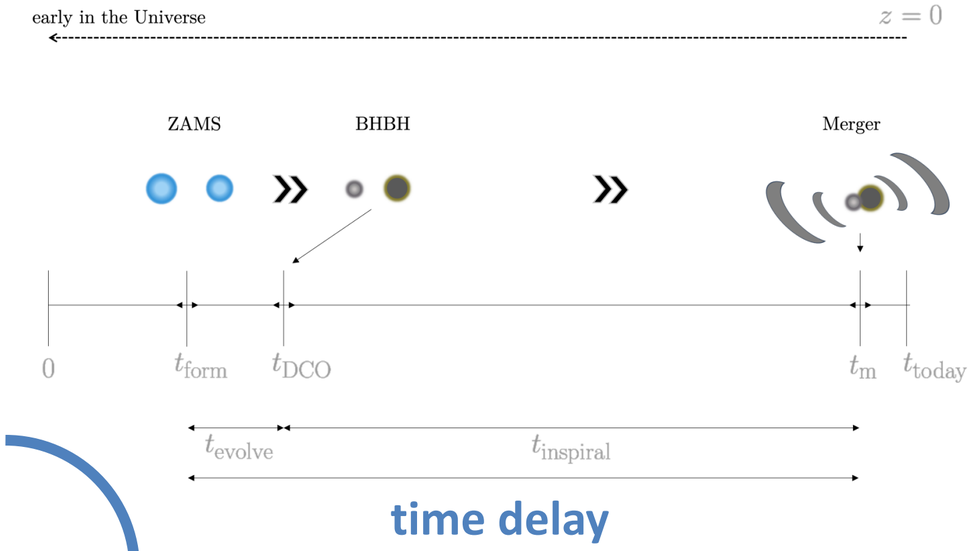

time delay

$$\int d\log\mathcal{M}$$

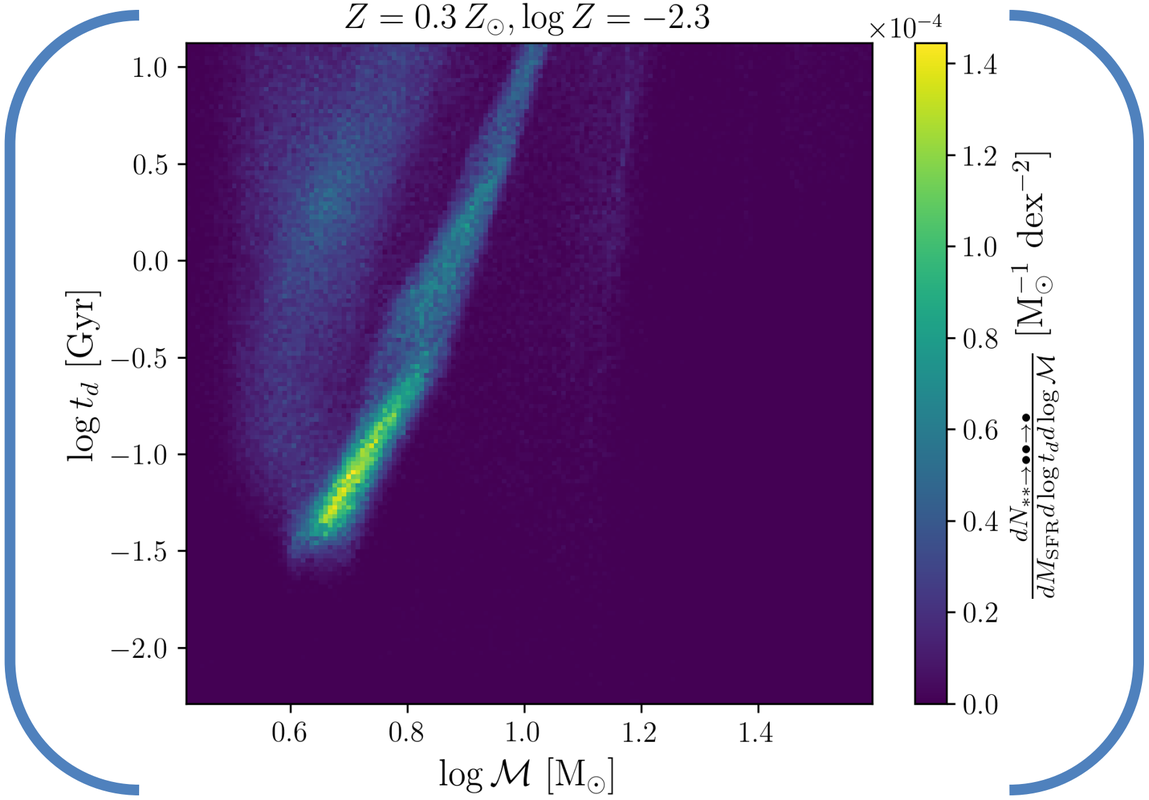

$$= \eta(Z)\frac{dp}{d\log t_d}$$

Merger efficiency: Number of merging BBH within a Hubble time per unit star mass formed

Model details

1. **SFRD computed with empirical relations from latest galaxy survey data** (more flexible than cosmological simulations and consistent with recent JWST data)
2. **Refined time delay distributions using simulations** (used SEVN but other pop synth codes can be used)
   An Example of construction:

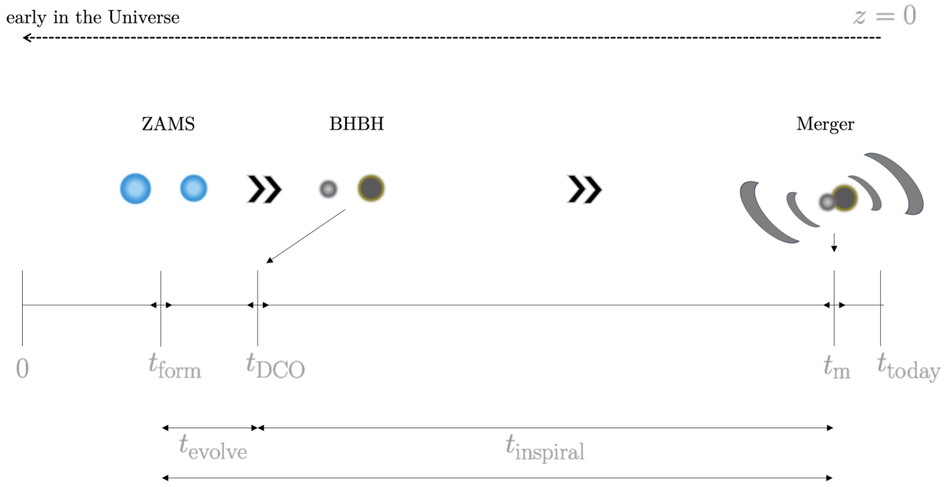

time delay

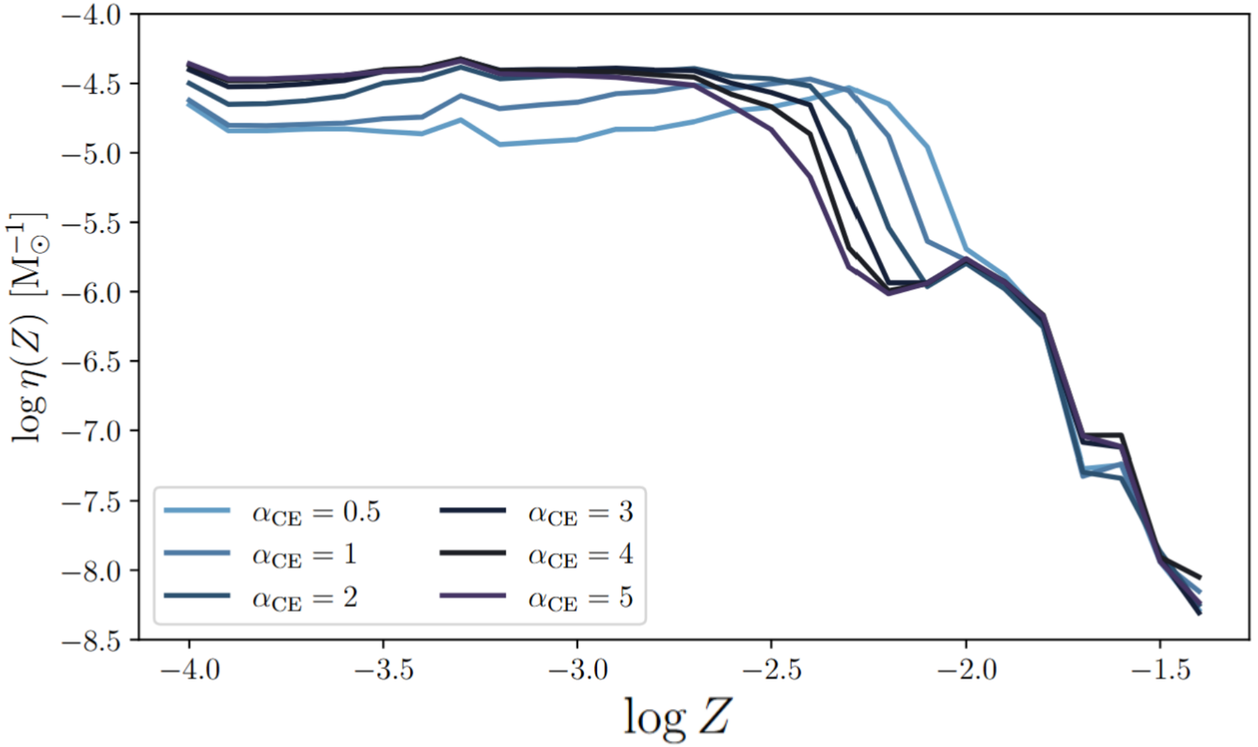

$$\eta(Z)\frac{dp}{d\log t_d}$$

Merger efficiency: varies with **metallicity** (e.g. **winds**) and with **common envelope** phase energy **efficiency** (**CE hardening**), **formation channel** (**IB, YC, GC, NC**)

2

Model details

1. **SFRD computed with empirical relations from latest galaxy survey data** (more flexible than cosmological simulations and consistent with recent JWST data)
2. **Refined time delay distributions using simulations** (used SEVN but other pop synth codes can be used)
   An Example of construction:

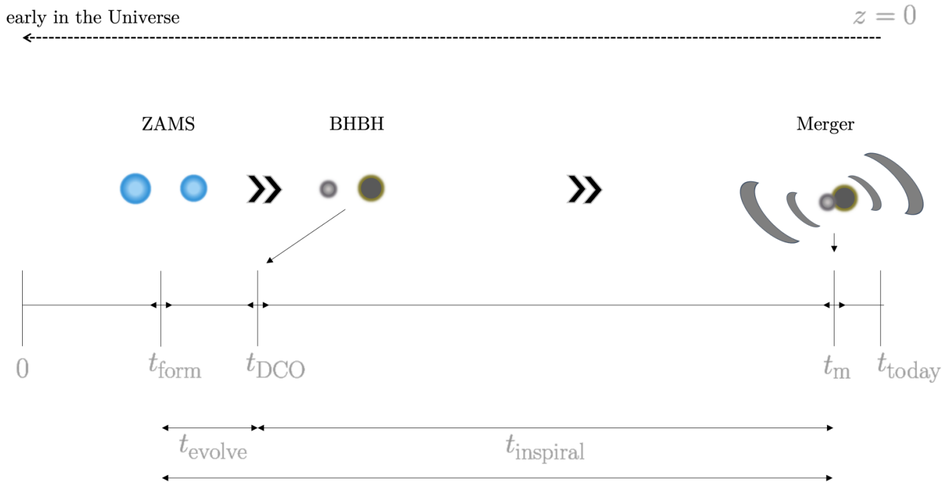

time delay

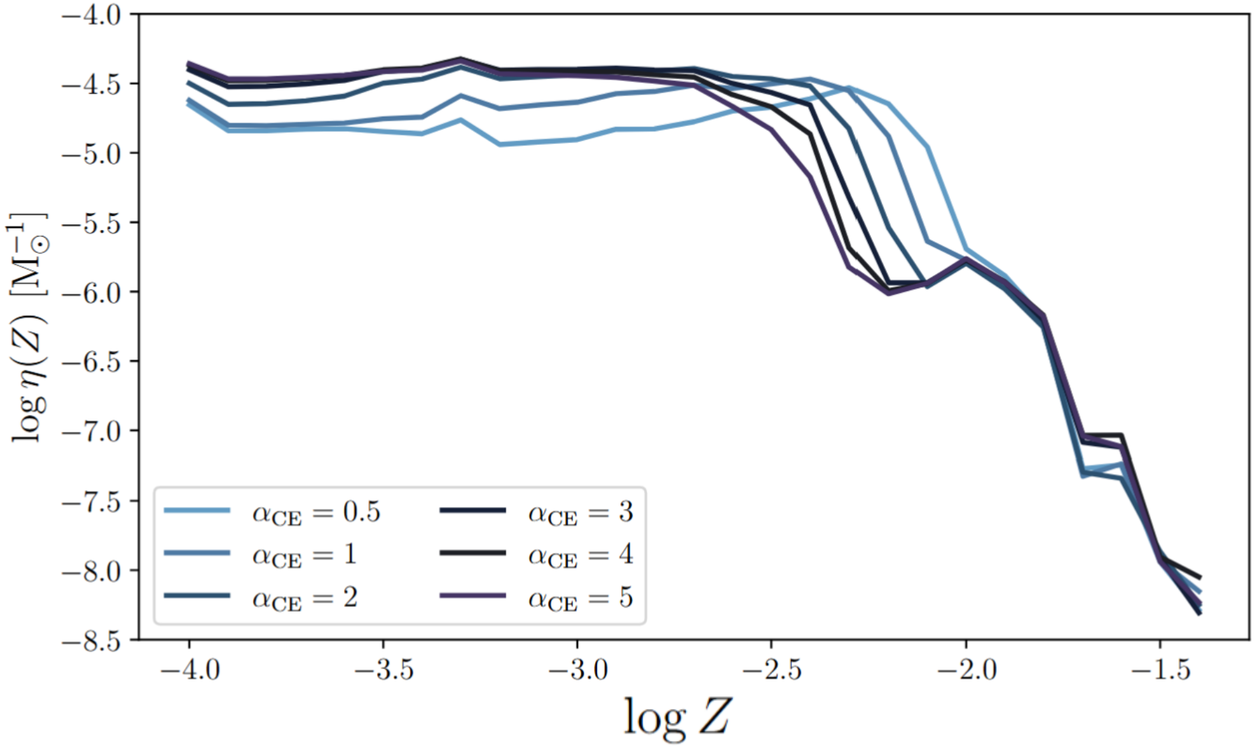

$$\eta(Z)\frac{dp}{d\log t_d}$$

Merger efficiency: varies with **metallicity** (e.g. **winds**) and with **common envelope** phase energy **efficiency** (**CE hardening**), **formation channel** (**IB, YC, GC, NC**)

Caveat: only isolated channel

Model details

1. **SFRD computed with empirical relations from latest galaxy survey data** (more flexible than cosmological simulations and consistent with recent JWST data)
2. **Refined time delay distributions using simulations** (used SEVN but other pop synth codes can be used)
3. **High speed population model computation with JAX** (necessary for population inference)

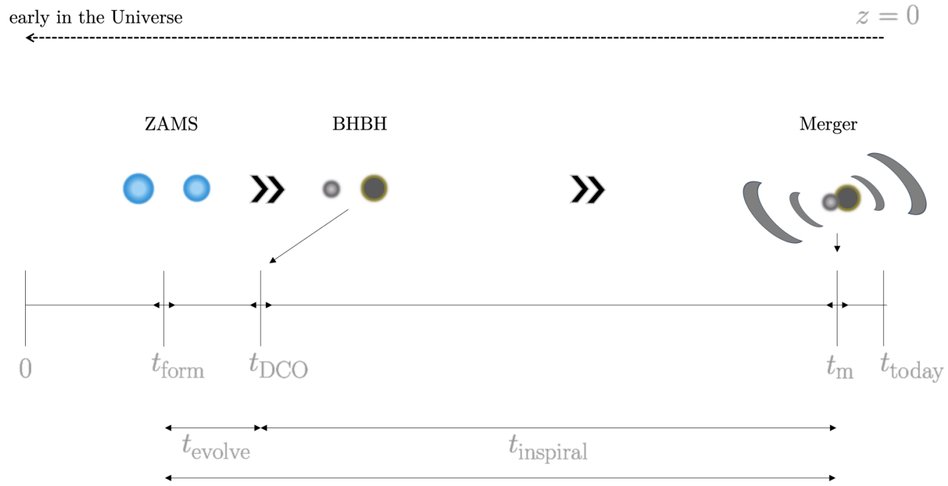

time delay

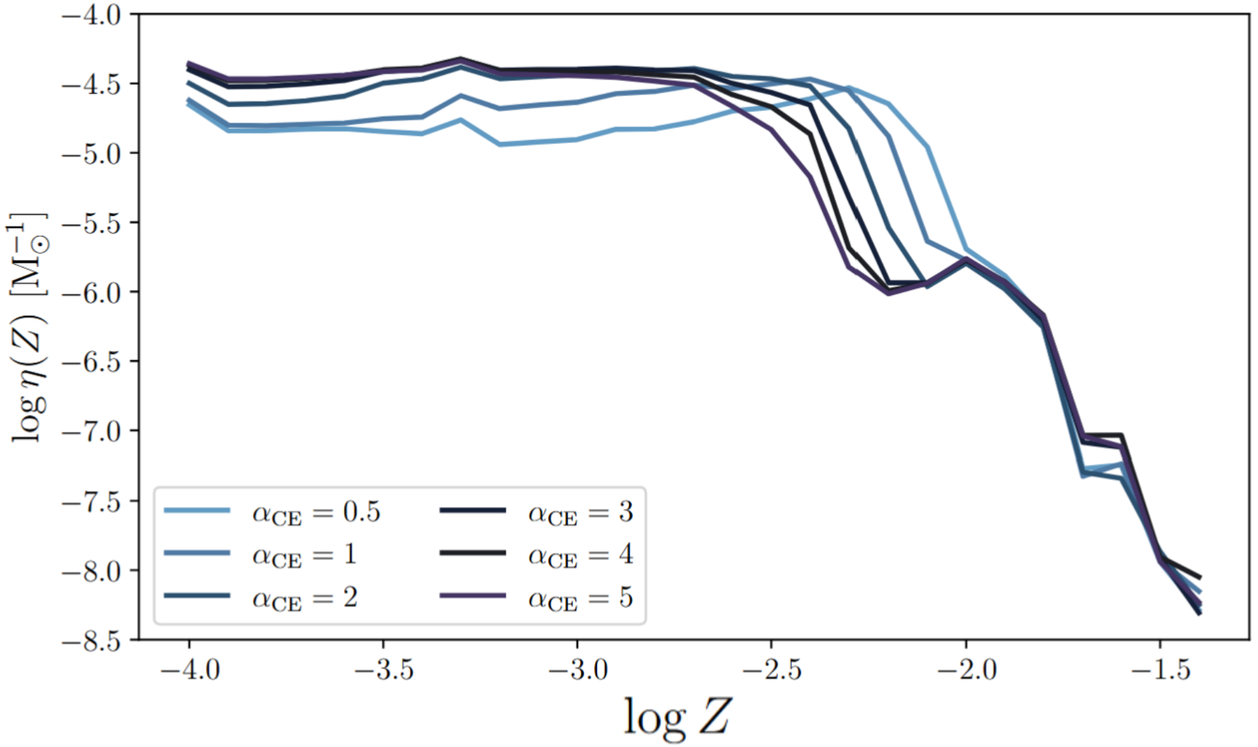

$$\eta(Z)\frac{dp}{d\log t_d}$$

Merger efficiency: varies with **metallicity** (e.g. **winds**) and with **common envelope** phase energy **efficiency** (**CE hardening**), **formation channel** (**IB, YC, GC, NC**)

Caveat: only isolated channel

2

Astro-cosmo parameters

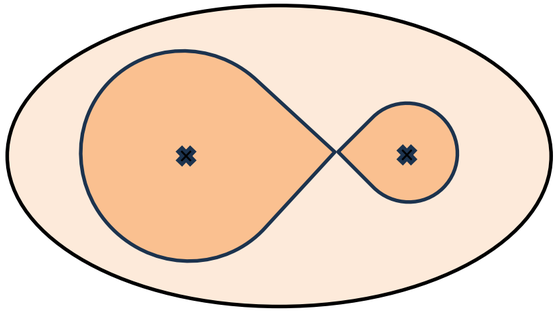

$$E_{\mathrm{bind,i}} = \alpha_{\mathrm{CE}} \, \Delta E_{\mathrm{orb}}$$

2

Astro-cosmo parameters

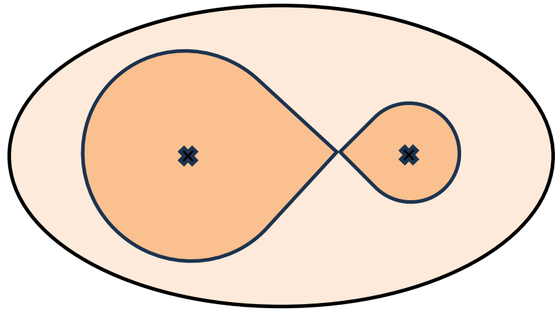

$$E_{\mathrm{bind,i}} = \alpha_{\mathrm{CE}}\,\Delta E_{\mathrm{orb}}$$

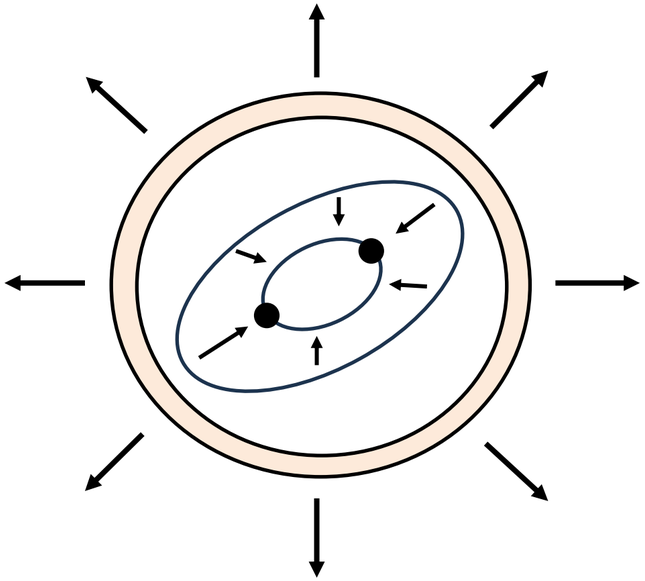

2

Astro-cosmo parameters

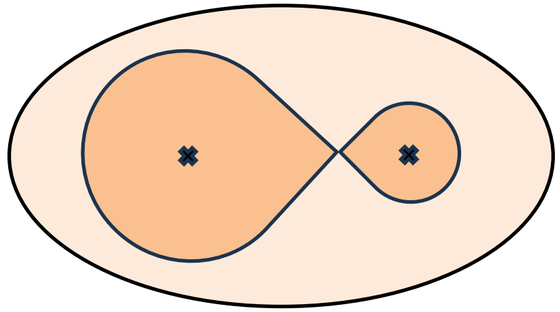

$$E_{\mathrm{bind,i}} = \alpha_{\mathrm{CE}}\,\Delta E_{\mathrm{orb}}$$

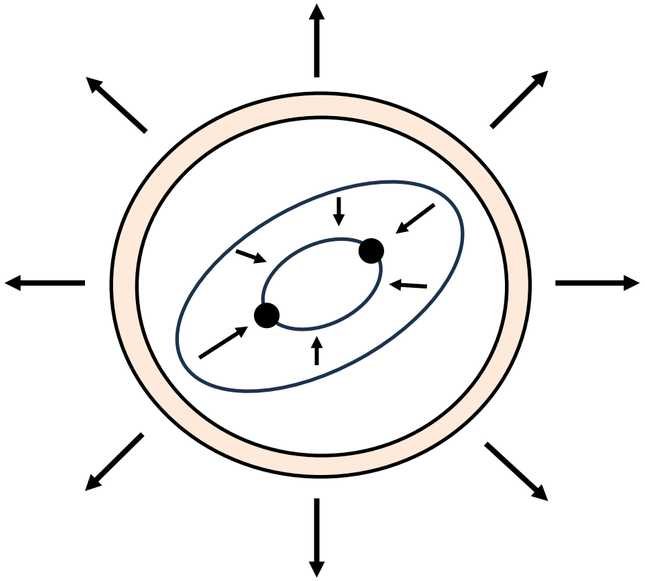

$$\alpha \nearrow \Rightarrow N_{\mathrm{det}} \searrow$$

Larger α : lower gas kinetic energy : more loose binaries than lower αs : longer GW merger time : less are observed within a Hubble time

2

Astro-cosmo parameters

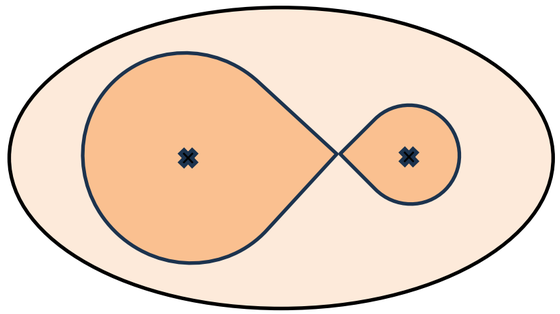

$$E_{\mathrm{bind,i}} = \alpha_{\mathrm{CE}}\,\Delta E_{\mathrm{orb}}$$

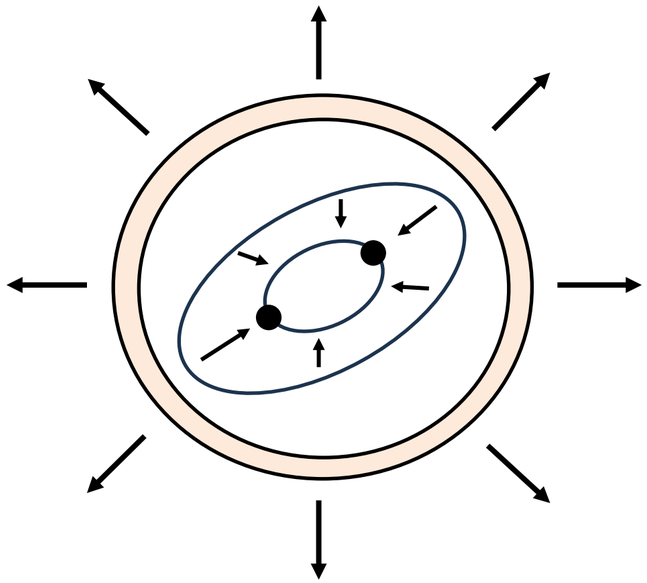

$$\alpha \nearrow \Rightarrow N_{\mathrm{det}} \searrow$$

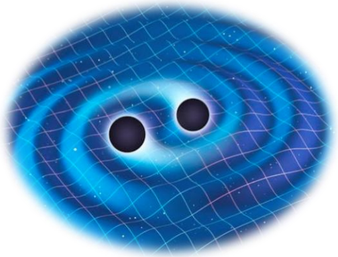

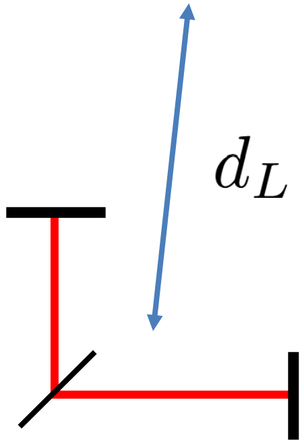

$$h_{+,\times} \propto 1/d_L \propto H_0$$

$$H_0 \nearrow \Rightarrow N_{\mathrm{det}} \nearrow$$

Larger α : lower gas kinetic energy : more loose binaries than lower αs : longer GW merger time : less are observed within a Hubble time

Astro-cosmo parameters

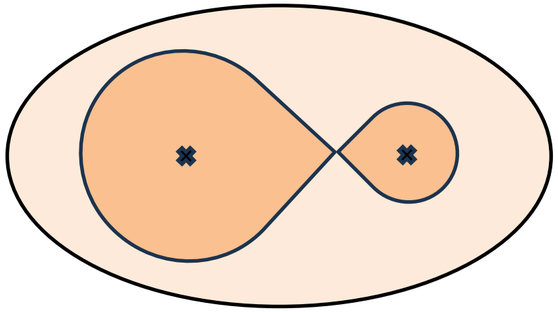

$$E_{\mathrm{bind,i}} = \alpha_{\mathrm{CE}}\,\Delta E_{\mathrm{orb}}$$

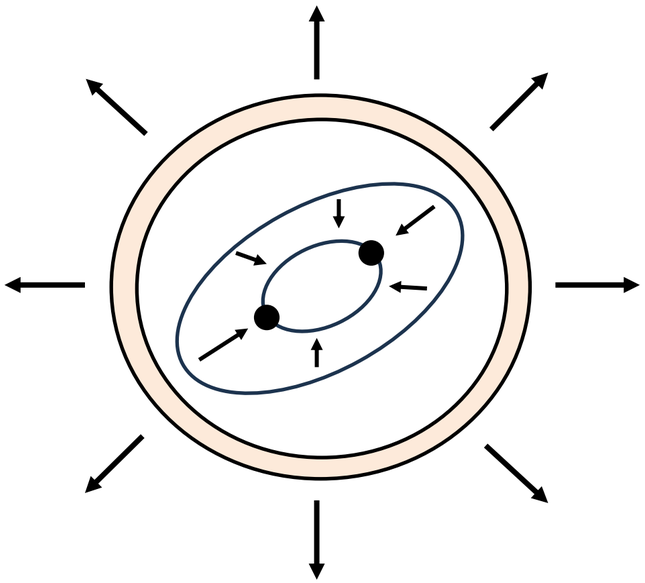

$$\alpha \nearrow \Rightarrow N_{\mathrm{det}} \searrow$$

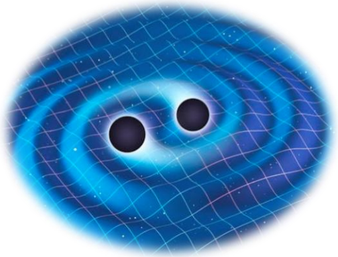

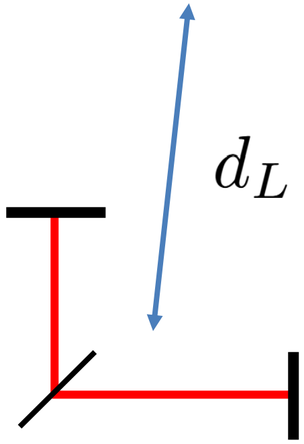

$$h_{+,\times} \propto 1/d_L \propto H_0$$

$$H_0 \nearrow \Rightarrow N_{\mathrm{det}} \nearrow$$

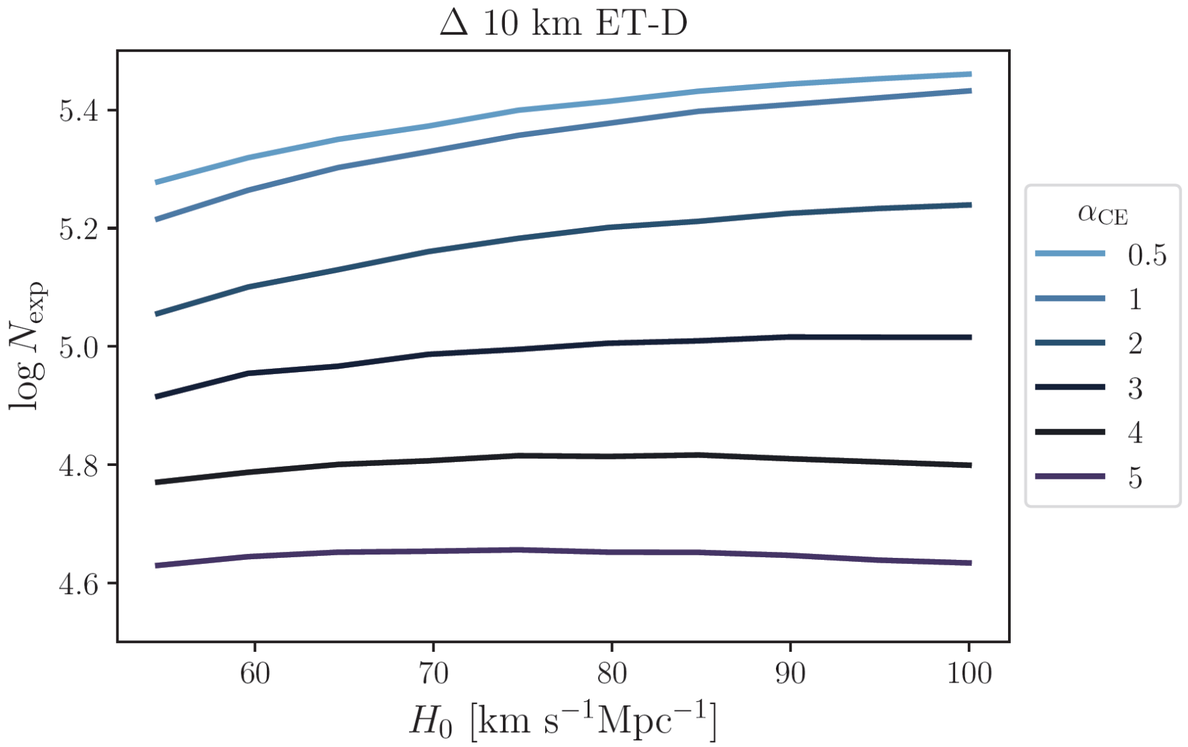

Larger α : lower gas kinetic energy : more loose binaries than lower αs : longer GW merger time : less are observed within a Hubble time

3.1 : Results

Model details

1. **SFRD computed with empirical relations from latest galaxy survey data** (more flexible than cosmological simulations and consistent with recent JWST data)
2. **Refined time delay distributions using simulations** (used SEVN but other pop synth codes can be used)
   An Example of construction:

Costa G., et al., arXiv:2311,15778

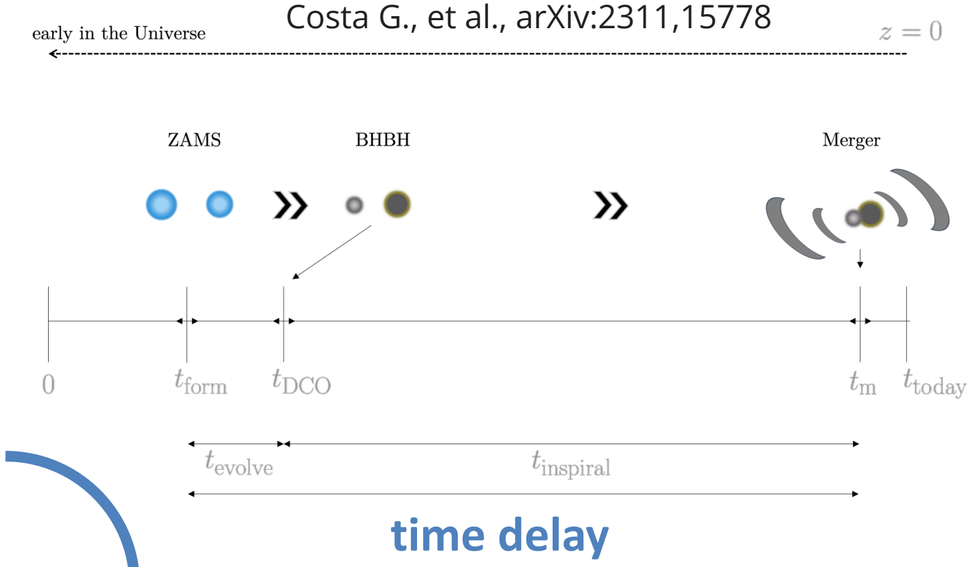

time delay

$$\int d\log\mathcal{M}$$

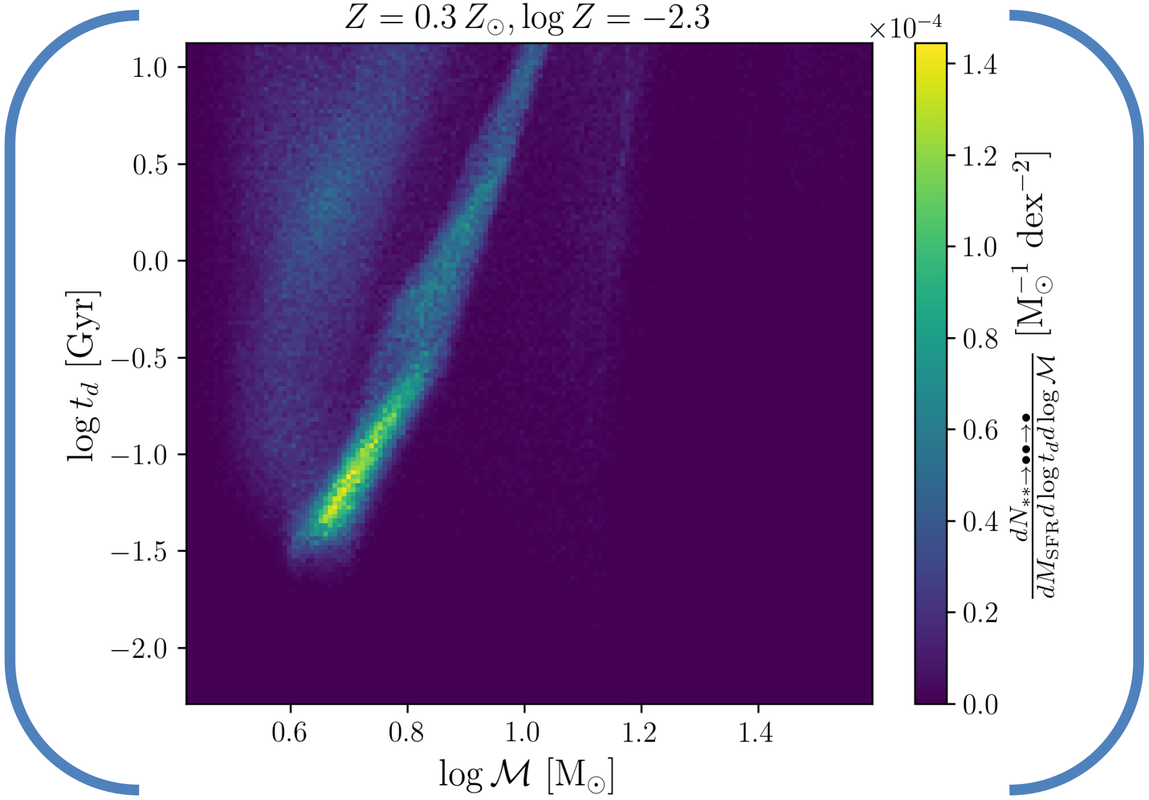

$$= \eta(Z)\frac{dp}{d\log t_d}$$

Merger efficiency: Number of merging BBH within a Hubble time per unit star mass formed

Resulting models and ET forecast

$$\frac{\mathrm{d}p}{\mathrm{d}q\,\mathrm{d}\mathcal{M}_\mathrm{s}\mathrm{d}\log\tau}(q,\mathcal{M}_\mathrm{s},\tau|Z,\alpha_\mathrm{CE}) = \begin{cases} \text{No factorization} & \mathrm{F0} \\ \dfrac{\mathrm{d}p}{\mathrm{d}q\,\mathrm{d}\mathcal{M}_\mathrm{s}}(q,\mathcal{M}_\mathrm{s}|Z,\alpha_\mathrm{CE})\dfrac{\mathrm{d}p}{\mathrm{d}\log\tau}(\tau|Z,\alpha_\mathrm{CE}) & \mathrm{F1} \\ C(\alpha_\mathrm{CE})\dfrac{\mathrm{d}p}{\mathrm{d}q\,\mathrm{d}\mathcal{M}_\mathrm{s}}(q,\mathcal{M}_\mathrm{s}|Z,\alpha_\mathrm{CE}) & \mathrm{F2} \end{cases}$$

3

Resulting models and ET forecast

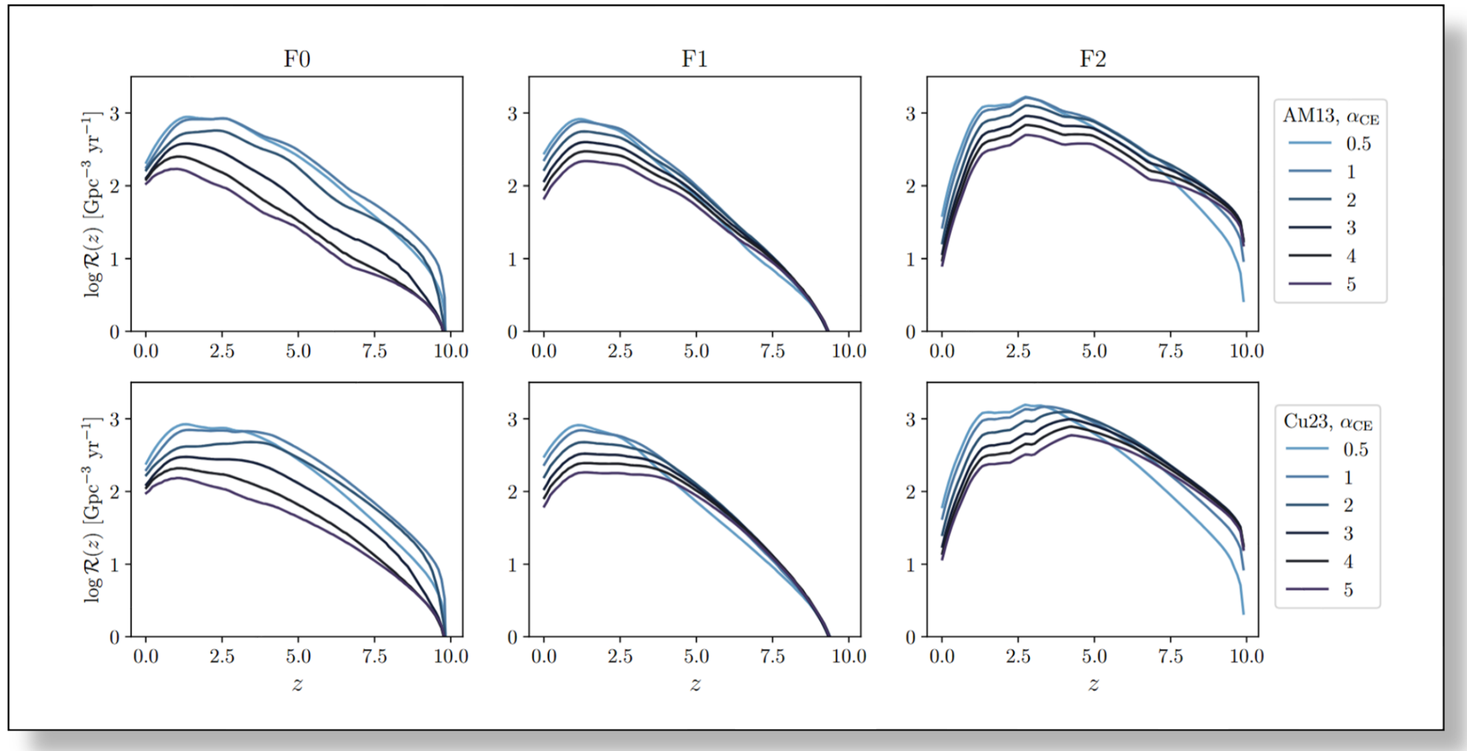

$$\frac{\mathrm{d}p}{\mathrm{d}q\,\mathrm{d}\mathcal{M}_{\rm s}\mathrm{d}\log\tau}(q,\mathcal{M}_{\rm s},\tau|Z,\alpha_{\rm CE}) = \begin{cases} \text{No factorization} & \text{F0} \\ \dfrac{\mathrm{d}p}{\mathrm{d}q\,\mathrm{d}\mathcal{M}_{\rm s}}(q,\mathcal{M}_{\rm s}|Z,\alpha_{\rm CE})\dfrac{\mathrm{d}p}{\mathrm{d}\log\tau}(\tau|Z,\alpha_{\rm CE}) & \text{F1} \\ C(\alpha_{\rm CE})\dfrac{\mathrm{d}p}{\mathrm{d}q\,\mathrm{d}\mathcal{M}_{\rm s}}(q,\mathcal{M}_{\rm s}|Z,\alpha_{\rm CE}) & \text{F2} \end{cases}$$

Resulting models and ET forecast

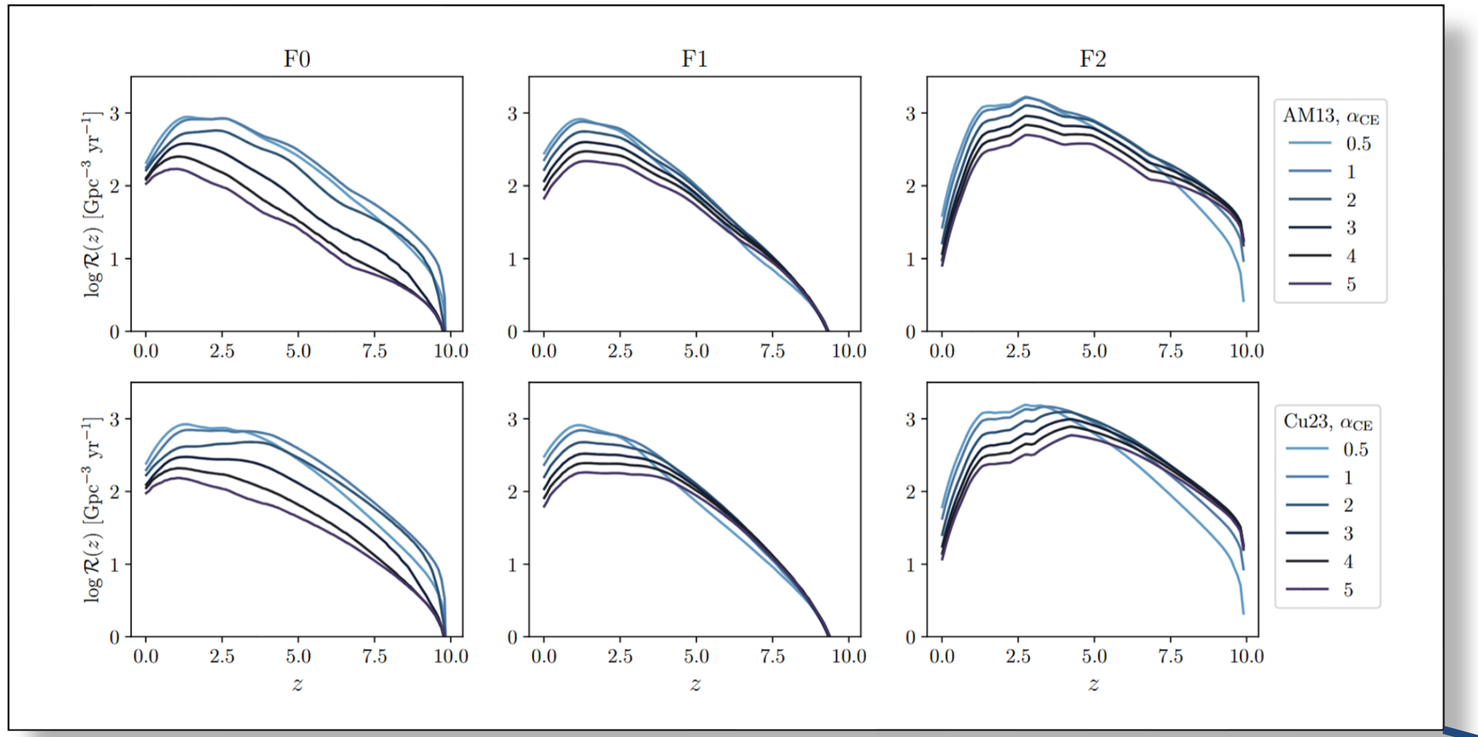

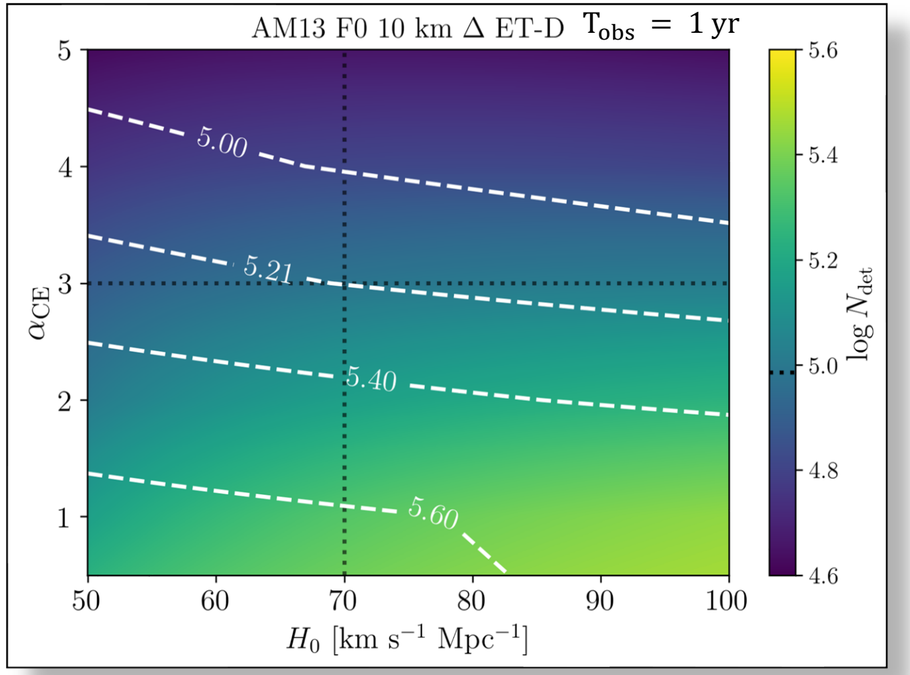

$$\frac{\mathrm{d}p}{\mathrm{d}q\,\mathrm{d}\mathcal{M}_\mathrm{s}\mathrm{d}\log\tau}(q,\mathcal{M}_\mathrm{s},\tau|Z,\alpha_\mathrm{CE}) = \begin{cases} \text{No factorization} & \text{F0} \\ \dfrac{\mathrm{d}p}{\mathrm{d}q\,\mathrm{d}\mathcal{M}_\mathrm{s}}(q,\mathcal{M}_\mathrm{s}|Z,\alpha_\mathrm{CE})\dfrac{\mathrm{d}p}{\mathrm{d}\log\tau}(\tau|Z,\alpha_\mathrm{CE}) & \text{F1} \\ C(\alpha_\mathrm{CE})\dfrac{\mathrm{d}p}{\mathrm{d}q\,\mathrm{d}\mathcal{M}_\mathrm{s}}(q,\mathcal{M}_\mathrm{s}|Z,\alpha_\mathrm{CE}) & \text{F2} \end{cases}$$

$$N_\mathrm{det}(\Lambda) = T_\mathrm{obs}\int \mathrm{d}\theta\, p_\mathrm{det}(\theta,\Lambda)\frac{\mathrm{d}N}{\mathrm{d}t_\mathrm{d}\,\mathrm{d}\theta}(\theta|\Lambda)$$

Einstein Telescope **detection function**: selects parameters that can produce detectable events

3

Hierarchical/population inference

Our population models on source-frame mass parameters $\vec{\theta} = (\mathrm{m}_1, \mathrm{m}_2)$ or $(\mathrm{q}, \mathcal{M})$ (other parameters could be included e.g. spin) depends on a set of **hyper-**parameters $\Lambda = (\alpha_{\mathrm{CE}}, H_0)$. Because of noise, the measured parameters $\vec{\mathrm{x}}$ will differ from $\vec{\theta}$, hence a hierarchy links measurements to hyper-parameters.

Hierarchical/population inference

Our population models on source-frame mass parameters $\vec{\theta} = (m_1, m_2)$ or $(q, \mathcal{M})$ (other parameters could be included e.g. spin) depends on a set of **hyper-**parameters $\Lambda = (\alpha_{CE}, H_0)$. Because of noise, the measured parameters $\vec{x}$ will differ from $\vec{\theta}$, hence a hierarchy links measurements to hyper-parameters.

Hierarchical inference is the approach to tackle this problem (Vitale S., Gerosa D., Farr W.M. Taylor S.R. HGWA Springer 2022 45):

$$\mathcal{L}(\{\vec{x}_i\}, N_{\rm obs}|\Lambda) \propto e^{-N_{\rm det}} N_{\rm det}^{N_{\rm obs}} \prod_{i=1}^{N_{\rm obs}} \frac{\int {\rm d}\vec{\theta}\, p(\vec{x}_i|\vec{\theta})\, p(\vec{\theta}|\Lambda)}{\int {\rm d}\vec{\theta}\, p({\rm det}|\vec{\theta})\, p(\vec{\theta}|\Lambda)}$$

Hierarchical/population inference

Our population models on source-frame mass parameters $\vec{\theta} = (m_1, m_2)$ or $(q, \mathcal{M})$ (other parameters could be included e.g. spin) depends on a set of **hyper-**parameters $\Lambda = (\alpha_{CE}, H_0)$. Because of noise, the measured parameters $\vec{x}$ will differ from $\vec{\theta}$, hence a hierarchy links measurements to hyper-parameters.

Hierarchical inference is the approach to tackle this problem (Vitale S., Gerosa D., Farr W.M. Taylor S.R. HGWA Springer 2022 45):

$$\mathcal{L}(\{\vec{x}_i\}, N_{\rm obs}|\Lambda) \propto e^{-N_{\rm det}} N_{\rm det}^{N_{\rm obs}} \prod_{i=1}^{N_{\rm obs}} \frac{\int {\rm d}\vec{\theta}\, p(\vec{x}_i|\vec{\theta})\, p(\vec{\theta}|\Lambda)}{\int {\rm d}\vec{\theta}\, p({\rm det}|\vec{\theta})\, p(\vec{\theta}|\Lambda)}$$

The *hierarchical likelihood* is composed of the **poissonian** occurence of N_{obs} events and the contribution from the **shape of the spectrum** modified by **selection effects** $p(det|\vec{\theta})$.

Hierarchical/population inference

Our population models on source-frame mass parameters $\vec{\theta} = (m_1, m_2)$ or $(q, \mathcal{M})$ (other parameters could be included e.g. spin) depends on a set of **hyper-**parameters $\Lambda = (\alpha_{CE}, H_0)$. Because of noise, the measured parameters $\vec{x}$ will differ from $\vec{\theta}$, hence a hierarchy links measurements to hyper-parameters.

Hierarchical inference is the approach to tackle this problem (Vitale S., Gerosa D., Farr W.M. Taylor S.R. HGWA Springer 2022 45):

$$\mathcal{L}(\{\vec{x}_i\}, N_{\rm obs}|\Lambda) \propto e^{-N_{\rm det}} N_{\rm det}^{N_{\rm obs}} \prod_{i=1}^{N_{\rm obs}} \frac{\int {\rm d}\vec{\theta}\, p(\vec{x}_i|\vec{\theta})\, p(\vec{\theta}|\Lambda)}{\int {\rm d}\vec{\theta}\, p({\rm det}|\vec{\theta})\, p(\vec{\theta}|\Lambda)}$$

The *hierarchical likelihood* is composed of the **poissonian** occurence of N_{obs} events and the contribution from the **shape of the spectrum** modified by **selection effects** $p(det|\vec{\theta})$.

Hierarchical/population inference

Our population models on source-frame mass parameters $\vec{\theta} = (m_1, m_2)$ or $(q, \mathcal{M})$ (other parameters could be included e.g. spin) depends on a set of **hyper-**parameters $\Lambda = (\alpha_{CE}, H_0)$. Because of noise, the measured parameters $\vec{x}$ will differ from $\vec{\theta}$, hence a hierarchy links measurements to hyper-parameters.

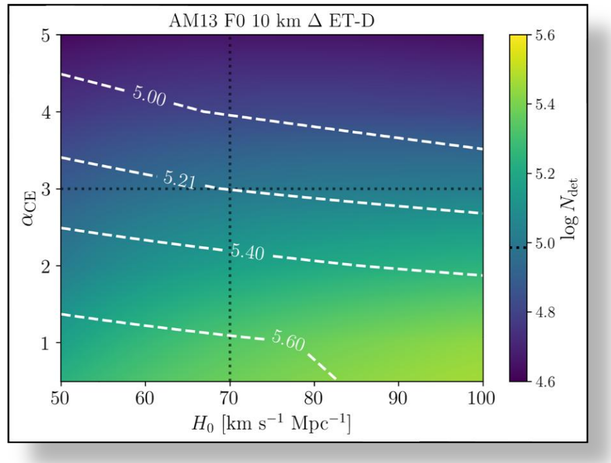

Hierarchical inference is the approach to tackle this problem:

$$\mathcal{L}(\{\vec{x}_i\}, N_{obs}|\Lambda) \propto e^{-N_{det}} N_{det}^{N_{obs}} \prod_{i=1}^{N_{obs}} \frac{\int d\vec{\theta}\, p(\vec{x}_i|\vec{\theta})\, p(\vec{\theta}|\Lambda)}{\int d\vec{\theta}\, p(det|\vec{\theta})\, p(\vec{\theta}|\Lambda)}$$

The *hierarchical likelihood* is composed of the **poissonian** occurence of N_{obs} events and the contribution from the **shape of the spectrum** modified by **selection effects** $p(det|\vec{\theta})$.

Hierarchical/population inference

Our population models on source-frame mass parameters $\vec{\theta} = (m_1, m_2)$ or $(q, \mathcal{M})$ (other parameters could be included e.g. spin) depends on a set of **hyper-**parameters $\Lambda = (\alpha_{CE}, H_0)$. Because of noise, the measured parameters $\vec{x}$ will differ from $\vec{\theta}$, hence a hierarchy links measurements to hyper-parameters.

Hierarchical inference is the approach to tackle this problem:

$$\mathcal{L}(\{\vec{x}_i\}, N_{\rm obs}|\Lambda) \propto e^{-N_{\rm det}} N_{\rm det}^{N_{\rm obs}} \prod_{i=1}^{N_{\rm obs}} \frac{\int {\rm d}\vec{\theta}\, p(\vec{x}_i|\vec{\theta})\, p(\vec{\theta}|\Lambda)}{\int {\rm d}\vec{\theta}\, p({\rm det}|\vec{\theta})\, p(\vec{\theta}|\Lambda)}$$

The *hierarchical likelihood* is composed of the **poissonian** occurence of N_{obs} events and the contribution from the **shape of the spectrum** modified by **selection effects** $p(det|\vec{\theta})$.

Poisson contribution

$$\mathcal{L}(\{\vec{x}_i\}, N_{\rm obs}|\Lambda) \propto e^{-N_{\rm det}} N_{\rm det}^{N_{\rm obs}}$$

3

Poisson contribution

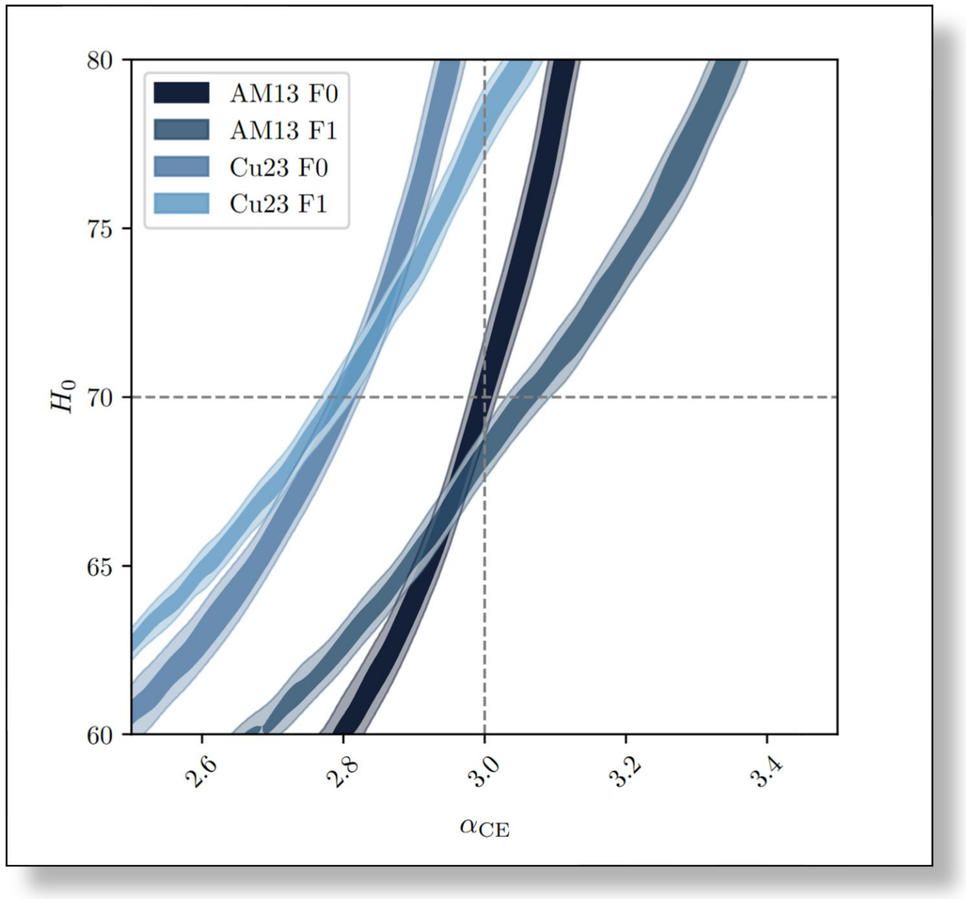

$$\mathcal{L}(\{\vec{x}_i\}, N_{\rm obs}|\Lambda) \propto e^{-N_{\rm det}} N_{\rm det}^{N_{\rm obs}}$$

The largest bias is given by an incorrect FMR relation (AM13 or Cu23) and less by the factorizations F0-1, unless the correct factorization is F2.

The strong dependence on the factorization is a strong dependence on the time delay model which can determine a concerning bias in the estimates of the hyperparameters.

3

Alternative SFRD model

$$\rho_{\rm SFR}^{\rm MF}(z) = 0.01 \frac{(1+z)^{2.6}}{1+[(1+z)/3.2]^{6.2}}$$

$$\frac{{\rm d}p}{{\rm d}\log Z}(Z|z) = \frac{1}{\sqrt{2\pi\tilde{\sigma}_Z^2}} e^{-\frac{[\log(Z/Z_\odot) - \langle\log(Z/Z_\odot)\rangle]^2}{2\tilde{\sigma}_Z^2}}$$

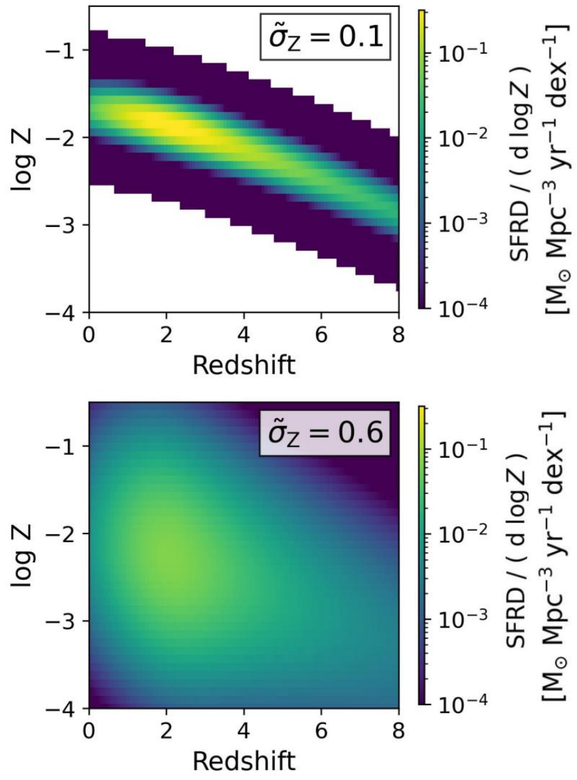

Sgalletta C., et al. A&A 698 144 2025

Alternative SFRD model

$$\rho_{\rm SFR}^{\rm MF}(z) = 0.01 \frac{(1+z)^{2.6}}{1+[(1+z)/3.2]^{6.2}}$$

$$\frac{{\rm d}p}{{\rm d}\log Z}(Z|z) = \frac{1}{\sqrt{2\pi\tilde{\sigma}_Z^2}} e^{-\frac{[\log(Z/Z_\odot) - \langle\log(Z/Z_\odot)\rangle]^2}{2\tilde{\sigma}_Z^2}}$$

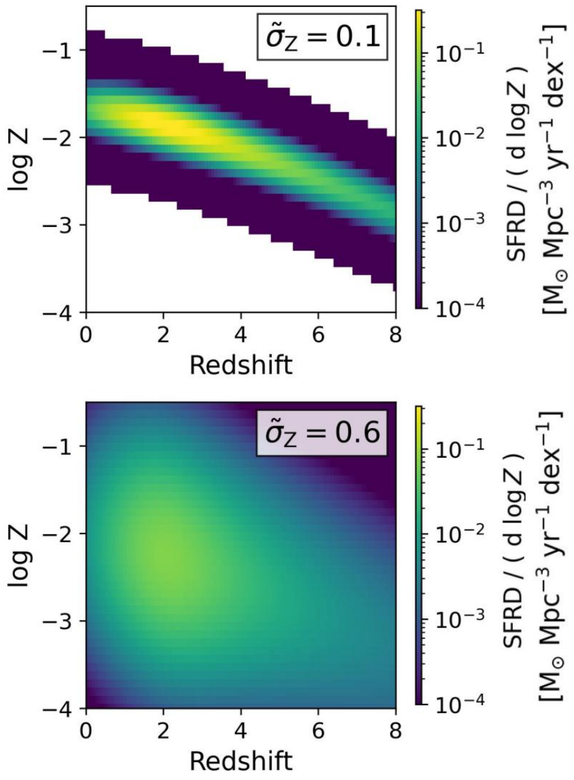

Sgalletta C., et al. A&A 698 144 2025

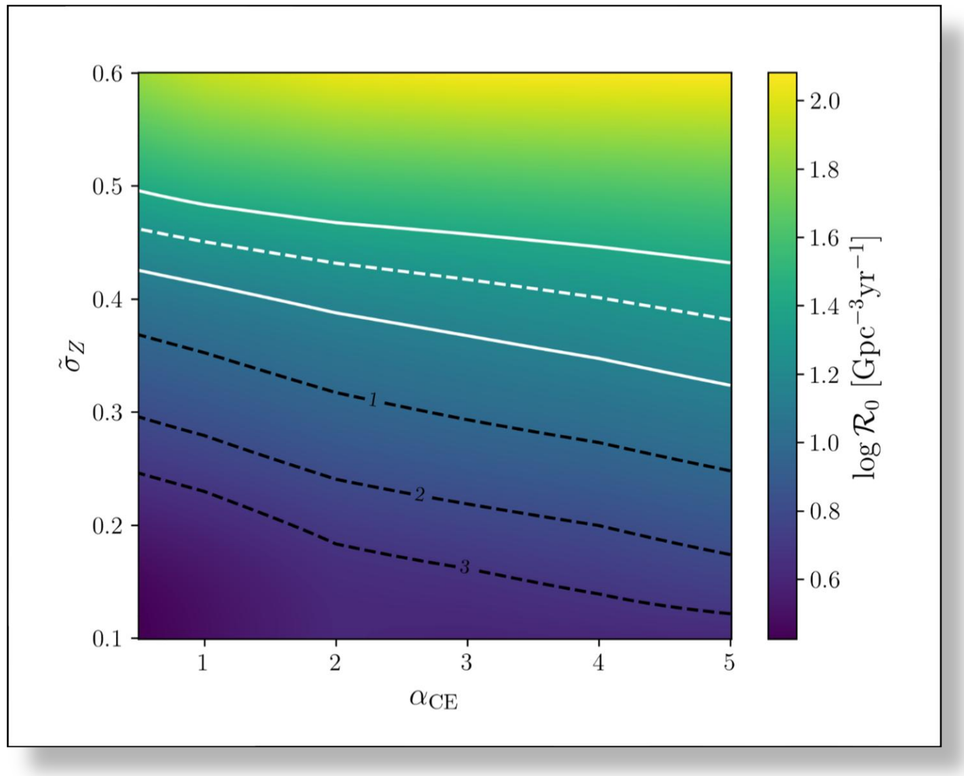

We find $\tilde{\sigma}_Z \leq 0.5$ from matching the local merger rate from LVK to our models. If other channels are added to isolate binary, value up to 0.15 can be reached depending on α_{CE}.

This GW constrain is unfortunately in tension with galaxy formation requirements (M. Chruslinska, Annalen der Physik 536 (2024)) of $\tilde{\sigma}_Z > 0.5$…

Local rates and stable mass transfer

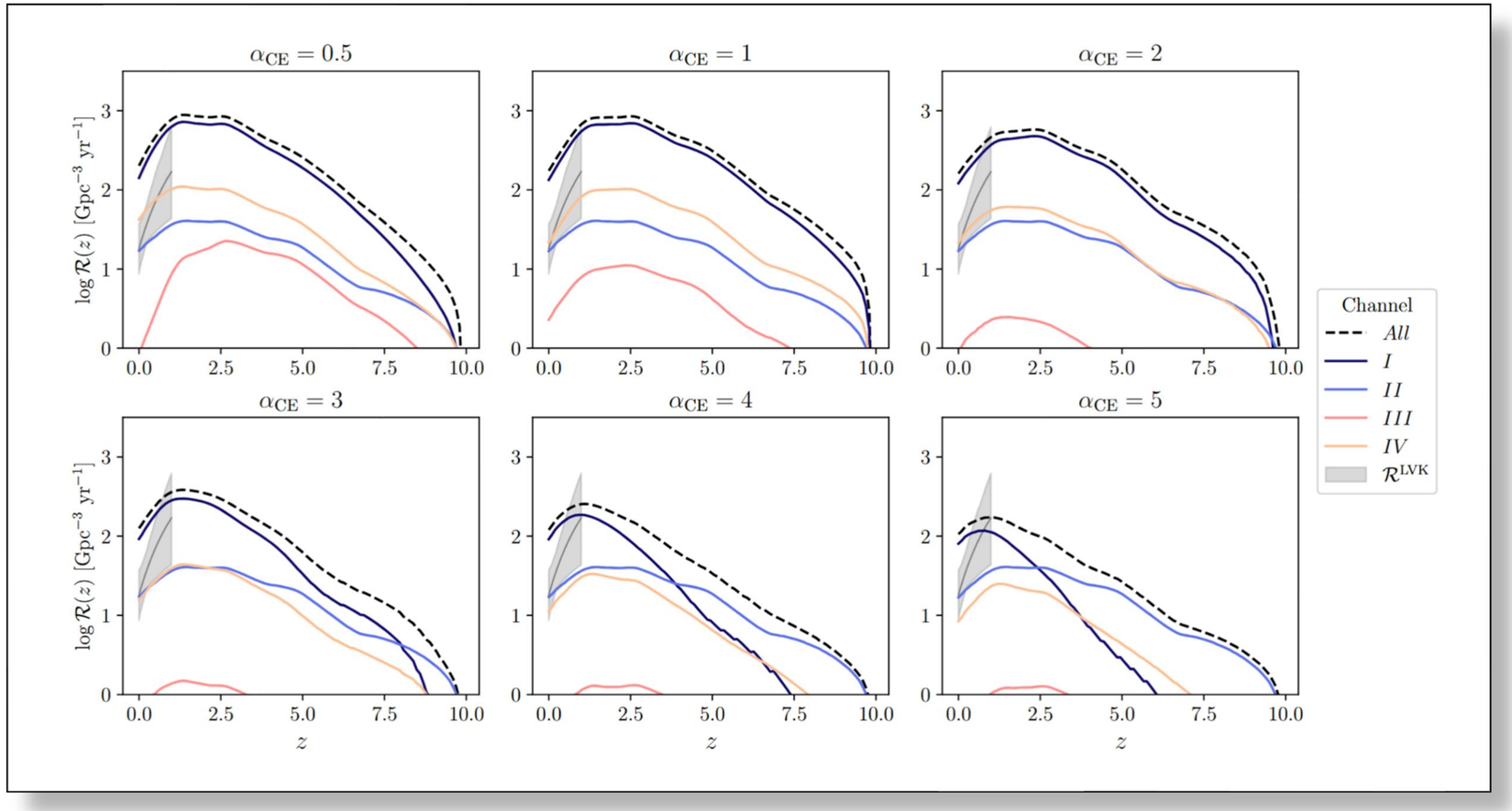

Channel I: SMT before Compact Object formation, then > 1 CE
Channel II: only SMT
Channel III: CE >1 before Cof, only one stripped star
Channel IV: Same but two stripped stars

F.S. Broekgaarden, et al., MNRAS 516 (2022) 5737

$\alpha_{CE} > 1$ are required, especially when adding additional formation channels.
Less CE systems and same order of SMT systems could be more appropriate to explain the merger rates.
The strong dependence on time-delay distribution suggests a revision of the criteria for unstable mass transfer.

3.2 : Open questions

m_2 PISN gap

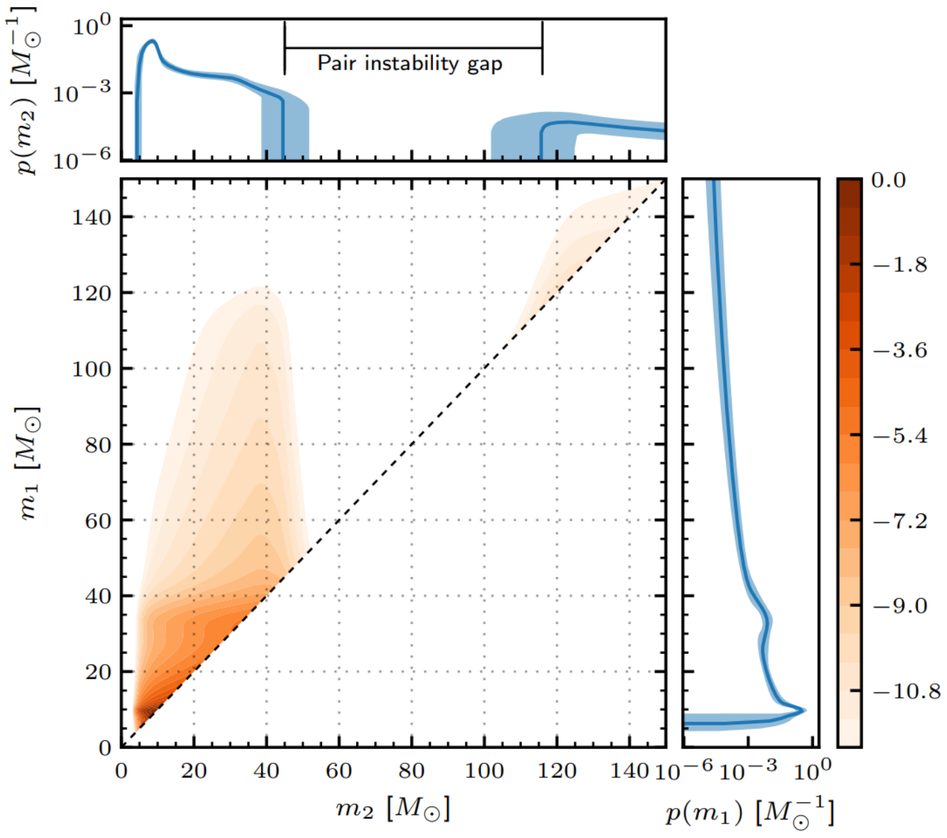

The recent work from Tong H., et al., Nature 652 8111 2026 showed the presence of a PISN gap in the secondary mass spectrum.

Motivation:

Primary BH PISN gap filled with 2G BHs, but mergers of 2G+2G are very rare, hence if the 2G+1G are the only possibility and the 1G is the least massive, then m2 spectrum should show signs of PISN gap.

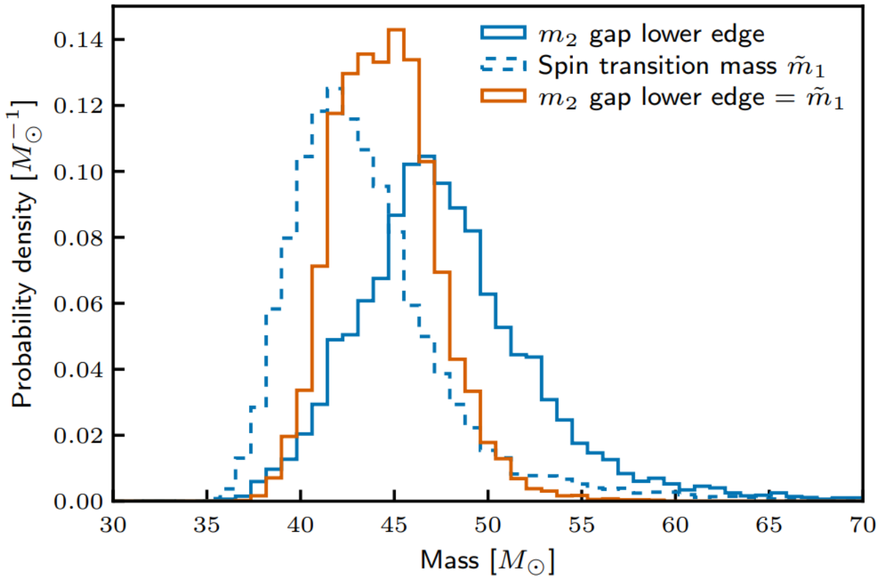

2G should have very high spin wrt 1G, therefore there is a spin transition mass that informs on the 1G->2G transition; this is compatible with the m2 PISN gap lower limit

How does cosmology affect the PISN gap?

Can the m_2 PISN gap depend on the cosmic SFR model?

3

How does cosmology affect the PISN gap?

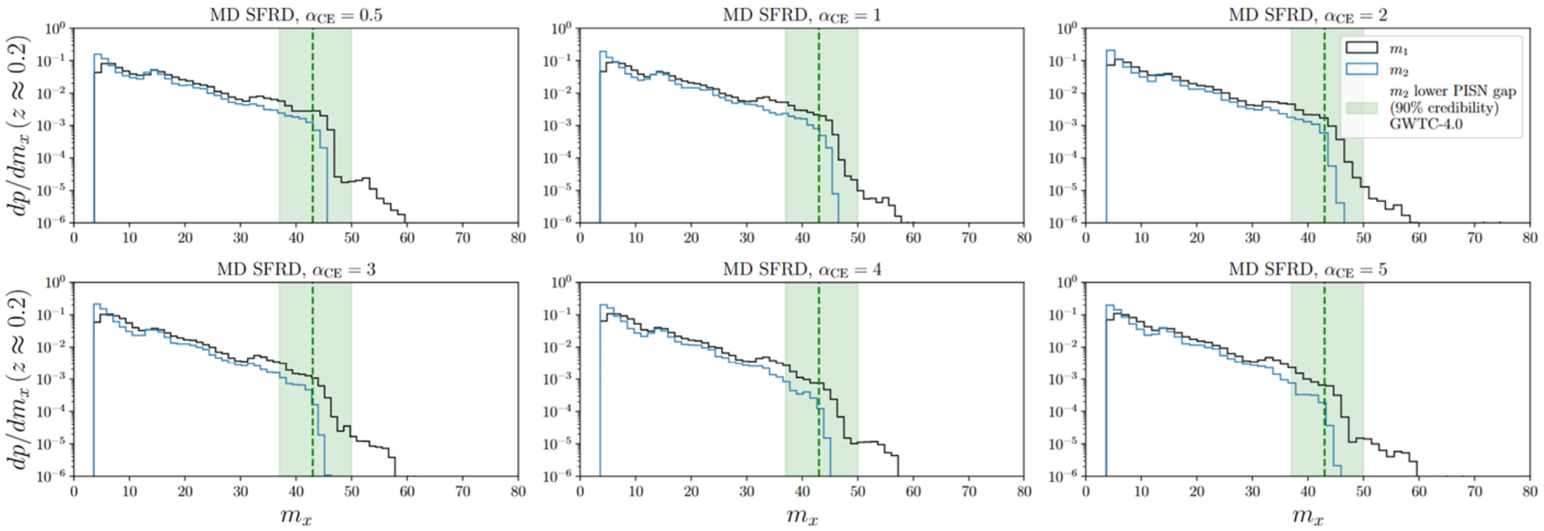

Can the m_2 PISN gap depend on the cosmic SFR model?

1. The standard Madau Dickinson model reproduces the expected PISN cut from O4

How does cosmology affect the PISN gap?

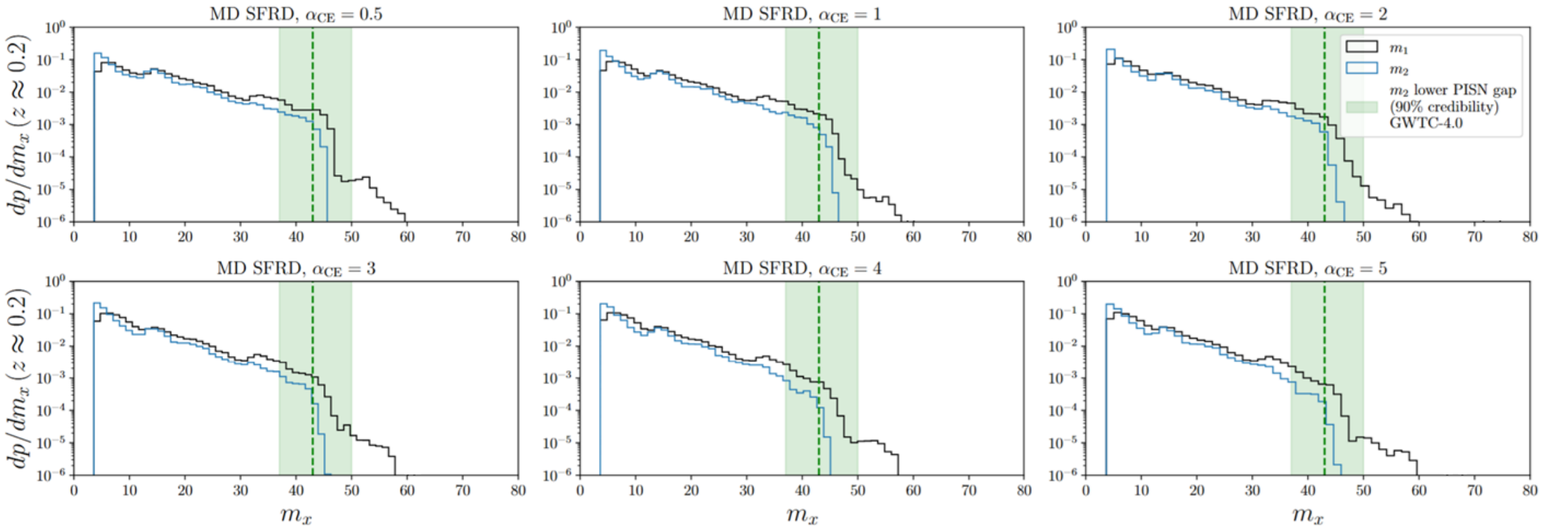

Can the m_2 PISN gap depend on the cosmic SFR model?

1. The standard Madau Dickinson model reproduces the expected PISN cut from O4

2. A data driven cosmic SFR seems to produce a different PISN cut for the same common envelope efficiency -> **Cosmological dependence**

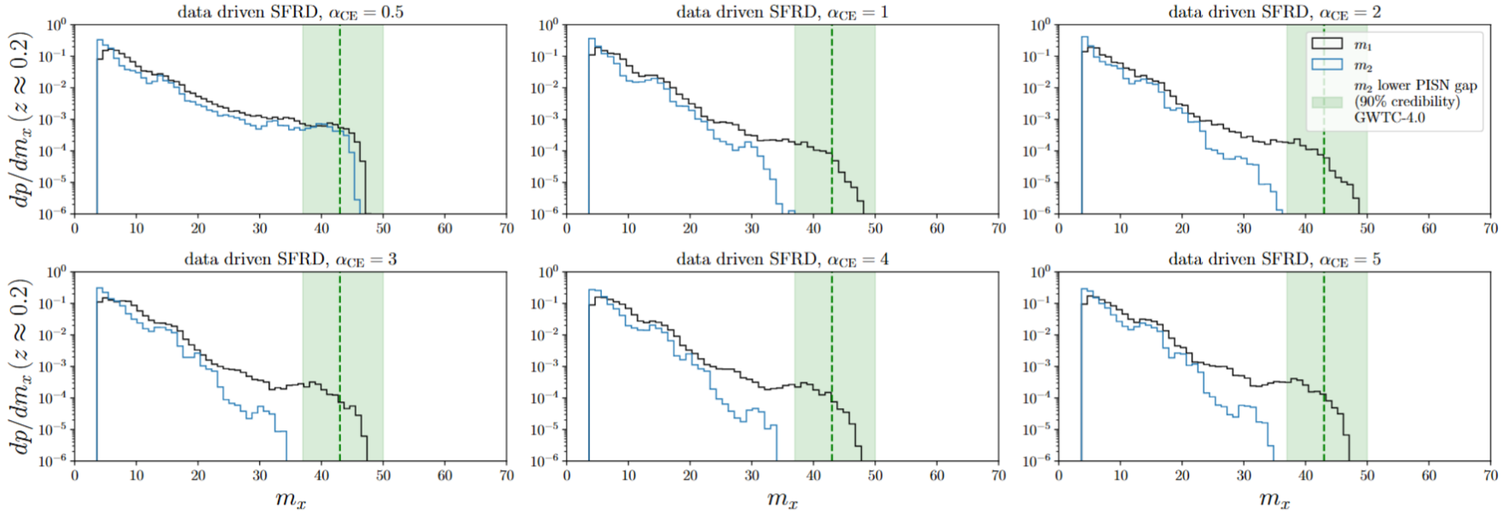

How does cosmology affect the PISN gap?

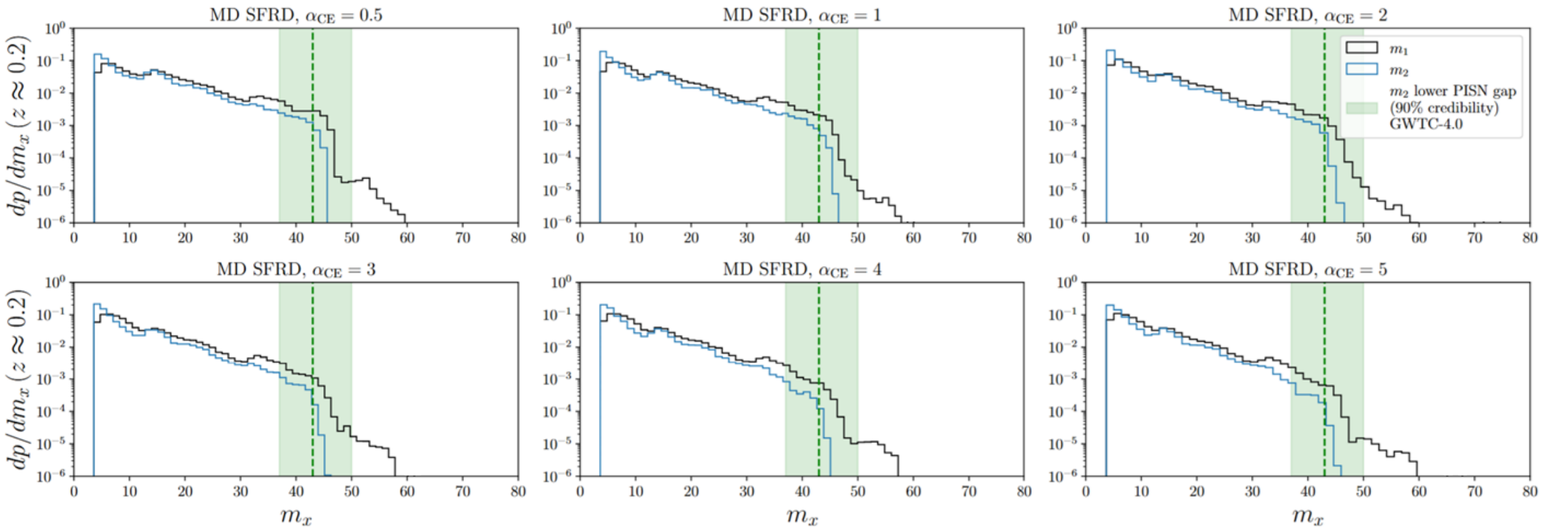

Can the m_2 PISN gap depend on the cosmic SFR model?

1. The standard Madau Dickinson model reproduces the expected PISN cut from O4

2. A data driven cosmic SFR seems to produce a different PISN cut for the same common envelope efficiency -> **Cosmological dependence**

3. In our model we find a transition around $\alpha_{CE} = 1$

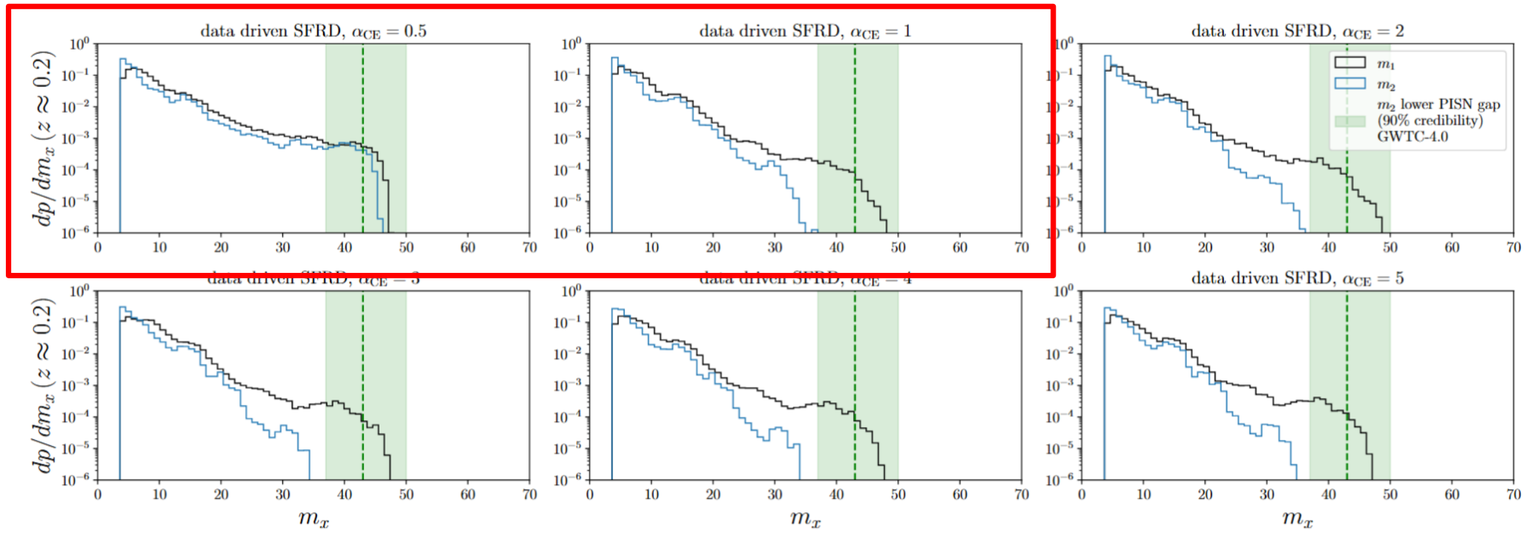

$\alpha_{CE} = 1$ transition?

$\alpha_{CE} = 1$ trans

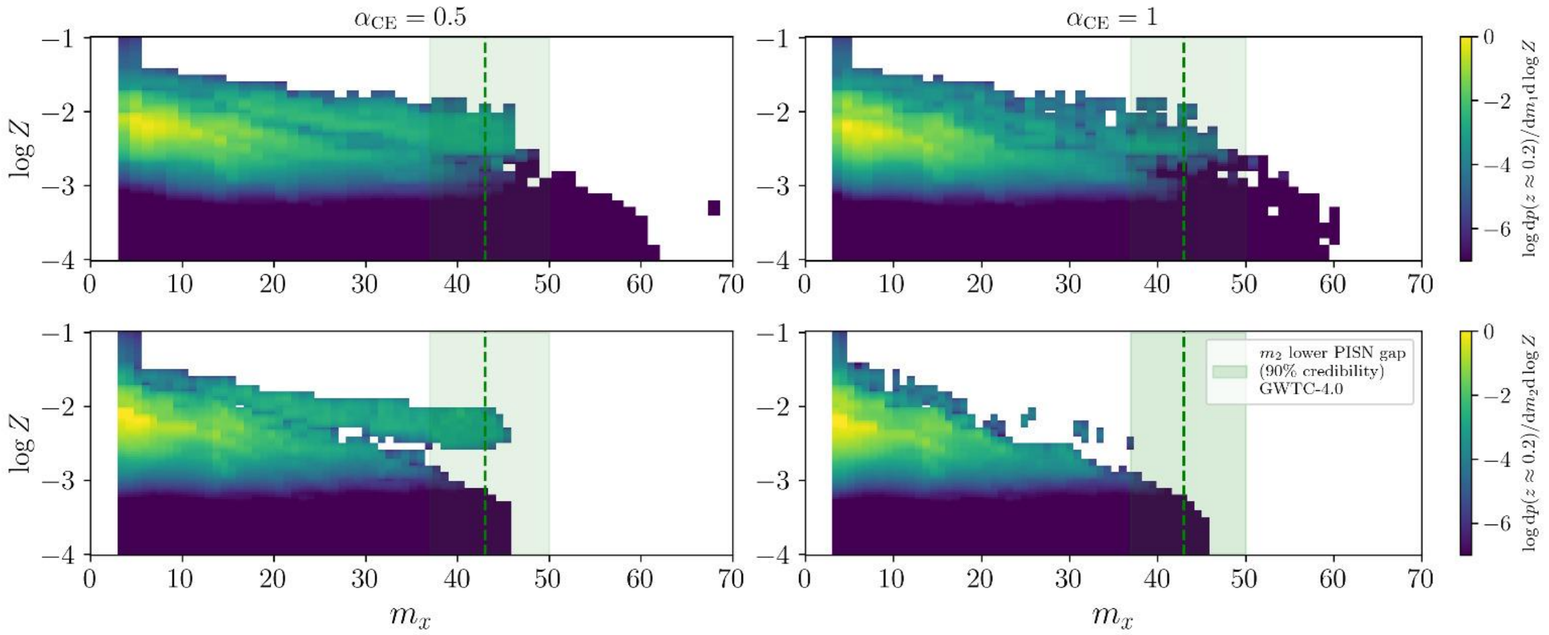

$\alpha_{CE} = 1$ transition?

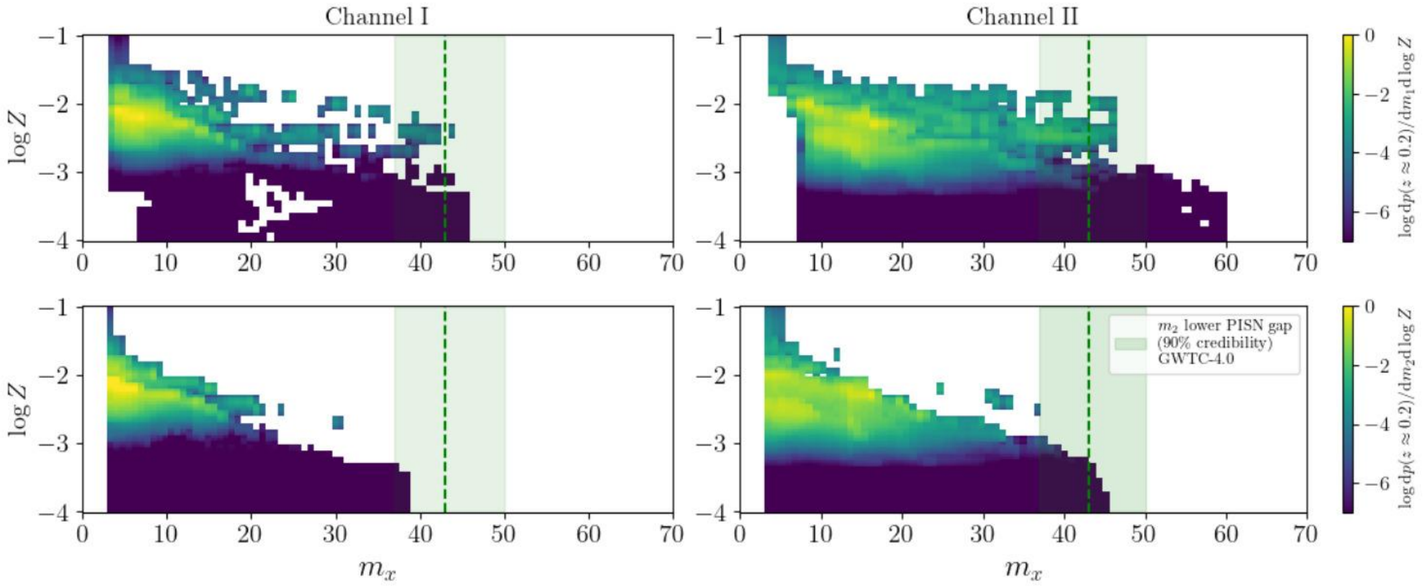

Channel I: SMT before Compact Object formation, then > 1 CE
Channel II: only SMT
Channel III: CE >1 before Cof, only one stripped star
Channel IV: Same but two stripped stars

F.S. Broekgaarden, et al., MNRAS 516 (2022) 5737

Interpretation: The data driven SFR gives a lot of weight to higher metallicities, and this feature gets picked up, differently from MD.

These systems survive because they can get really close by a double combination of low CE efficiency and double envelope ejection (double naked core system)

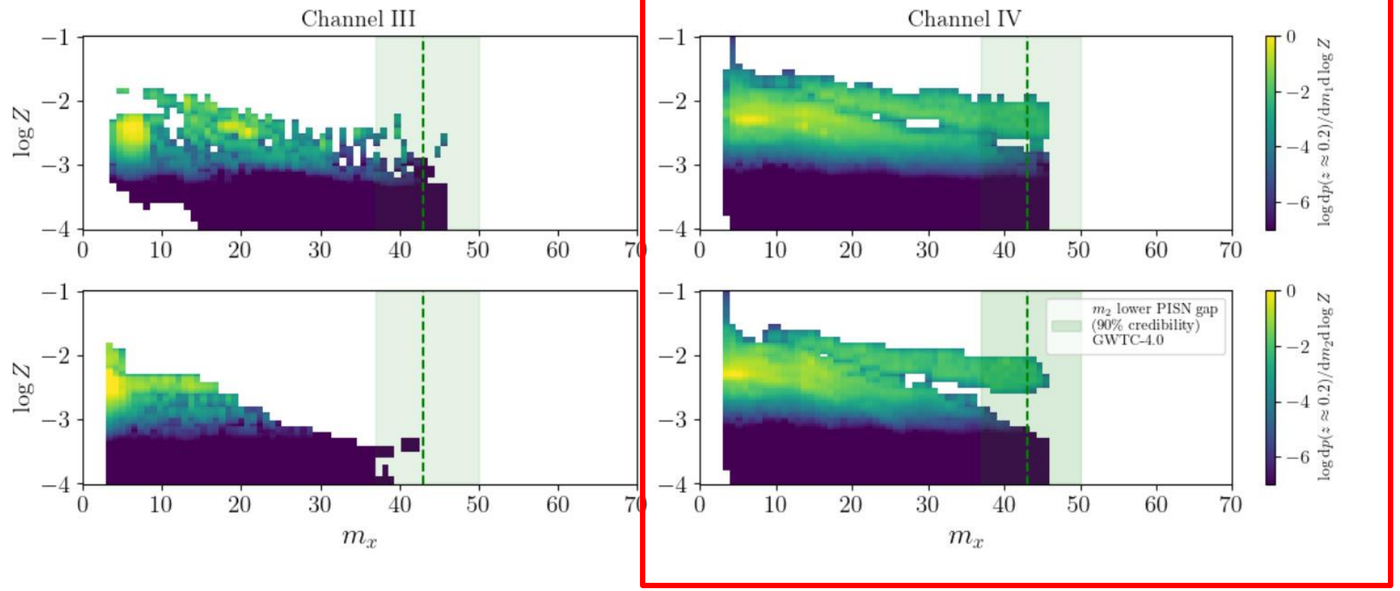

Comparing extremes: PISN vs. No PISN

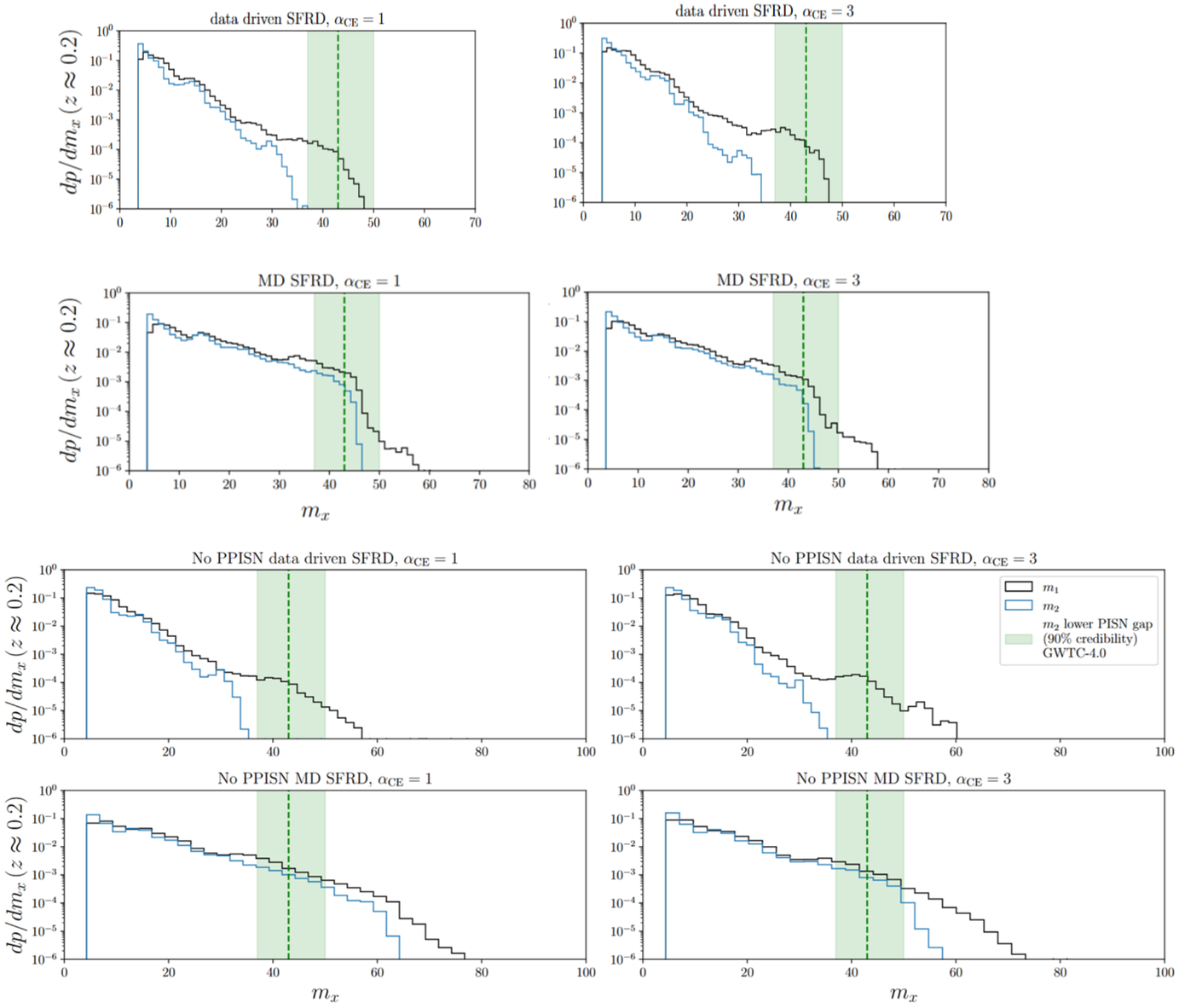

4. Similarly to what was found by Olejak A., arXiv 2026, binary stellar evolution (**different PISN prescriptions**) influence the position of the PISN gap for m_1.

However, it seems to be slightly insensitive to the position of the PISN cut in m2, therefore **Cosmological model could be dominant over the $^{12}\mathbf{C}(\boldsymbol{\alpha},\boldsymbol{\gamma})^{16}\mathbf{O}$ rate.**

Stellar mergers in Young Star Clusters

Collaborator: Ugo Niccolò Di Carlo
Aim: run N-body simulations for a young stellar cluster to investigate IMF upper limits, initial conditions and formation pathways of the most massive R136 stars
Methods:
used PeTar latest version github.com/lwang-astro/PeTar a hybrid Nbody code: force of distant particles computed w/ Barnes-Hut tree algorithm, Hermite integrator for closer particles, SDAR for close distance multiples
tested different initial conditions (SC of M=10^5 $M_{\odot}$, R = 0.8 pc):
2.1) 5 Kroupa mass upper limits (20, 50, 80, 100, 150) Msun
2.2) 10 realizations for 2 different density distributions (*Spherical* and *Fractal* w/ fractal dimension 1.6) integrated up to 10 Myrs (actually 5 fractal realizations reach 10 Myrs, but 10 reach up to 2 Myrs)
Results: (in preparation)

BH mass spectra

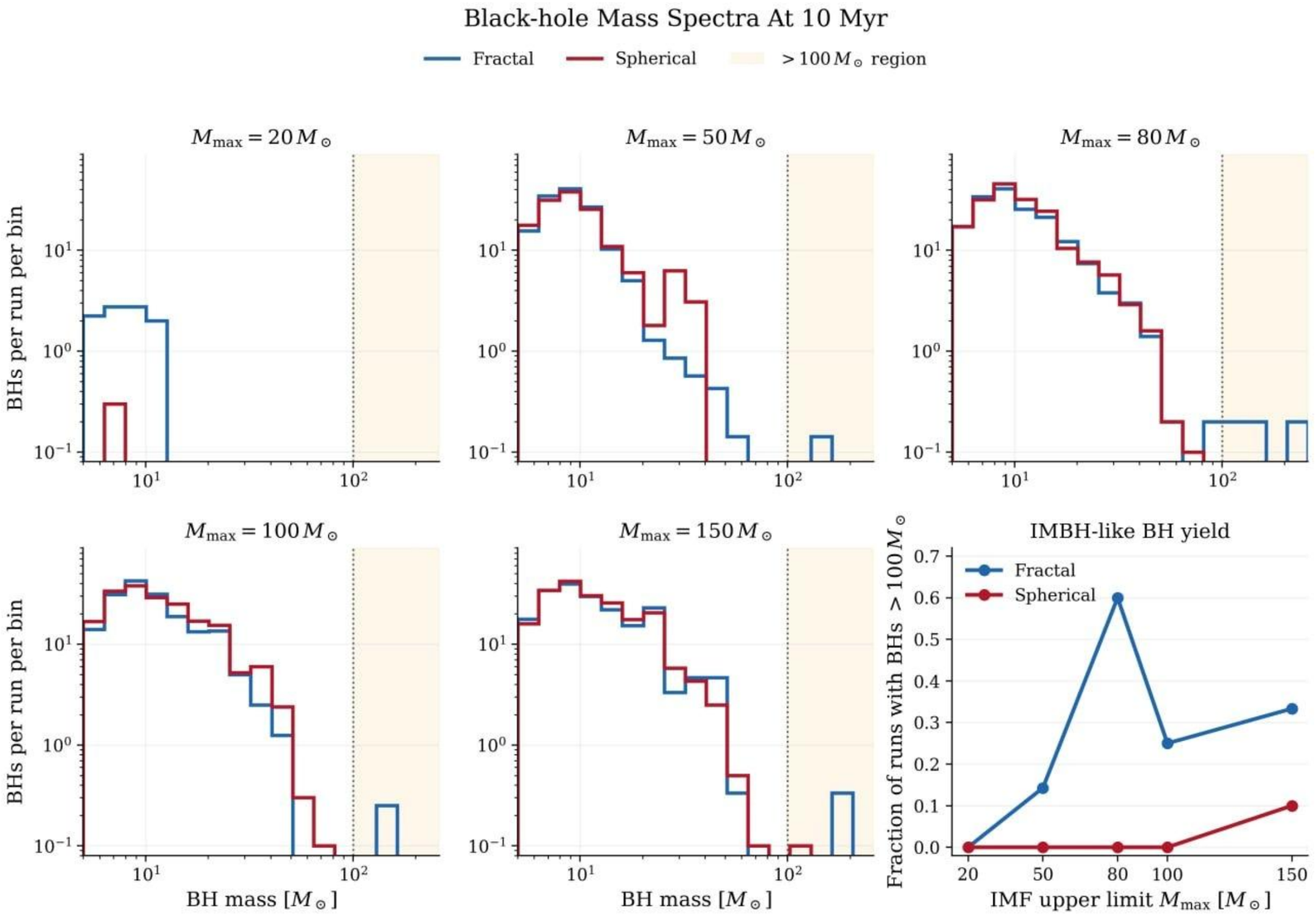

a) Simulations up to 10 Myr for a total of 50 (S) + 28 (F)

b) Heavier BHs formed with **Fractal initial condition**

c) w/ Fractal IMBH formed from 50 $M_\odot$ IMF limit, w/ Spherical only at 150 $M_\odot$

Next steps:

1) check formation pathways of IMBHs

2) increase statistics: run more simulations and for longer

Initial conditions and IMBH formation

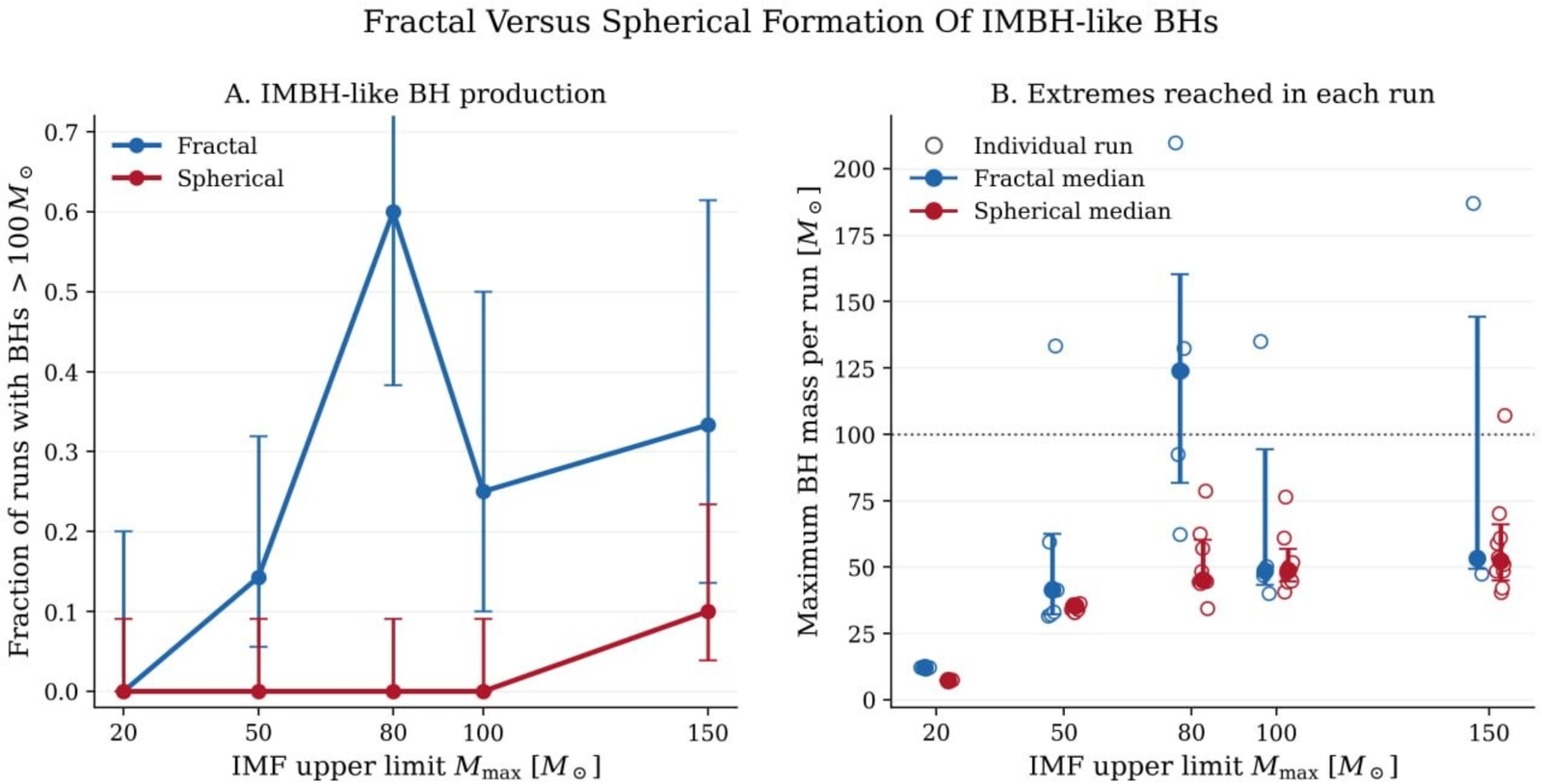

IMF limit of 80 $M_\odot$ and Fractal gave the maximum yield of IMBH in each run

Generally more IMBH for Fractal IC and more massive BH masses formed

Even with more simulations (error bars) the same picture would hold

3

IMBH in binaries

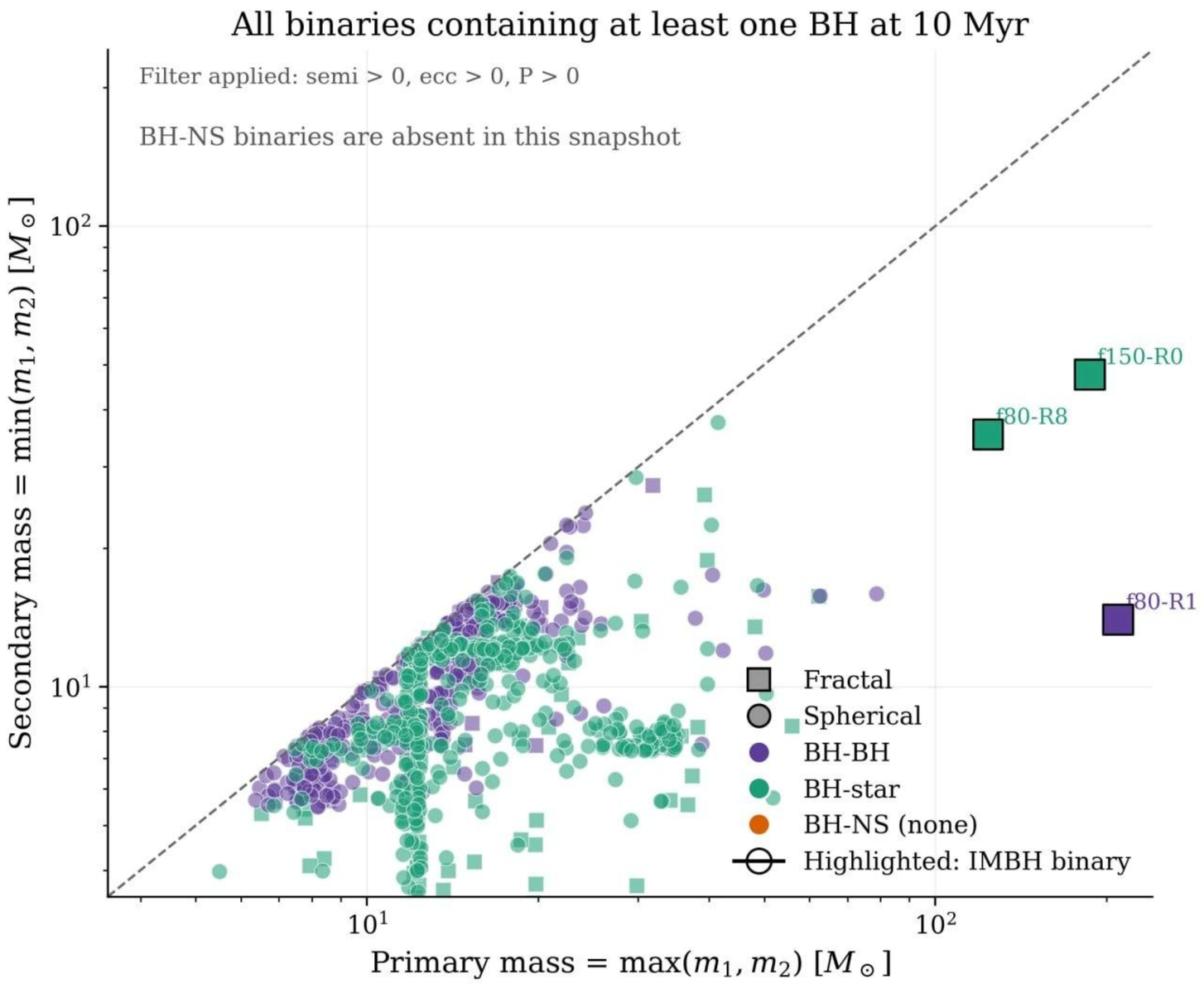

At 10 Myr we have only 3 IMBH binary candidates, 1 in a BBH
No NSBH binaries

IMBH binaries

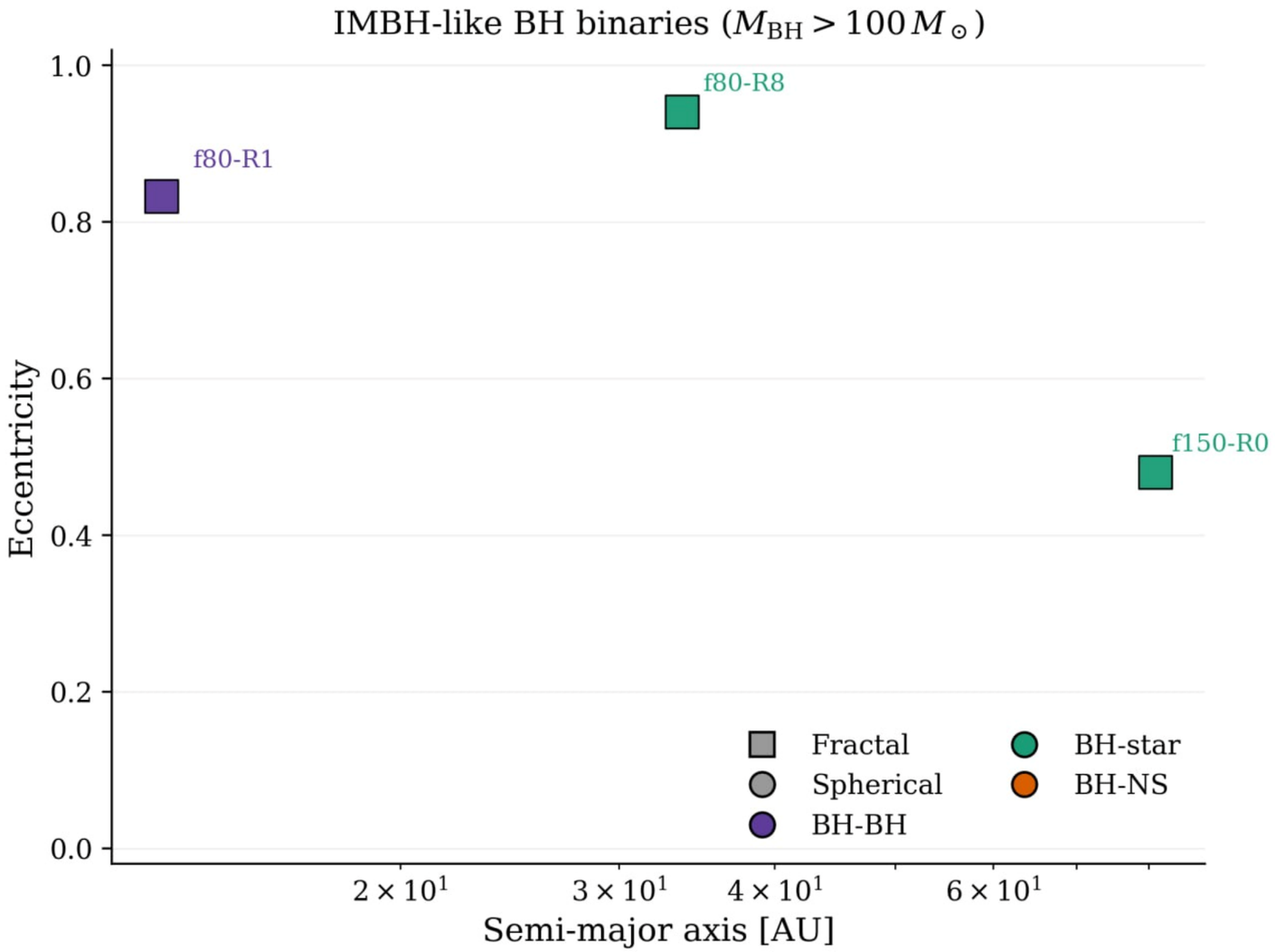

We have one hard binary of stellar BH - IMBH (F, 80 IMF): **GW inspiral time of 10^5 Gyr…**

It is located in the core of the star cluster and we expect **repeated hardenings** following a **merger in 100-200 Myr**

Two eccentric BH-star binaries: MS - BH and CHeB - BH

BH binary status

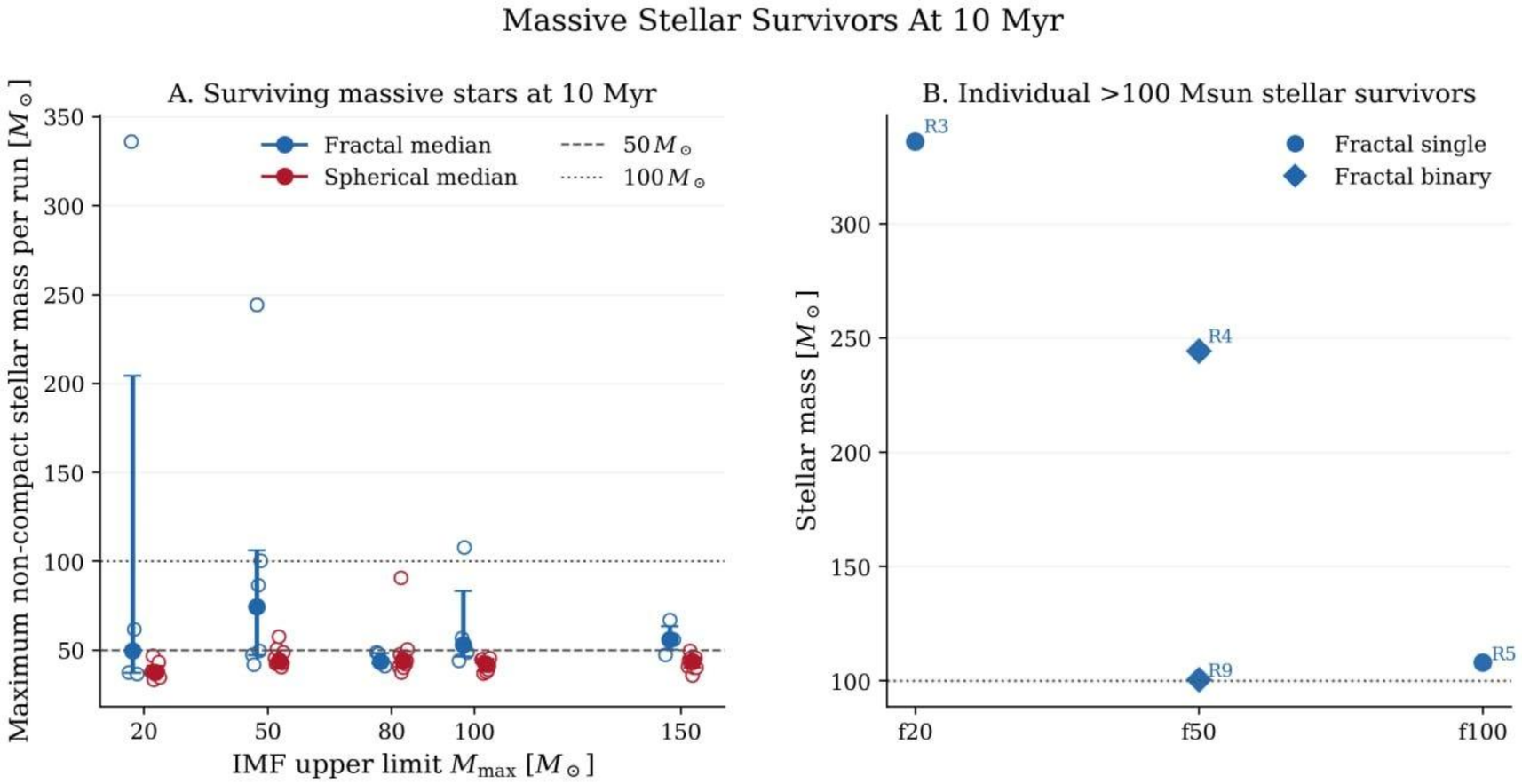

Massive stars w/ $M > 100\ M_\odot$ are found only w/ Fractal IC at different IMF limits. Stars in Spherical IC are mostly below 50 $M_\odot$

Understanding the formation and evolution of massive progenitors can give insights on R136 most massive stars.

3

Simulation based population inference

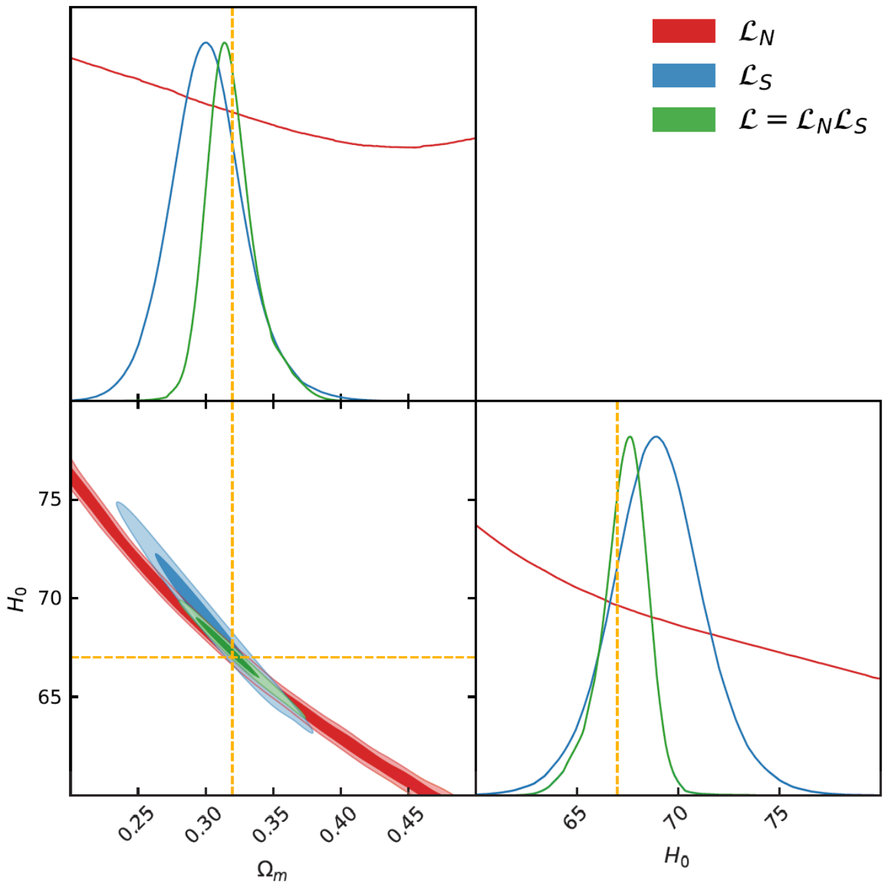

$$\mathcal{L}(\{\vec{x}_i\}, N_{\rm obs}|\Lambda) \propto e^{-N_{\rm det}} N_{\rm det}^{N_{\rm obs}} \prod_{i=1}^{N_{\rm obs}} \frac{\int {\rm d}\vec{\theta}\, p(\vec{x}_i|\vec{\theta})\, p(\vec{\theta}|\Lambda)}{\int {\rm d}\vec{\theta}\, p({\rm det}|\vec{\theta})\, p(\vec{\theta}|\Lambda)}$$

Computing the hierarchical likelihood for the next generation is computationally expensive due to large data-parameter space: $O(10^5 \times 10 \times 10)$

New methods are required: e.g. SBI (B.K. Miller, et al., Adv.NIPS 7, 2021)

Simulation based population inference

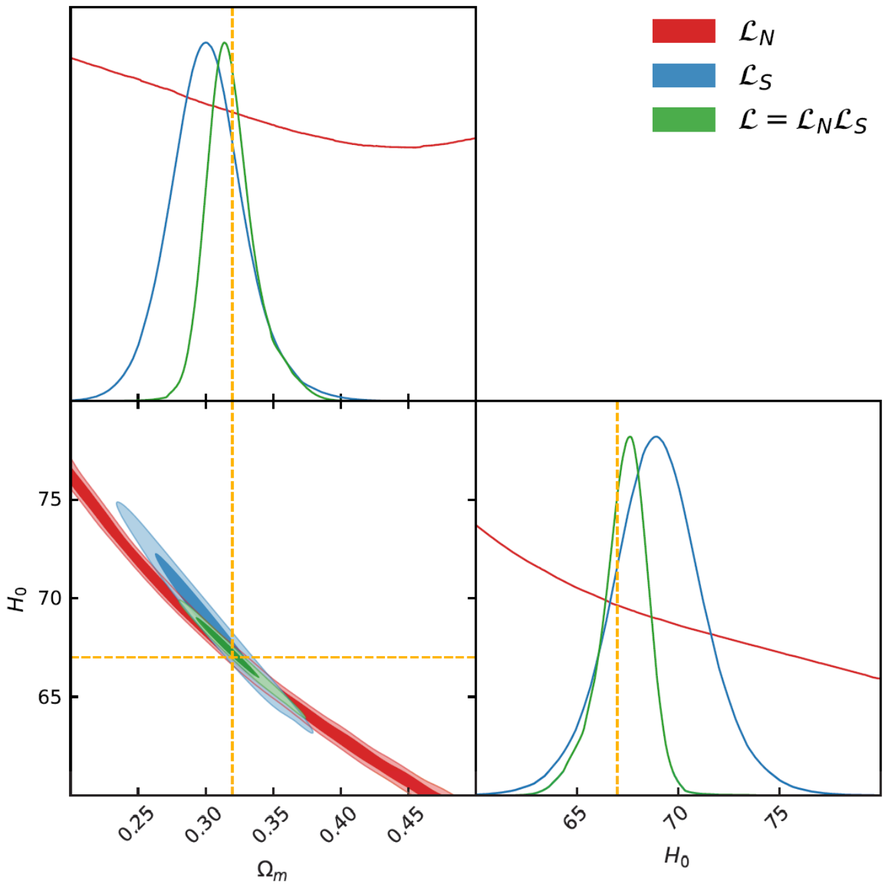

$$\mathcal{L}(\{\vec{x}_i\}, N_{\rm obs}|\Lambda) \propto e^{-N_{\rm det}} N_{\rm det}^{N_{\rm obs}} \prod_{i=1}^{N_{\rm obs}} \frac{\int \mathrm{d}\vec{\theta}\, p(\vec{x}_i|\vec{\theta})\, p(\vec{\theta}|\Lambda)}{\int \mathrm{d}\vec{\theta}\, p(\mathrm{det}|\vec{\theta})\, p(\vec{\theta}|\Lambda)}$$

Computing the hierarchical likelihood for the next generation is computationally expensive due to large data-parameter space: $O(10^5 \times 10 \times 10)$

New methods are required: e.g. SBI (B.K. Miller, et al., Adv.NIPS 7, 2021)

Simulator: a code that produces data realizations $\vec{\mathrm{x}}_j$ given a set of hyper-parameters Λ_j , for j =1,…,R

1) Extract R Λs from a prior $\pi(\Lambda)$ and construct the set $\{(\vec{\mathrm{x}}_1, \Lambda_1), \ldots, (\vec{\mathrm{x}}_{\mathrm{R}}, \Lambda_{\mathrm{R}})\}$ **these will behave as samples from $\boldsymbol{p(\vec{x}, \Lambda)}$**
2) **Reshuffle randomly the samples** in the set to obtain samples from marginals $\mathrm{p}(\vec{\mathrm{x}})$ and $\mathrm{p}(\Lambda)$
3) **Train a neural network** that computes the **marginal posterior-to-prior ratio (Swyft:** github.com/undark-lab/swyft**)**

$$\mathrm{r}(\vec{\mathrm{x}}, \Lambda) = \frac{p(\vec{\mathrm{x}}, \Lambda)}{p(\vec{\mathrm{x}})p(\Lambda)}$$

4) **Reweight r by $\boldsymbol{p(\Lambda)}$** and get posterior samples

3

Simulation based population inference